### BISHOP'S UNIVERSITY

### MASTER'S THESIS

# Predicting the Host Galaxies of Supermassive Black Hole Binaries from their Stellar Kinematic Signatures

Author: Supervisor:

Patrick HORLAVILLE Dr. John J. RUAN

A thesis submitted in fulfillment of the requirements for the degree of Master of Science

in the

Multi-Messenger Astrophysics Research Group

Department of Physics & Astronomy

**Declaration of Authorship** 

I, Patrick HORLAVILLE, declare that this thesis titled, "Predicting the Host Galaxies

of Supermassive Black Hole Binaries from their Stellar Kinematic Signatures" and

the work presented in it are my own. I confirm that:

• This work was done wholly or mainly while in candidature for a research de-

gree at this University.

• Where any part of this thesis has previously been submitted for a degree or

any other qualification at this University or any other institution, this has been

clearly stated.

• Where I have consulted the published work of others, this is always clearly

attributed.

• Where I have quoted from the work of others, the source is always given. With

the exception of such quotations, this thesis is entirely my own work.

• I have acknowledged all main sources of help.

• Where the thesis is based on work done by myself jointly with others, I have

made clear exactly what was done by others and what I have contributed my-

self.

Signed:

Date: July 22<sup>nd</sup>, 2025

L'univers comme tel n'a pas de Sens. Il est silence. Personne n'a mis du Sens dans le monde, personne d'autres que nous. Le Sens dépend de l'humain, et l'humain dépend du Sens.

– Nancy Huston, L'espèce fabulatrice

#### BISHOP'S UNIVERSITY

### Abstract

Faculty of Arts and Science

Department of Physics & Astronomy

Master of Science

Predicting the Host Galaxies of Supermassive Black Hole Binaries from their Stellar Kinematic Signatures

by Patrick HORLAVILLE

Supermassive black hole binaries (SMBHBs) at the centers of galaxies emit continuous gravitational waves (GWs) at nanohertz frequencies, and ongoing pulsar timing array (PTA) experiments aim to detect the first individual system. Identifying the exact host galaxy of a SMBHB detected in GWs is paramount for a variety of multi-messenger science cases, but it will be challenging due to the large number of candidate galaxies in the sky localization region. The present thesis reflects the work of Horlaville et al. (2025), in which recent insights on the distinct characteristics of SMBHB host galaxies are applied to archival galaxy datasets to predict which nearby massive galaxies are most likely to host SMBHBs detectable by PTAs. Specifically, we use archival galaxy integral field unit (IFU) surveys to search for nearby galaxies with distinct stellar kinematic signatures of SMBHB host galaxies, as informed by cosmological simulations. These distinct stellar kinematic signatures, including slow rotation and strong kinematic/photometric misalignments, are a hallmark of recent major galaxy mergers that led to the formation of SMBHBs in these galaxies. This work resulted in a list of nearby massive galaxies that may currently host SMBHBs, ranked by a combination of their host galaxy stellar kinematic properties and their hypothetical GW strain. After an introduction of the relevant history and overarching scientific themes in Chapter 1, this thesis delves into the methods and results of the search for SMBHB host galaxies in Chapters 2 and 3, presents the practical uses and caveats of the results of this search in Chapter 4, and concludes in Chapter 5.

### Acknowledgements

First and foremost, I would like to express my most sincere gratitude towards my supervisor, John Ruan, who has not only provided everlasting help and guidance in the development and completion of this research project, but who also helped me navigate through the maze of scholarship and graduate school applications with success. Thank you also to Jaeden Bardati for never failing to answer my questions regarding his project, which was pivotal in the completion of my own. I would also like to express my friendship to my partners in crime, fellow Bishop's physics graduate students – Matthew, Élodie, and Julien – with whom I have shared both memorable singular moments and everyday office life, and who I am happy to call friends. I am also thankful to all the members of the Bishop's Physics and Astronomy community who I have had the chance to bond with during my studies: summer interns, postdocs - including Weixiang and Reza - as well as the undergraduate students who help stimulate academic life on campus. Thank you also to Bishop's Physics and Astronomy faculty for all of their support, and in particular to Lorne Nelson for managing the Physics Help Center and coordinating activities for the 2024 solar eclipse, which was spectacular thanks both to the weather and the people who have helped organize activities on campus. Beyond our department, I am also thankful to many people from the Bishop's community: the Knowledge Mobilization folks, in particular Heather Lawford and Wade Lynch, research officer Joannie St-Germain, and graduate studies coordinator extraordinaire Jimmy Couturier. I would also like to thank my past research supervisors: Matt Dobbs, Saurabh Singh, Dallas Wulf, Dick Bond and Dongwoo Chung, who have been so instrumental in helping me navigate the complex world of research and academia.

I would also like to use this opportunity to thank all those who have helped me and continue to help me growing and learning. I am deeply indebted in their love, kindness, and I certainly wouldn't be the person I am (and becoming) without them. To my family, of course: Louis, Jean, Papa and Maman. And Pipun! To my roommate for this last year (and now dear friend) Ali: I will come back to Sherbrooke just to try your chili! To my best friends in Montreal and across the globe: Samuel, Samer, and Rodion, who I always hold close to my heart and always will. To my

spiritual mentors: Eugen Pascu, who introduced me to the beauty in the rigor of mathematics, and Victor Arcos, who, at a time when I was constantly blinded by an attention to detail, helped me understand the importance of the bigger picture. And to my dear love Lily, with whom I am looking forward to start our new life together in Montreal. And Goeuffrey!

To conclude, I would like to acknowledge that I was financially supported by a Graduate Entrance Scholarship from the Bishop's University Foundation, a Master's Training Scholarship from the Fonds de recherche du Québec – Nature et technologie (FRQNT) and a Canada Graduate Scholarship from the Natural Sciences and Engineering Research Council of Canada (NSERC) throughout the completion of this thesis research project, and I am thankful to them and my supervisor for their continued support. Lastly, I would like to highlight that Bishop's University is located on the traditional territory of the Abenaki people (the people of the rising sun), and that I feel grateful for having had the opportunity to complete my Master's degree on their land.

## **Contents**

D	eclara	ation of	f Authorship	iii
Al	bstrac	ct		viii
A	cknov	wledge	ments	ix
1	His	tory &	Modern Paradigm of Supermassive Black Hole Binaries	1
	1.1	A Brie	ef History of Black Holes	. 1
	1.2	The C	osmic Origin and Evolution of SMBHs	. 6
		1.2.1	Origins and Seeds	. 6
		1.2.2	Growth Mechanisms	. 8
			Gas Accretion	. 8
			Merging with Other SMBHs	. 10
	1.3	Obser	vational Signatures of SMBH pairs and SMBHBs	. 11
		1.3.1	Searching for Dual AGNs	. 11
		1.3.2	Searching for SMBHBs	. 14
			Electromagnetic Signatures	. 14
			Gravitational Wave Signatures	. 16
	1.4	A No	vel Approach Towards Identifying the Host Galaxies of SMBHBs	19
2	Idei	ntifying	g SMBHB Host Galaxy Signature and Relevant Datasets	23
	2.1	Deriv	ing the Kinematic LDA	. 23
	2.2	Comp	paring Stellar Kinematic Signatures to Morphological Signatures .	. 25
	2.3	Archi	val Galaxy IFU Datasets	. 28
		2.3.1	Sample Selection	. 28
		2.3.2	Stellar Mass, Metallicity, and Star-Formation Rate as SMBHB	
			Host Galaxy Discriminants	. 28

3	Cha	racteriz	zing SMBHB Host Galaxy Candidates with Stellar Kinematics	
	and	GWs		33
	3.1	Identi	fying SMBHB Host Galaxy Candidates in Archival IFU Surveys.	33
		3.1.1	Retrieval of Stellar Kinematic Parameters	33
		3.1.2	Selection of Massive Galaxies	34
		3.1.3	LDA Score and Correlations	
			with $\lambda_{R_e}$ , $\Delta PA$ , $M_*$ , $Z$ , and sSFR	36
	3.2	Calcu	lating the GW strain of Hypothetical SMBHBs	38
4	App	olicatio	ns & Caveats of SMBHB Host Galaxy Identification	41
	4.1	Interp	pretations of the Ranked List of Galaxies	41
	4.2	Use C	ases of the Ranked List of Galaxies	42
		4.2.1	Targeted Searches for Individual Continuous GW Sources by	
			PTAs	42
		4.2.2	Independent Corroboration of Candidate SMBHBs Discovered	
			Through Other Means	43
		4.2.3	Identifying Candidate Dual AGNs and Recoiling AGNs for	
			Follow-Up Observations	44
	4.3	Uncer	tainties in Calculating the GW Strain $h_0$	45
		4.3.1	Black Hole Mass	45
		4.3.2	Black Hole Mass Ratio	45
		4.3.3	Binary Separation	46
	4.4	Cross	-Referencing with Multi-AGN Catalogs	46
	4.5	Discre	epancies Among Overlapping Galaxies Between Different Surveys	48
	4.6	Redsh	nift Difference Between	
		the Si	mulated and Observational Galaxy Datasets	48
5	Con	clusion	ns	51
	5.1	Science	ce Summary	51
	5.2	Gener	al Perspectives	53
A	Ran	ked Lis	st of Galaxies	55
Ri	hlion	ranhy		65

# **List of Figures**

1.1	Chandra X-ray image of galaxy NGC 6240, with a zoom-in on its cen-	
	ter, which hosts a dual AGN. The red color represents 'soft' (less en-	
	ergetic) X-rays while the blue color represents 'hard' (more energetic)	
	X-rays. Both nuclei are at a separation of $\sim 1$ kiloparsec from each	
	other (Komossa et al., 2003)	13
2.1	Accuracy of the LDA predictor when trained with individual param-	
	eters. The stellar kinematic parameters are indicated with the yellow	
	vertical bars, while the morphological parameters are indicated with	
	the green vertical bars. The dotted green and dashed yellow horizon-	
	tal lines indicate the accuracies of the full LDA predictors correspond-	
	ing to Equations 2.1 and 2.2, respectively. Additional parameters not	
	listed in Section 2.1 are the ellipticity $\varepsilon$ , the Sérsic index $n$ , and the	
	shape asymmetry $A_S$ (Pawlik et al., 2016). We also show the LDA	
	classification accuracy using the stellar mass $M_*$ , the stellar metallic-	
	ity Z, and the specific star formation rate sSFR with the gray vertical	
	bars, which are between $\sim$ 65% and $\sim$ 50%	26
2.2	Sky map of the location of the galaxies we use for our search of the po-	
	tential host galaxies of SMBHBs. The archival galaxy datasets we use	
	(MASSIVE, ATLAS <sup>3D</sup> and CALIFA) cover most of the local massive	
	galaxies in the northern sky. The gray line traces the Galactic plane	29

2.3	Galaxies within our sample obey well-known global scaling relations.	
	Top panel: stellar mass-metallicity relation $(M_* - Z)$ for the MAS-	
	SIVE, ATLAS <sup>3D</sup> , and CALIFA galaxies for which $\lambda_{R_e}$ and $\Delta$ PA are	
	available. The solid black line represents the empirical $M_{st}$ – $Z$ re-	
	lation from SDSS galaxies from Gallazzi et al. (2005), with the dashed	
	lines representing the $\pm 1\sigma$ interval. Bottom panel: stellar mass-sSFR	
	relation ( $M_*$ -sSFR) for all ATLAS <sup>3D</sup> , MASSIVE and CALIFA galax-	
	ies in the top panel for which SFR has also been derived. The con-	
	tour lines enclose 68%, 95%, 99% of galaxies from the JHU-MPA SDSS	
	galaxy catalog (Brinchmann et al., 2004)	31
3.1	Distribution of the SMBH mass $M_{\rm BH}$ of the galaxies in the archival	
	IFU surveys. We search for PTA-detectable SMBHB host galaxies only	
	among galaxies that host the most massive SMBHs ( $M_{\rm BH} \gtrsim 10^{8.4} {\rm M}_{\odot}$ ,	
	corresponding to $M_{chirp} \gtrsim 10^8 M_{\odot}$ ). This minimum SMBH mass thresh-	
	old is indicated by a black dashed line. The bins with darker lines	
	correspond to galaxies above this threshold	35
3.2	Correlations between various galaxy properties and the LDA score	
	(from top to bottom: $\lambda_{R_e}$ , $\log \Delta PA$ , stellar mass $M_*$ , stellar metallicity	
	Z, and specific star formation rate sSFR). Overall, the LDA score has	
	a strong negative correlation with $\lambda_{R_e}$ , and a weaker positive correla-	
	tion with $\log \Delta PA$ , but little to no correlation with stellar mass, $Z$ , and	
	sSFR	37

## **List of Tables**

3.1	The top ten highest-ranking galaxies using the total score from Equa-	
	tion 3.2. Columns include: galaxy name, total score rank, luminos-	
	ity distance $D$ , IFU survey, log of the black hole mass $M_{\rm BH}$ , log of	
	the hypothetical GW strain $h_0$ , LDA score (Equation 2.2), normal-	
	ized log hypothetical strain $\widehat{\log h_0}$ , normalized LDA score $\widehat{\text{LDA}}$ , to-	
	tal score (Equation 3.2), and the inner light profile classification from	
	the literature, when available (where 'C'=core, 'P'=power-law, and	
	'I'=intermediate). The full list is provided in Table A.1 of the Ap-	
	pendix	40
A.1	Extended Table 3.1 for all the massive galaxies in our sample (with	
	a SMBH mass $M_{ m BH} > 10^{8.4} M_{\odot}$ , or equivalently with a chirp mass	
	$M_{chirp} > 10^8 M_{\odot}$ ). Columns include: galaxy name, total score rank,	
	luminosity distance $D$ , IFU survey, log of the black hole mass $M_{\rm BH}$ ,	
	log of the hypothetical strain $h_0$ , LDA score (Equation 2.2), normal-	
	ized log hypothetical GW strain $\widehat{\log h_0}$ , normalized LDA score $\widehat{\text{LDA}}$ ,	
	total score (Equation 3.2), and the inner light profile classification from	
	the literature, when available (where 'C'=core, 'P'=power-law, and	
	(I'=intermediate)	55

xix

### **List of Abbreviations**

SMBH(B) SuperMasssive Black Hole (Binary)

**GW** Gravitational Wave

**AGN** Active Galactic Nucleus

PTA Pulsar Timing Array

VLBI Very Long Baseline Interferometry

SGWB Stochastic Graviational Wave Background

BLR Broad Line Region

NLR Narrow Line Region

IFU Integral Field Unit

LDA Linear Discriminant Analysis

VMS Very Massive Star

SMS SuperMassive Star

## **Physical Constants & Conversions**

Speed of Light  $c = 2.99792458 \times 10^8 \,\mathrm{m \, s^{-1}}$  (exact)

Gravitational Constant  $G = 6.6743 \times 10^{-11} \,\mathrm{m}^3 \,\mathrm{kg}^{-1} \,\mathrm{s}^{-2}$ 

Solar mass  $1~M_{\odot}=1.989\times10^{30}~{\rm g}$ 

Light-year  $1 \text{ light-year} = 9.461 \times 10^{15} \text{ m}$ 

Parsec  $1 \text{ parsec} = 3.086 \times 10^{16} \text{ m}$ 

xxiii

# **List of Symbols**

q mass ratio (unitless)

 $\sigma_e$  stellar velocity dispersion km/s

 $h_0$  gravitational wave strain (unitless)

f gravitational wave frequency  $s^{-1}$ 

Dedicated to my grandparents:

Papi, Manou, Papounet & Ghislaine, who are and will always be with me.

### Chapter 1

# History & Modern Paradigm of Supermassive Black Hole Binaries

### 1.1 A Brief History of Black Holes

Even before the advent of the theory of general relativity by Albert Einstein in the beginning of the twentieth century, the existence of black holes was first conceptualized in the late 18th century from the precepts of Newtonian gravity. The idea of a black hole is rather simple: if an object is massive enough, its gravitational pull will be strong enough such that the velocity required for any object to escape its surface will be greater than the speed of light. As a result, the object would not be directly visible, since light leaving its surface would inevitably come back to it. John Michell, an English astronomer and geologist, first came up with that idea (Michell, 1784), going as far as predicting that while such objects (then called 'dark stars') could not be seen, the motion of luminous objects in their surroundings could reveal their presence. Shortly after Michell, French mathematician Pierre-Simon Laplace published essentially the same idea (Laplace, 1796), albeit these objects remained for many years merely a mathematical curiosity.

At the beginning of the twentieth century, novel theoretical insights in fundamental physics brought further mathematical significance to black holes and shed light on their possible formation pathways. With the emergence of general relativity by Einstein (1915) as the new theory of gravitation, Schwarzschild (1916) was the first one to solve its field equations, with his solution describing the gravitational field in the vicinity of a spherically symmetric and non-rotating mass. In particular,

the gravitational field of a black hole of mass M as described by Schwarzschild's solution diverges at a non-zero distance away from the mass known as the Schwarzschild radius and equal to  $R_s \equiv \frac{2GM}{c^2}$ , where G is the universal gravitational constant dating back from Newtonian mechanics, and c is the speed of light. This limit corresponds, in fact, to the radius derived by Laplace which describes the surface at which the escape velocity from an enclosed body of mass M is the speed of light. While the unknown origin and nature of such dense (and, perhaps most importantly, hypothetical) objects persisted for many years, the work of Chandrasekhar (1931) and Oppenheimer and Volkoff (1939) later showed that the life cycle of massive enough stars would inexorably result in the formation of a space-time singularity. Such peculiar objects would come from the unstoppable infall of matter originating from the stellar remnant, whose gravity, opposed by no counteracting force, condenses the remains of the star into a single point of infinite density. These resulting singularities satisfy the conditions of a 'dark star' imagined by Michell and Laplace, such that no object can escape their gravitational pull within their Schwarzschild radius, and in the late 1960s, John Archibald Wheeler popularized the term 'black hole' for their denomination.

In the 1970s, observations of the Cygnus X-1 source was the first observational and indirect evidence for the existence of black holes, which bolstered black hole astrophysics into an observational science. In 1970, NASA space satellite Uhuru revealed second-scale X-ray fluctuations originating from Cygnus X-1, which pointed towards X-ray generation from a compact region (where the light emitted from an object of size L will typically exhibit fluctuations on the order of a timescale  $\tau$  with  $L \sim c\tau$ ; Oda et al., 1971). Soon after, radial velocity measurements of HDE 226868, the companion star to Cygnus X-1, by Webster and Murdin (1972) at the Royal Greenwich Observatory and by Bolton (1972) at the David Dunlap Observatory at the University of Toronto, constrained the mass of Cygnus X-1 to be larger than the maximum theoretical mass for a neutron star  $^1$ , strongly hinting that Cygnus X-1 is a black hole. Today, it is believed that Cygnus X-1 is a 21  $M_{\odot}$  black hole born from the collapse of a  $\sim$ 40  $M_{\odot}$  star (Miller-Jones et al., 2021), making it a part of a class of black holes known as stellar-mass black holes, which are thought to be the end

<sup>&</sup>lt;sup>1</sup>about 3  $M_{\odot}$ ; where 1  $M_{\odot}$  is one solar mass, or about 1.989 ×10<sup>30</sup> g

product of stars with a mass  $\gtrsim 20 M_{\odot}$  (see, e.g., Casares, 2007).

In the second half of the twentieth century, the observation of distant, luminous and small objects later known as quasars were the first evidence for a new class of black holes called supermassive black holes (SMBHs). Throughout the 1950s and 1960s, the discovery of numerous radio sources with no optical counterpart was a challenge for astronomers to interpret (see, e.g., Matthews and Sandage, 1963). These "quasi-stellar" radio sources (also called quasi-stellar objects (QSOs), later shortened as quasars) displayed strongly redshifted emission lines (which could either come from their physical motion, or their large distance due to the expansion of the Universe) and significant radio and X-ray variability (on the timescale of years), which pointed to very compact origins. By the 1970s, multiple lines of evidence suggested that their redshift were of cosmological origin, meaning that quasars are extraordinarily luminous objects located in the center of galaxies that emit light in multiple parts of the electromagnetic spectrum (a class of objects known as active galactic nuclei, or AGNs) very far away from our Galaxy. The extreme luminosity and small sizes of quasars was first explained to originate from material accreting onto a very massive black hole (known as supermassive black hole, or SMBH, with masses in the range of  $10^6 - 10^{10} M_{\odot}$ ) by Zel'dovich (1964), Salpeter (1964) and Lynden-Bell (1978). Nowadays, quasars have been detected at many different epochs of the Universe, up to redshift  $z \sim 6$  (within the first billion years of the Universe; see, e.g. Barth et al., 2003; Willott et al., 2005), although quasar activity is a phase of galaxy evolution peaking near redshift  $z \sim 2.5$  (when the Universe was less than 20% of its current age; Richards et al., 2006), such that galaxies nowadays should host dormant, inactive SMBHs (Haehnelt and Rees, 1993; Soltan, 1982).

Beginning in the 1990s, the study of gaseous and stellar kinematics in the surroundings of extragalactic nuclei unveiled the presence of SMBHs in the centers of many massive local galaxies. In 1994, the Faint Object Spectrograph (FOS) aboard the Hubble Space Telescope (HST) studied the motion of gas in the nuclear region of the center of the galaxy M87. The high velocity of the gas, about 500 km/s, revealed a high concentration of mass ( $\sim 2 \times 10^9 M_{\odot}$ ) contained in a small region in the center of the galaxy, which was a strong evidence for the presence of a SMBH (Harms et al., 1994). In 1995, the Very Long Baseline Array (VLBA; which uses very long

4

baseline interferometry (VLBI) by observing the same target with many different radio telescopes at large separations to enhance the resolution of its observations) was able to study the rotating gas in the center of the galaxy M106, and deduced a high concentration of mass ( $\sim 4 \times 10^7 M_{\odot}$ ) in its nucleus, which suggested that it harbored a SMBH (Miyoshi et al., 1995). Since then, such techniques have been extensively employed to uncover many more SMBHs lurking in the center of local massive galaxies. As another example, the mass of Sagittarius A\*, the SMBH in the center of our Galaxy, was calculated by tracking the motion of stars in eccentric orbits around it (and estimated to be of a  $\sim$ a few million solar masses; see, e.g., Ghez et al., 1998; Ghez et al., 2000).

We now know that SMBHs are omnipresent in the center of massive galaxies, with which they co-evolve through cosmic time. Since the 1990s, many more SMBHs have been evidenced in most local massive galaxies, which enabled the study of their relationship with their host galaxy (see, e.g., Richstone et al., 1998; Silk and Rees, 1998; Ferrarese and Ford, 2005; Di Matteo, Springel, and Hernquist, 2005). In particular, numerous scaling relations have been found between the properties of the host galaxy and their central black hole. For example, the mass of SMBHs  $M_{BH}$  has been shown to correlate with the stellar mass of the host galaxy  $M_*$  (the total mass of its stars), the bulge mass  $M_{\text{bulge}}$  (the mass in the central region of the galaxy) and the stellar velocity dispersion  $\sigma$  (the spread in the distribution of the velocity of the stars; see e.g., Kormendy and Richstone, 1995; Ferrarese and Merritt, 2000; Gebhardt et al., 2000; Kormendy and Ho, 2013). The origins of these scaling relations is intimately tied to the growth of SMBHs and the impact they have on their host galaxies. When SMBHs accrete gas, they radiate light across the electromagnetic spectrum (at which point they become an 'active galactic nucleus', or AGN; cf. Section 1.2.2), which injects energy and momentum into the surrounding gas. In particular, the  $M_{\rm BH}-\sigma$ relation is thought to arise from AGN feedback mechanisms: as a SMBH grows, it releases radiation and winds that couple to the surrounding interstellar medium, and when the feedback becomes strong enough to overcome the gravitational binding of the galaxy bulge, it halts further accretion and central star formation, leaving the hole with a critical mass set by the depth of the potential well, which is traced by  $\sigma$ . Such feedback from the AGN can be driven by momentum (provided by radiation

pressure on dusty gas or a rapidly cooling shocked wind; see, e.g., King, 2003), or energy (provided by a hot shocked wind whose thermal energy is retained and drives a blast wave; see, e.g., Silk and Rees, 1998). In comparison, the  $M_{\rm BH}-M_{*}$  relation is largely a statistical outcome of joint black-hole and galaxy assembly, where mergers and the additive growth of stars and black holes tend to drive galaxies toward a mean mass-ratio between SMBH mass and stellar mass. However, AGN feedback can play a role by quenching star formation and preventing further accretion, which sets the normalization of the  $M_{\rm BH}-M_{*}$  relation (see, e.g., Jahnke and Macciò, 2011).

In 2015, the first detection of gravitational waves originating from the merger of two stellar mass black holes was the first direct observation of black holes. If two stellar mass black holes are brought to merge with each other, then the event stretches the fabric of space-time to the point where it generates a ripple known as a gravitational wave (GW) which propagates through the cosmos. In September of 2015, the Laser Interferometer Gravitational-Wave Observatory (LIGO) and Virgo collaborations, respectively located in the USA and in Italy, detected one such event named GW150914 (Abbott et al., 2016). The analysis of the GW signal of GW150914 revealed that it came from the merger of two black holes of masses  $\sim 36 M_{\odot}$  and  $\sim 29 M_{\odot}$ , which formed a single black hole of mass  $\sim 62 M_{\odot}$ , at a distance of about 1.3 billion light-years (where 1 light-year is approximately equal to 9.461 imes 10 $^{15}$  m), such that the equivalent of three solar masses was converted to gravitational wave energy during the merger event, whose final phase lasted a fraction of a second. This discovery was the first direct observation of black holes, which confirmed their existence and nature. Since then, LIGO, Virgo and other gravitational wave observatories such as KAGRA, in Japan, have detected many more such GW events, further substantiating the presence of black holes in our Universe (LIGO, 2025).

In 2019, the Event Horizon Telescope (EHT) collaboration released images of the shadow of a SMBH for the first time, which became one of the most compelling proofs of their existence and nature, and cemented them as an integral and fundamental part of modern astronomy. By using a network of radio antennas spread throughout the globe, the EHT collaboration observed the very center of the galaxy M87 in April 2017. With the high angular resolution provided by the long baseline between its different telescopes, the EHT was able to resolve the visible outline of

the SMBH in the nucleus of M87 (which has the same size in the sky as that of a tennis ball as distant as the Moon), thus revealing its shadow caused by the extreme gravitational pull of light in its vicinity (Event Horizon Telescope Collaboration et al., 2019). Since then, the EHT has also captured the shadow of Sagittarius A\*, the SMBH in the center of our Galaxy, the Milky Way (Event Horizon Telescope Collaboration et al., 2022). Their observations further confirm the existence of SMBHs within the centers of massive galaxies, whose images exactly match expected results from general relativity.

In 2023, numerous collaborations across the globe reported a tentative detection of a stochastic gravitational wave background in the nHz frequency band, which is suspected to be produced by SMBH binaries (SMBHBs) in the local Universe. SMB-HBs are gravitationally bound SMBHs that are expected from galaxy and SMBH evolution (cf. Section 1.2.2), with typical separations ranging from  $10^{-4} - 10^{0}$  parsec (where 1 parsec is equal to approximately  $3.086 \times 10^{16}$  m). At such separations, the two SMBHs exert a strong enough strain on the fabric of space-time to generate GWs at nanohertz (nHz) frequencies. Such GWs have a small amplitude that is significantly challenging to detect, but numerous experiments such as pulsar timing arrays (PTAs) are dedicated to their search (cf. Section 1.3.2 for more details). In 2023, multiple PTA collaborations reported the detection of the overall GW signal in the nHz frequency band (also known as the stochastic gravitational wave background, or SGWB; see, e.g., EPTA Collaboration et al., 2023; Agazie et al., 2023a; Xu et al., 2023; Reardon et al., 2023). The SGWB is hypothesized to originate from the superposition of the ensemble of individual GWs produced by many SMBHBs in the local Universe, but no single system has been identified yet. In order to understand how to identify a single SMBHB in GWs, we need to understand what we know of their origins, evolution and observational signatures.

### 1.2 The Cosmic Origin and Evolution of SMBHs

### 1.2.1 Origins and Seeds

A prevalent theory to explain the origins of SMBHs is that they arise from the collapse of the first generation of stars, which were massive and formed out of gas

that was depleted of metals. The discovery of quasars with masses of  $\sim 10^9 M_{\odot}$  at redshift  $z \sim 6$  (in the first billion years of the Universe; see, e.g., Barth et al., 2003; Willott et al., 2005) left astronomers wondering how were SMBHs born and how did they grow to be so massive so early in the Universe. One way through which they could form is from the collapse of the first generation of stars (also known as Population III, or Pop III stars). While the initial mass function (IMF) of Pop III stars is not well constrained, it is likely that they were much heavier than modern day stars (with masses tens to hundreds times that of our Sun) and lived for a much shorter time (on the order of millions of years, compared to billions of years for stars like our Sun). This is expected since the metal-free environment in which they formed limited the cooling mechanisms (such as metal-line cooling) through which gas fragments into smaller stars, yielding massive stars which burned through their hydrogen much more quickly than modern and less massive stars (see, e.g., Klessen and Glover, 2023). As such, early very massive stars (VMSs, with masses  $> 100 M_{\odot}$ ), which are predicted to arise from the collapse of primordial molecular clouds, constitute natural seeds to modern day SMBHs as they would collapse to form black holes in the early days of our Universe (see, e.g., Carr, Bond, and Arnett, 1984).

Another possible formation channel for SMBHs is that they could come from the direct collapse of dense gas regions in proto-galaxies. The inner regions of gaseous proto-galaxies are ideal locations for the formation of SMBHs. Proto-galaxies were largely metal-free, as metals were only synthesized by subsequent generations of stars and dispersed through the interstellar medium over time. As a result, these environments were not conducive for efficient gas cooling, fragmentation and star formation, which left gas available for SMBH seed formation (see, e.g., Loeb and Rasio, 1994; Koushiappas, Bullock, and Dekel, 2004; Begelman, Volonteri, and Rees, 2006). Numerical simulations have shown that the typical gas masses accumulated in the centers of galaxies (within the central few parsecs) available for the formation of massive objects are of order  $10^4 - 10^6 M_{\odot}$  (Wise, Turk, and Abel, 2008; Regan and Haehnelt, 2009). Such gas structures could directly form the seeds of SMBHs, or collapse into supermassive stars (SMSs, with masses  $> 5 \times 10^4 M_{\odot}$ ) which would later collapse into a SMBH. The masses of such SMBH seeds vary, with a range of  $10^4 - 10^5 M_{\odot}$  (Volonteri, Lodato, and Natarajan, 2008).

It is also thought that SMBHs could have been formed by the collapse of later generations of stars, which, while individually less massive, could have formed more massive seeds by colliding with each other prior to collapsing into a SMBH. If large reservoirs of gas in proto-galaxies lead to star formation rather than the formation of SMBHs, subsequent star formation will be polluted by metals and thus yield lower mass stars (Omukai, Schneider, and Haiman, 2008). Such later generations of stars could yield compact nuclear star clusters in the galaxy center (Schneider et al., 2006; Clark, Glover, and Klessen, 2008), which would be conducive to stellar collisions and the formation of VMSs, and later collapse into SMBHs with a masses in the range of  $10^2 - 10^4 M_{\odot}$  (Devecchi and Volonteri, 2009).

Alternatively, SMBHs could have been formed in the early Universe as primordial black holes. Density fluctuations whose gravitational force is large enough to overcome environmental pressure can directly collapse into primordial black holes (Carr, 2003). Their predicted masses widely vary depending on the specific time at which they are formed, from a Planck mass ( $2.176 \times 10^{-5}$  g) up to  $10^5 M_{\odot}$  (Khlopov, Rubin, and Sakharov, 2005), although lower mass primordial SMBHs are limited because they would have evaporated due to Hawking radiation and higher mass ones can be constrained from microlensing techniques (Page and Hawking, 1976; Alcock et al., 2000; Tisserand et al., 2007).

#### 1.2.2 Growth Mechanisms

#### **Gas Accretion**

If gas is present in the vicinity of a SMBH, its infall towards the SMBH will increase its mass at a rate that depends on internal and external processes, which can notably help to constrain the mass of SMBH seeds. The specific rate at which a SMBH will accrete gas depends on both external and internal effects. Cosmological hydrodynamical simulations, which simulate the birth and growth of structures in the Universe over cosmic time for a wide range of spatial scales, have shown that the centers of proto-galaxies are gas rich environments, such that external conditions are favorable to SMBH growth through accretion of nearby gas (Pelupessy, Di Matteo, and Ciardi, 2007; Wise, Turk, and Abel, 2008). However, rapid accretion is expected to be

followed by internal feedback, through which the heat of the resulting accretion disk creates a pressure that prevents further gas from falling towards the SMBH (Johnson and Bromm, 2007). In some scenarios, numerical simulations found that the growth of a SMBH can alternate between gas infall from gravity and expulsion from radiative pressure (Milosavljević, Couch, and Bromm, 2009). In particular, the Eddington limit of a SMBH is the maximum rate at which it can accrete matter while still allowing the radiation pressure to balance the inward gravitational force, which gives an idea of the maximum growth that a SMBH can undergo through accretion alone. For example, with a SMBH accreting at the Eddington rate, its mass can be approximated to double every 100 million years (Mandel, <mark>n.d</mark>.) if we assume spherically symmetric accretion of material composed of ionized hydrogen at the innermost stable circular orbit (ISCO) of the SMBH (although an accretion rate above the Eddington rate, super-Eddington accretion, is possible under different assumptions, e.g., if accretion is not spherically symmetric; see, e.g, Massonneau et al., 2023). This is notably useful in constraining possible SMBH seed models, as SMBH 'light' seeds (with masses  $\lesssim$ tens of solar masses) cannot evolve through accretion-only growth fast enough to reproduce the masses of observed quasars (near  $\sim 10^9 M_{\odot}$ ) early enough in the Universe (near redshift  $z\sim 6$ , within the first billion years of the Universe), suggesting quasars either came from more massive seeds or grew through other mechanisms (e.g., Volonteri, 2010).

Accretion of gas onto the SMBH as well as other processes in its vicinity turn the SMBH into an active galactic nucleus (AGN) and radiate light across the electromagnetic spectrum. The presence of different AGN structures depends on the SMBH formation and environment, and their associated observational features help to classify AGNs into different categories. Some of the main structures that power AGN luminosity are listed below (see, e.g., Alexander and Hickox, 2012; Netzer, 2015; Padovani et al., 2017):

Viscous dissipation in the accretion disk will convert gravitational potential
energy into thermal energy radiated as a multi-temperature blackbody: inner and hotter regions of the disk will emit ultraviolet (UV) radiation whereas
outer and cooler regions of the disk will emit light in the optical part of the

spectrum.

- Outward from the accretion disk, the broad-line region (BLR) is made of dense clouds orbiting the SMBH at velocities of  $\sim\!1000s$  of km/s, within  $\sim 0.01-1$  parsec of the SMBH. Radiation coming from the SMBH will excite electrons in the clouds of the BLR which, upon returning to their energy level, will emit specific emission lines in the optical spectrum. It is called a 'broad-line region' because the high velocity of the clouds broaden the width of the observed lines. Clouds farther out from the SMBH (at a distance of  $\sim 100-1000$  parsecs) can undergo similar photoionization, but their lower velocity (of order  $\sim\!$ hundreds of km/s) makes their observed emission lines much more narrow, and hence constitute the narrow line region (NLR).
- The dust torus, which surrounds the accretion disk and the BLR, is made of dust grains which absorb UV and optical photons and re-radiates in the infrared.
- Above the accretion disk is the corona, where energetic electrons upscatter UV
  and optical photons from the disk (through inverse Compton scattering) to
  X-ray photons. Relativistic electrons in the corona, while spiraling in the magnetic field of the SMBH, will also emit synchrotron radiation (from radio to
  optical bands) and form a relativistic jet.

#### Merging with Other SMBHs

The merging of two galaxies each hosting a SMBH can be conducive to the merging of their respective SMBHs in the center of the newly formed galaxy, which is a crucial component of SMBH mass growth. As the two supermassive black holes (SMBHs) move through the merged galaxy, they experience dynamical friction, slowing them down through transfer of angular momentum and energy to surrounding stars and dark matter (Chandrasekhar, 1943). This enables them to sink towards the bottom of the gravitational potential well of the merged galaxy (Antonini and Merritt, 2012), where the two SMBHs will then form a bound binary at ~parsec separation, which hardens through further angular momentum loss from scattering of nearby stars

and torques from the surrounding gas (Valtaoja, Valtonen, and Byrd, 1989; Quinlan, 1996; Armitage and Natarajan, 2002; Sesana, Haardt, and Madau, 2008; Kelley, Blecha, and Hernquist, 2017; De Rosa et al., 2019). At  $\sim 10^{-3}$  parsec separations, the binary system emits continuous GWs at nHz frequencies detectable by pulsar timing array (PTA) experiments (cf. Section 1.3.2), before the binary inspirals and coalesces into a single SMBH with a recoil kick (Volonteri, Haardt, and Madau, 2003; Burke-Spolaor et al., 2019). Since galaxy mergers are an important component of galaxy mass assembly whose rate peaks near redshift  $z \sim 1-3$  (when the Universe was between two and six billion years old; see, e.g., Hopkins et al., 2010; Romano et al., 2021), SMBH mergers are estimated to have contributed significantly to SMBH mass growth through cosmic time.

## 1.3 Observational Signatures of SMBH pairs and SMBHBs

The search for dual AGNs with separations  $\lesssim 10^3$  parsecs and SMBHBs is difficult and their discovery is serendipitous. Dual AGNs are gravitationally unbound pairs of SMBHs (with typical separations of  $\sim 10^0-10^5$  parsecs) that are both accreting and hence active. They arise as a stage of SMBH merger evolution (as described in the previous paragraph) upon the merging of two galaxies each hosting a SMBH and are the precursors to gravitationally bound SMBHBs. They are relatively rare (present in  $\sim$ a few percent of galaxies at most; Yu et al., 2011; Rosas-Guevara et al., 2019) and potential candidates can be identified in wide field surveys if their separation is larger than the spatial resolution in imaging data (which corresponds to  $\sim 10^4-10^3$  parsec scale separation (depending on the specific redshift of the galaxy) for typical optical surveys such as the Sloan Digital Sky Survey (SDSS), which have an angular resolution of  $\sim$ a few arcseconds; York et al., 2000). Hence, discovering dual AGNs with  $\lesssim 10^3$  parsec (sub-kiloparsec) separations and SMBHBs (which have sub-parsec separations) requires different strategies, although most of them cannot be applied systematically (see, e.g., De Rosa et al., 2019).

#### 1.3.1 Searching for Dual AGNs

In the optical band, dual AGN candidates at sub-kiloparsec separation scale can be

selected through the identification of double-peaked emission lines. As explained in Section 1.2.2, some AGNs possess a narrow-line region (NLR) corresponding to narrow emission lines in the optical spectrum originating from clouds at a distance of ~ 1 kiloparsec from the SMBH. If the system is a dual AGN possessing two distinct NLRs, then the two NLRs would display emission lines at offset wavelengths due to their relative motion with each other, which would be observable as a double-peaked narrow emission line. This technique has uncovered many dual AGN systems (see, e.g., Gerke et al., 2007; Xu and Komossa, 2009; Benítez et al., 2013), although double-peaked narrow lines can also be caused by, for example, compact rotating gas disks (e.g., Villforth and Hamann, 2015) or illumination of interacting companion galaxies (e.g., Sun et al., 2016). Therefore, double-peaked narrow lines typically require further investigation to confirm the presence of a dual AGN.

Integral field unit (IFU) observations can be used to confirm the presence of dual AGNs among selected candidates. IFU data provides both imaging and spatially resolved spectroscopy from the optical to near-infrared wavelengths, which helps to probe gaseous and stellar kinematics across different locations within the galaxy (see, e.g., Baldwin, Phillips, and Terlevich, 1981; Bundy et al., 2014). This can notably be helpful to distinguish single AGNs from dual AGNs that display double-peaked narrow lines. For example, Fu et al. (2012) performed IFU follow-up observations to dual AGN candidates previously identified with double-peaked narrow lines. They found that the double-peaked emission lines for most of their candidates (98%) can be explained with gas kinematics from a single AGN, while 2% display the radial velocities of merging systems, which supports the presence of dual AGNs. However, the wealth of information that IFU provides comes at a cost of a long exposure time (proportional to the IFU spatial and spectral resolution), which limits a wide use and application. Also, IFU observations are subject to dust obscuration (as with optical observations), which motivates using complementing techniques in other parts of the electromagnetic spectrum.

X-ray observations provide another avenue towards identifying dual AGNs, where the presence of two X-ray sources in imaging and/or specific spectral features can hint towards the presence of a dual AGN. X-ray light is relevant for dual AGN searches because it pierces through dusty environments, which are prominent around

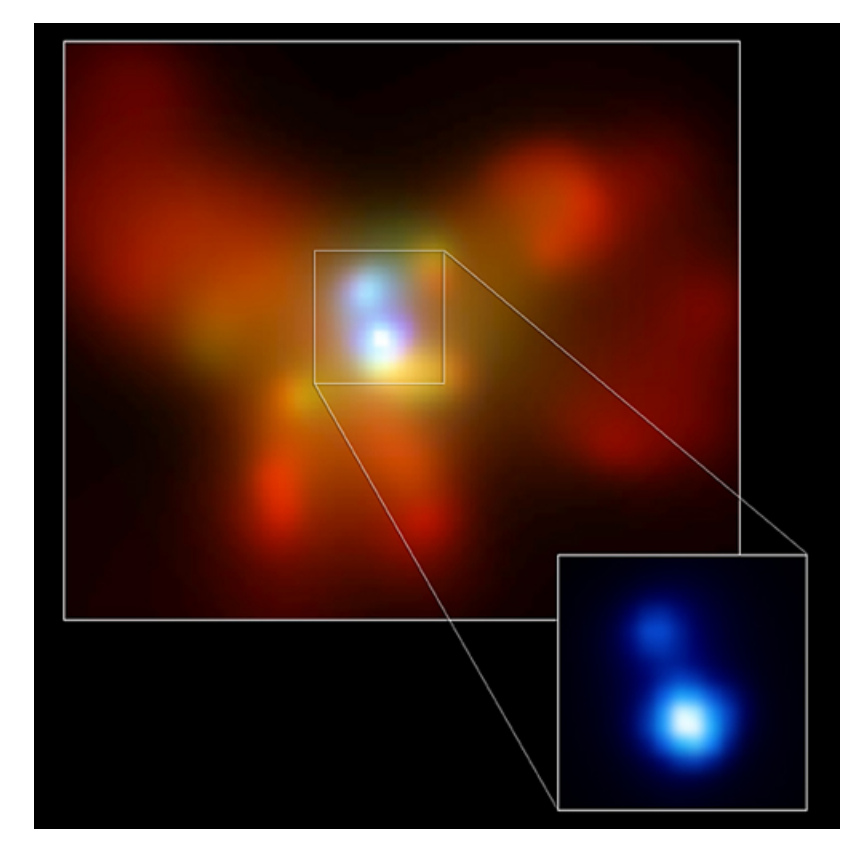


FIGURE 1.1: Chandra X-ray image of galaxy NGC 6240, with a zoomin on its center, which hosts a dual AGN. The red color represents 'soft' (less energetic) X-rays while the blue color represents 'hard' (more energetic) X-rays. Both nuclei are at a separation of  $\sim 1$  kiloparsec from each other (Komossa et al., 2003).

rapidly accreting SMBHs at redshift  $z\lesssim 1$  (Mateos et al., 2017). If both AGNs are X-ray emitters at a separation of  $\lesssim 1$  kiloparsec, then X-ray imaging (e.g., with the Chandra space observatory) can resolve their separation. Komossa et al. (2003) used this technique to uncover the first spatially resolved dual AGN, which was found in the galaxy NGC 6240 (see Figure 1.1). One caveat to X-ray imaging for dual AGN identification is that a single AGN with dual jets can be mistaken as two individual sources. For NGC 6240, both sources have a similar X-ray spectrum and display a strong neutral iron line, which is hypothesized to arise from the reprocessing of X-ray radiation by material accreting onto the SMBH (Komossa et al., 2003; Ricci et al., 2014), which confirms that both sources are individual AGNs.

Specific features in spectroscopic and imaging infrared data can help to identify dual AGNs enshrouded in dust. The presence of double-peaked infrared lines (equivalent to optical methods), two continuum components in infrared spectra or two spatially resolved nuclei in infrared imaging can reveal the presence of two

AGNs (e.g., Pfeifle et al., 2019).

In the radio band, the small angular resolution provided by imaging through very long baseline interferometry (VLBI) can also confirm the presence of a dual AGN. Extragalactic radio emission typically originates either from AGNs or star formation activity, but high-resolution radio observations can entangle the compact AGN radio emission from the more diffuse star-formation activity radio light (see, e.g., Condon, 1992). Such resolutions are attained by radio telescopes using very long baseline interferometry (VLBI). At cm wavelength, VLBI can spatially resolve the separation between two SMBHs as close as  $\sim$ one parsec in the local Universe, and  $\sim$ 10 parsecs at any redshift, which makes it an ideal technique to search for sub-kiloparsec dual AGNs (An, Mohan, and Frey, 2018; De Rosa et al., 2019). However, only a handful ( $\lesssim$ 10%) of AGNs are strong radio emitters ('radio-loud'), limiting the applicability of VLBI to search for dual AGNs (Ivezić et al., 2002), although some 'radio-quiet' AGNs can have compact radio emission observable with VLBI (Herrera Ruiz et al., 2016).

#### 1.3.2 Searching for SMBHBs

#### **Electromagnetic Signatures**

Since SMBHBs have an even smaller separation than dual AGNs, VLBI alone can resolve their separation in imaging, and can only do so for the most widely separated and nearby systems. For example, Rodriguez et al. (2006) used VLBI to uncover a SMBHB with a projected separation of 7.3 parsec in the radio galaxy 0402+379, which is one of the SMBHB candidates with the smallest orbital separation found to date. However, with a physical resolution power between  $\sim 1-10$  parsecs, VLBI cannot detect SMBHBs with much closer separations (which go down to  $\sim 10^{-4}$  parsec, at which point the binary is predicted to emit GWs detectable by PTAs). Radio observations can also be used to find rotationally symmetric helical S-shaped radio structures, which could be the result of periodic perturbations in the structure of the relativistic jet of one of the SMBHs in a binary system, although such features could also be attributed to a tilted accretion disk in a single AGN (see, e.g., Begelman, Blandford, and Rees, 1980; Lobanov and Roland, 2005; Deane et al., 2014).

At sub-parsec separation scale, SMBHB candidates can be identified through offsets and velocity shifts in their broad emission lines. As explained in Section 1.2.2, the BLR of a SMBH is a region made of dense clouds orbiting the SMBH at a distance of  $\sim 0.01-1$  parsec. Just like double-peaked narrow emission lines originating from two NLRs can help to identify dual AGNs, if a SMBHB (whose two black holes are active) has two distinct BLRs, the binary system can be detectable with double-peaked broad emission lines, or with a velocity shift of the broad emission line (see, e.g., Eracleous and Halpern, 1994; Popović, 2012). For this signature to be observable, the binary separation must not be too small (in which case the BLRs become truncated and eventually merge; see, e.g., Roedig, Krolik, and Miller, 2014; Krolik et al., 2019) or too far (in which case the velocity difference between the two BLRs becomes imperceptible; see, e.g., Shen and Loeb, 2010; Eracleous et al., 2012). However, double-peaked broad emission lines could also originate from complex kinematics due to AGN inflows and outflows or star formation activity, and broad emission line velocity shift could be mimicked by quasar variability (e.g., Eracleous et al., 1997). Therefore, such signatures are not straightforwardly associated with the presence of a SMBHB.

SMBHB candidates with sub-parsec separation scale can also be identified through time-domain searches for periodic variability in AGN lightcurves. Numerical simulations have demonstrated that AGN photometric variability can be modulated by the presence of a SMBHB (see, e.g., D'Orazio, Haiman, and MacFadyen, 2013; Ragusa, Lodato, and Price, 2016). For example, the accretion of gas can periodically produce a burst in brightness which can be enhanced by gravitational lensing (see, e.g., Hu et al., 2020). It is also possible for the luminosity of SMBHBs to be Doppler boosted, through which the most massive SMBH is observed to move towards and away from the line of sight periodically due to being in a binary system (see, e.g., Graham et al., 2015). However, such signatures would only be observable if the SMBHB is actively accreting and the nucleus is not dust-obscured, which may be a minority of cases (Koss et al., 2018; Izquierdo-Villalba, Sesana, and Colpi, 2023; Dong-Páez et al., 2023; Truant et al., 2025).

#### **Gravitational Wave Signatures**

At the smallest binary separations ( $\lesssim 10^{-3}$  parsec scale), SMBHBs are expected to produce GWs in the nHz band, whose signal differ largely from the GWs emitted by stellar-mass black hole mergers. The detection of GWs constitute one of the most compelling proofs for the observation of black holes (cf. the detection of the first GWs from a stellar-mass black hole merger, Section 1.1). Notably, the GW signal from SMBHBs is significantly different from that of stellar-mass black holes. While stellar-mass black hole mergers emit a 'chirp' of GWs that is observable by GW observatories on Earth for typically less than a second and which has a frequency ranging from  $\sim$ a few Hz to  $\sim$ hundreds of Hz, SMBHBs emit continuous nHz GWs which last for millions of years prior to their merger. This is because stellar-mass black holes are much less massive and thus emit detectable GWs when they are much closer to each other. As a result of their close separation, their orbital frequency is also much higher, and so is their GW frequency (where the GW frequency is equal to twice the orbital frequency for circular orbits). For example, the GW chirp of GW150914 lasted  $\sim$ 0.2 s and emitted peak-amplitude GWs when its separation was an estimated  $\sim$ 350 km (Abbott et al., 2017). On the other hand, SMBHBs emit GWs detectable by PTAs when they close in at  $\lesssim 10^{-3}$  parsec, which corresponds to an orbital period of  $\sim$ tens of years for masses of  $\sim 10^9 M_{\odot}$ . However, SMBHBs can take up to millions of years to merge after starting to emit detectable GWs, which makes their GW signal a continuous 'siren' (see, e.g. Burke-Spolaor et al., 2019). Therefore, if the local Universe is populated with SMBHBs, they are continuously emitting nHz GWs which are traveling through our Galaxy and will continue to do so virtually indefinitely during our observing time scale, although no individual SMBHB has been found in GWs as of yet.

Pulsar timing array (PTA) experiments are designed to measure the GWs emitted by SMBHBs in the local Universe by timing the arrival of light from pulsars in our Galaxy. Pulsars are highly magnetized neutron stars emitting strong electromagnetic radiation out of their magnetic poles which is passing through Earth. Because the arrival of their signal is periodic (and with a typical period of ~milliseconds) and very regular, pulsars appear as 'cosmic lighthouses', or reliable cosmic clocks.

However, if GWs originating from outside our Galaxy come to disturb the travel of pulsar light by distorting the space-time fabric between the pulsar and Earth, the signal will be offset from its regular period. Pulsar timing arrays (PTAs) are radio telescopes monitoring pulsar light arrival, and as such they are sensitive to the GW signature from SMBHBs in the local Universe (see, e.g., Burke-Spolaor et al., 2019). Such an effect is better identified when pulsars are timed on the timescale of the period of the GW, which in the case of nHz GWs, is between  $\sim$ a few years to  $\sim$ tens of years, depending on the specific GW frequency, which depends on the SMBH separation.

Numerous PTA experiments have recently reported a tentative detection of the stochastic gravitational wave background (SGWB), which is hypothesized to be produced by the ensemble of SMBHBs in the local Universe. Ongoing PTA experiments (e.g., the Parkes PTA (PPTA; Hobbs, 2013), the European PTA (EPTA; Kramer and Champion, 2013) and the North American Nanohertz Observatory for Gravitational Waves (NANOGrav; Agazie et al., 2023b)), have been in operation and taking data for a few years already (~20 years, 16 years and 20 years, respectively). In June 2023, multiple PTA experiments reported a tentative detection of the stochastic GW background (SGWB; see, e.g., EPTA Collaboration et al., 2023; Agazie et al., 2023a; Xu et al., 2023; Reardon et al., 2023). The SGWB is hypothesized to arise from the interference of all the individual nHz GWs emitted by all the SMBHBs in the local Universe, although there are alternative cosmological origins which could contribute to it (such as inflation and cosmic strings; see, e.g., Vilenkin, 1985; Chiara Guzzetti et al., 2016).

The next step for PTAs will be to identify the location in the sky of the source that contributes the most to the SGWB, which will be paramount to addressing many key science questions, in particular regarding the evolution of SMBHs with their host galaxies. Since the preliminary detection of the SGWB, PTA experiments aim to localize the strongest nHz GW source in the sky. When its host galaxy is found, numerous follow-up electromagnetic observations will investigate the environment of the SMBHB, which will be paramount to addressing many key science questions. For example, combining GWs and the electromagnetic information originating from the binary environment and its host galaxy will constrain binary orbit parameters,

such as the total mass and separation of the binary system (Arzoumanian et al., 2014; Shannon et al., 2015; Lentati et al., 2015; Liu and Vigeland, 2021). These multimessenger observations will also constrain the interactions that take place in the galaxy nucleus, such as core scouring through three-body interactions with nearby stars (cf. Section 1.2.2; Rajagopal and Romani, 1995; Jaffe and Backer, 2003; Wyithe and Loeb, 2003; Enoki et al., 2004; Sesana et al., 2004). Furthermore, if the information from the GW signal can constrain the distance to the source, follow-up electromagnetic observations can determine the redshift of the source to constrain the Hubble constant, in which case SMBHBs act as standard sirens (Schutz, 1986; Holz and Hughes, 2005). These science goals will only be realized if the exact host galaxy of the SMBHB detected in GWs can be identified (Bogdanović, Miller, and Blecha, 2022).

At present, there are no reliable methods to identify the host galaxy of a GW source detected with PTAs. The expected GW sky localization region of the individual SMBHBs detected by PTAs is expected to be of order  $10^2 - 10^3$  deg<sup>2</sup> (Sesana and Vecchio, 2010; Goldstein et al., 2018; Truant et al., 2025). While the mass and distance of SMBHBs detected in continuous GWs are degenerate, they can be determined individually if the gravitational radiation produces a frequency drift, which occurs when the frequency of the GW changes over time (e.g., if the separation between the two SMBHs changes due to an eccentric orbit; Sesana and Vecchio, 2010). These constraints can be used to make galaxy stellar mass and redshift cuts on the galaxies in the PTA localization region based on empirical galaxy scaling relations. However, the total number of candidate host galaxies even after these selection cuts is still expected to be of order  $\sim 10^2$  (Goldstein et al., 2019; Petrov et al., 2024; Truant et al., 2025). A complementary method would be to look for the modulation of a SMBHB in AGN photometric variability (as explained earlier in 'Electromagnetic Signatures of SMBHBs'), but only a handful of SMBHB systems are expected to exhibit such features (and only a fraction of them would be detectable, e.g. if they are not dust-obscured), which motivates the use of additional approaches.

# 1.4 A Novel Approach Towards Identifying the Host Galaxies of SMBHBs

The development of cosmological simulations in the last few years have enabled indepth studies of the evolution of galaxies and SMBHs. Cosmological simulations encode known physical interactions over an ensemble of particles (which can be modeled as, e.g., gas, dark matter, stars, or SMBH seeds) which evolve through cosmic time. The resulting physical structures and their properties can be analyzed to 1) compare them to observations and 2) gain insight on physical phenomena and dynamics that cannot be assessed observationally. Every cosmological simulation studies different cosmological volumes at different resolutions with different encoded components and interactions, all depending on the specific astrophysical and cosmological interests targeted (see, e.g., the Illustris or the Feedback In Realistic Environments (FIRE) cosmological simulations; Vogelsberger et al., 2014; Hopkins et al., 2014).

Specifically, the ROMULUS25 cosmological simulation has been used for the study of SMBHs and their evolution with their host galaxies. ROMULUS25 is a  $25 \times 10^6$  parsec per side volume simulation which includes gas, star, dark matter and SMBH particles that evolve from initial conditions set in the early Universe until present day (redshift z=0; Tremmel et al., 2017). Notably, ROMULUS25 is a simulation large enough to conduct a statistical study of the host galaxies of SMBHBs (i.e., which contains enough galaxies), and its sub-grid model enables sophisticated SMBH evolution physics such as dynamical friction, which is an important mechanism that leads to the formation of dual AGNs and SMBHBs (cf. Section 1.2.2). As such, cosmological simulations like ROMULUS25 are well-suited for the study of the evolution of SMBHs.

Some studies have notably characterized the population of PTA-detectable SMBHB host galaxies in cosmological simulations, but these results are influenced by galaxy scaling relations. By comparing the properties of the host galaxies of all SMBHBs in the Illustris cosmological simulations to the host galaxies of PTA-detectable SMB-HBs, Cella, Taylor, and Kelley (2024) found that PTAs are sensitive to SMBHBs in

galaxies that are more massive, redder in color, more metal-rich and less star forming. Saeedzadeh et al. (2024) used the ROMULUS25 cosmological simulations to compare the properties of SMBHB hosts to the overall population of galaxies in the simulation, and found similar results. However, PTAs are only sensitive to the most massive SMBHBs ( $M_{\rm BH} \gtrsim 10^8 M_{\odot}$ ; Sesana, Vecchio, and Volonteri, 2009; Ellis et al., 2023). These naturally correspond to more massive, metal-rich, redder, and less starforming galaxies, due to empirical galaxy scaling relations such as the stellar massblack hole mass relation ( $M_* - M_{\rm BH}$ ; Häring and Rix, 2004; Torbaniuk et al., 2024), the stellar mass-metallicity relation ( $M_* - Z$ ; Tremonti et al., 2004; Ma et al., 2016), the stellar mass-color relationship ( $M_*$  –color; Law-Smith and Eisenstein, 2017), and the stellar mass-specific star formation rate relation ( $M_*$ -sSFR; Brinchmann et al., 2004; Bauer et al., 2013). Thus, these properties may not be distinct to SMBHB host galaxies, but instead reflect the sensitivity of PTAs to nHz GWs, which arise from massive SMBHBs in massive galaxies. As a result, characterizing the distinct properties of galaxies that host PTA-detectable SMBHBs beyond their difference in mass relative to the broader galaxy population will require a comparison with a massmatched control galaxy sample.

Recently, Bardati et al. (2024a, hereafter B24A) and Bardati et al. (2024b, hereafter B24B) used the ROMULUS25 cosmological simulations of galaxy formation to find that galaxies hosting SMBH mergers and binaries have distinctive morphological and stellar kinematic properties, in comparison to a mass- and redshift-matched control galaxy sample. Their results suggest that the host galaxies of closely separated (\$\times\$100 pc) SMBH pairs, bound SMBHBs, and recent SMBH mergers tend to have bulge-dominated morphologies in imaging, and have slower rotation with stronger kinematic/photometric misaligned stellar kinematics in integral field spectroscopy. Critically, because their control sample is mass- and redshift-matched to their SMBH merger and binary sample, these characteristics are distinct to SMBHB host galaxies, and do not simply arise from galaxy scaling relations. As such, these results can be used to search for candidate galaxies hosting SMBHBs using archival galaxy datasets, even before PTA detections, effectively making a prediction of which nearby galaxies are likely to host future PTA sources of continuous GWs.

Other investigations have aimed to predict the host galaxies of individual SMB-HBs that will be detected by PTAs among local galaxies by computing the GW strain of hypothetical SMBHBs. Simon et al. (2014) and Schutz and Ma (2016) computed the GW strain  $h_0$  (which is a measure of the amplitude of a GW signal) of hypothetical SMBHBs in local galaxies by using the distance and SMBH mass of each galaxy. However, those studies do not incorporate any information on the potential presence of a SMBHB in each galaxy, which is needed to make a more informed prediction.

The following chapters of this thesis cover the work conducted in Horlaville et al. (2025), which led to predicting potential host galaxies of the first SMBHBs that will be detected in GWs by PTAs, by searching archival galaxy datasets for the distinct signatures of SMBH merger and binary host galaxies identified by B24A and B24B. Since most local massive galaxies have already been observed by imaging and integral field spectroscopy surveys, their morphological and stellar kinematic parameters are already available in the literature. We use this information to predict which galaxies among them are the most likely to host SMBHB systems. We also calculate the GW strain  $h_0$  of their hypothetical SMBHBs, to identify the potentially strongest individual sources of GWs. Finally, we present a ranked list of galaxies within our sample that both possess the signatures of SMBHB host galaxies and whose hypothetical SMBHBs have the strongest GW strain. These top-ranking galaxies are thus the most likely to be the host galaxy counterpart to individual sources of continuous GWs that will be detected by PTAs in the near future.

# **Chapter 2**

# Identifying SMBHB Host Galaxy Signature and Relevant Datasets

## 2.1 Deriving the Kinematic LDA

To identify the distinct morphological and stellar kinematic properties of SMBHB host galaxies in the ROMULUS25 cosmological simulations, B24A and B24B constructed a sample of SMBH merger and binary host galaxies, as well as a massand redshift-matched control sample. In ROMULUS25, SMBHs numerically merge in the simulation at a separation of  $\sim$ 700 pc. However, at this stage, the two SMBHs have yet to form a bound binary system. Further loss of angular momentum that hardens the binary separation down to  $\sim 10^{-3}$  parsec (milliparsec) scales, and the eventual physical merger of the SMBHB, are below the resolution limit of the simulation. The time delay between numerical and physical merger is poorly-constrained, and estimates vary widely between 0.1 to 10 Gyr (e.g., Volonteri et al., 2020; Li et al., 2022). B24A identified 201 SMBH numerical merger events within the simulation, and tracked their host galaxies up to 1 Gyr after their numerical merger in order to construct a galaxy sample representative of SMBH merger and binary host galaxies. Due to their ignorance of the exact time of the physical SMBHB merger, this sample includes galaxies hosting SMBHBs at separations from <700 pc to galaxies hosting SMBHBs that have merged in the past <1 Gyr. They also built a control galaxy sample, by selecting galaxies in ROMULUS25 whose mass and redshift distributions matched those of the SMBH merger and binary host galaxy sample.

After measuring the morphological and stellar kinematic parameters of both

their SMBH merger and binary sample as well as their control sample galaxies, B24A and B24B trained a linear discriminant analysis (LDA) predictor to identify the distinct signatures of SMBH merger and binary host galaxies. They first performed stellar population synthesis and radiative transfer simulations to produce synthetic images and stellar kinematic maps of their simulated galaxies, from which they extracted morphological and stellar kinematic parameters. They then trained an LDA predictor, which identifies the linear combination of parameters that optimally distinguishes the SMBH merger and binary host galaxy sample from the control sample. The resultant LDA predictor assigns a score to each galaxy based on their morphological or stellar kinematic parameters, where high (positive) LDA scoring galaxies are predicted to be more likely to host a SMBH merger or binary.

The findings of B24A and B24B suggest that SMBH merger and binary host galaxies have distinct morphological and stellar kinematic properties in comparison to a mass- and redshift-matched control sample. Specifically, B24A found that SMBH merger and binary host galaxies are characterized by a more prominent classical bulge in their morphology as probed by imaging, while B24B found that they are characterized by slower rotation and stronger kinematic/photometric misalignments through their stellar kinematics as probed by integral field unit (IFU) spectroscopy. These distinctions are strongest for SMBH merger and binary host galaxies with high chirp mass ( $M_{chirp} > 10^{8.2} M_{\odot}$ ) and high mass ratio ( $q \equiv M_2/M_1 > 0.5$ , with  $M_1 > M_2$ ), where the chirp mass of a SMBHB system composed of  $M_1$  and  $M_2$ is defined as  $M_{chirp} \equiv \frac{(M_1 M_2)^{3/5}}{(M_1 + M_2)^{1/5}}$ , or, equivalently,  $M_{chirp} = \left[\frac{q}{(1+q)^2}\right]^{3/5} (M_1 + M_2)$ . Those results are consistent with the standard picture of hierarchical galaxy formation, in which major mergers of massive galaxies produce SMBHBs, which result in galaxies with more bulge-dominant morphologies, slower rotation, and more complex stellar kinematics (e.g., Bois et al., 2011; Naab et al., 2014). B24A used morphological parameters to derive the LDA predictor:

$$LDA = 1.23Gini + 0.51M_{20} + 0.52C - 1.04S - 0.01,$$
 (2.1)

where the Gini coefficient is a measure of how evenly the galaxy flux is distributed, the  $M_{20}$  parameter describes the concentration of light in a galaxy, C (concentration) measures the concentration of light in a galaxy relative to its center, and S (smoothness) is a measure of the fraction of light found in clumpy distributions (Lotz, Primack, and Madau, 2004; Pawlik et al., 2016). The LDA predictor from Equation 2.1 distinguishes the SMBH merger and binary host galaxies from the mass- and redshift-matched control group with a mean accuracy of 82.6  $\pm$  3.3%. B24B then used stellar kinematic parameters to derive the LDA predictor:

$$LDA = 0.51 \log \Delta PA - 2.81 \lambda_{R_e} + 0.04, \tag{2.2}$$

where  $\Delta PA$  is the difference between the photometric position angle as measured in the galaxy image and the kinematic position angle as measured in the galaxy stellar kinematic map, and  $\lambda_{R_e}$  is the spin angular momentum of the galaxy measured at one effective radius  $R_e$ , where the effective radius of a galaxy is the radius of a galaxy which encloses half of its total emitted light (Emsellem et al., 2007). The LDA predictor from Equation 2.2 distinguishes the SMBH merger and binary host galaxies from the mass- and redshift-matched control group with a mean accuracy of  $85.7 \pm 4.5\%$ . Because the LDA equation was constructed by first normalizing the parameters, the absolute value of the coefficients are indicative of each parameter's importance towards the LDA classification. For example, the most important parameter in Equation 2.2 is the  $\lambda_{R_e}$  parameter. Note that this result is coherent with galaxy evolution paradigms through which galaxy mergers, which are conducive to the formation of SMBHBs, also lower the spin angular momentum of the newly formed galaxy.

# 2.2 Comparing Stellar Kinematic Signatures to Morphological Signatures

We identify the optimal combination of parameters to search for PTA-detectable SMBHB host galaxies, which will determine which archival datasets we need for

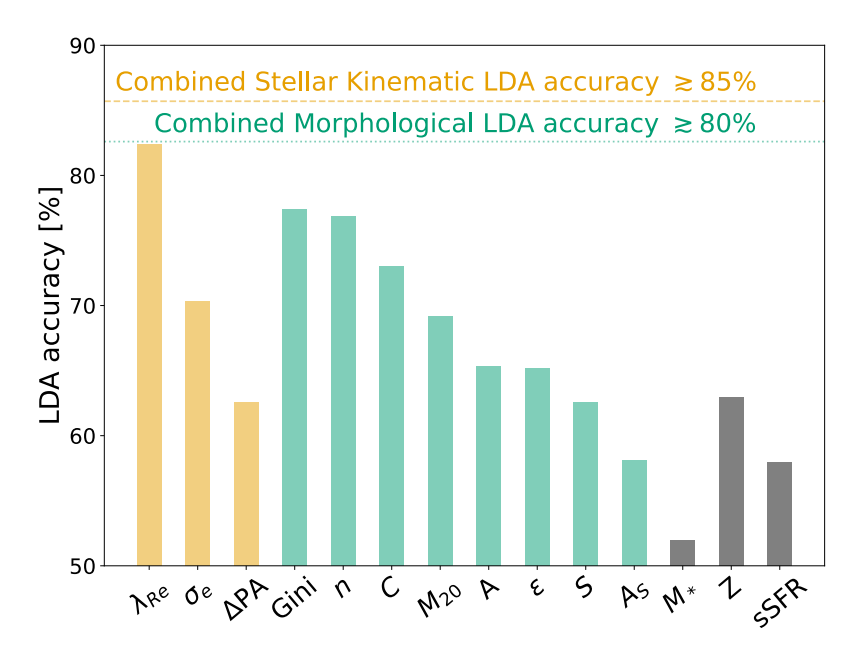


FIGURE 2.1: Accuracy of the LDA predictor when trained with individual parameters. The stellar kinematic parameters are indicated with the yellow vertical bars, while the morphological parameters are indicated with the green vertical bars. The dotted green and dashed yellow horizontal lines indicate the accuracies of the full LDA predictors corresponding to Equations 2.1 and 2.2, respectively. Additional parameters not listed in Section 2.1 are the ellipticity  $\varepsilon$ , the Sérsic index n, and the shape asymmetry  $A_S$  (Pawlik et al., 2016). We also show the LDA classification accuracy using the stellar mass  $M_*$ , the stellar metallicity Z, and the specific star formation rate sSFR with the gray vertical bars, which are between  $\sim$ 65% and  $\sim$ 50%.

our search. In Figure 2.1, we show the accuracy of the LDA predictor, which we train using one parameter at a time while ignoring the others. For the stellar kinematic parameters (yellow bars), the spin angular momentum ( $\lambda_{R_e}$ ) and the stellar velocity dispersion ( $\sigma_e$ ) measured at the effective radius ( $R_e$ ) are the two parameters whose LDA equations are the most accurate at discriminating the SMBH merger and binary host galaxies from the control group. However, when training the LDA using both parameters, the accuracy remains the same as using  $\lambda_{R_e}$  alone, because the discriminatory information contained in  $\sigma_e$  is degenerate with that from  $\lambda_{R_e}$ . In contrast, even though  $\log \Delta PA$  individually has an accuracy of only  $\gtrsim$ 60%, it contains discriminatory information that is not degenerate with  $\lambda_{R_e}$ , which causes the accuracy of the LDA trained over both  $\lambda_{R_e}$  and  $\log \Delta PA$  to be higher than  $\lambda_{R_e}$  alone. This is why the optimal stellar kinematic equation of the LDA as derived by B24B (Equation 2.2) contains  $\lambda_{R_e}$  and  $\log \Delta PA$ , but not  $\sigma_e$ .

Among all morphological (green bars) and stellar kinematic (yellow bars) parameters shown in Figure 2.1 and present in Equations 2.1 and 2.2, we find that the set of stellar kinematic parameters is the optimal discriminant, motivating the use of archival galaxy IFU surveys. While B24A and B24B separately identified each set of parameters that best classified SMBH merger and binary host galaxies, it is possible that combining both sets of parameters increases the accuracy of the LDA equation. To test this, we train the LDA over the ensemble of both the morphological and stellar kinematic parameters. We use the same approach as B24A and B24B by performing forward stepwise selection to optimally reduce the number of parameters in the LDA equation, through which parameters are added one by one to the LDA. At each step, the corresponding LDA equation is computed to determine whether adding the parameter increases the LDA accuracy or not. This process is repeated until the LDA accuracy decreases. We find that all the morphological parameters as analyzed by B24A are degenerate with either  $\lambda_{R_e}$  or log  $\Delta$ PA, such that the optimal LDA equation that maximizes the classification accuracy and minimizes the number of parameters is the set of stellar kinematic parameters as derived by B24B, and described in Equation 2.2. As such, we will mine through archival galaxy IFU surveys to conduct our search of PTA-detectable SMBHB host galaxies.

## 2.3 Archival Galaxy IFU Datasets

#### 2.3.1 Sample Selection

We conduct our search for SMBHB host galaxies using archival IFU data from the MASSIVE (Ma et al., 2014), ATLAS<sup>3D</sup> (Cappellari et al., 2011), and CALIFA (Sánchez et al., 2012) galaxy surveys. Since PTAs are sensitive to GWs originating from nearly the full sky, we specifically choose these three IFU surveys because they cover a wide sky footprint. Furthermore, these three surveys are also approximately volumelimited, which mitigates the Malmquist bias that would preferentially select increasingly massive galaxies with increasing distance (Malmquist, 1922; Sandage, 2000). By doing so, we explore all the galaxies in the northern sky within a distance D <108 Mpc and with a stellar mass  $M_* \gtrsim 3 \times 10^{11} M_{\odot}$  for MASSIVE (Ma et al., 2014), and D < 42 Mpc,  $M_* \gtrsim 6 \times 10^9 M_{\odot}$  for ATLAS<sup>3D</sup> (Cappellari et al., 2011). Although the CALIFA survey is not strictly volume-limited, it has been shown to be > 95% complete for galaxies with stellar mass  $5 \times 10^9 M_{\odot} \lesssim M_* \lesssim 2.5 \times 10^{11} M_{\odot}$  and distance 22 Mpc < D < 128 Mpc (Sánchez et al., 2012; Walcher et al., 2014), so we limit our study to this range. In total, the main MASSIVE, CALIFA, and ATLAS<sup>3D</sup> surveys contain 116, 667, and 260 galaxies, respectively. A few galaxies overlap between multiple surveys, and we address how we take this into account in our analysis in Section 4.5. We also note that the redshift ranges of these IFU surveys are different than the redshift range of simulated galaxies used to derive the stellar kinematic signatures of SMBH merger and binary host galaxies, and we discuss why this does not impact our results in Section 4.6. With this selection of galaxies, we cover most of the local massive galaxies in the northern sky that are not in the Galactic plane (see Figure 2.2).

# 2.3.2 Stellar Mass, Metallicity, and Star-Formation Rate as SMBHB Host Galaxy Discriminants

We first demonstrate that the most massive galaxies within our sample naturally correspond to the most metal-rich and least star-forming, as expected from galaxy scaling relations. As such, identifying the distinct signatures of the host galaxies of

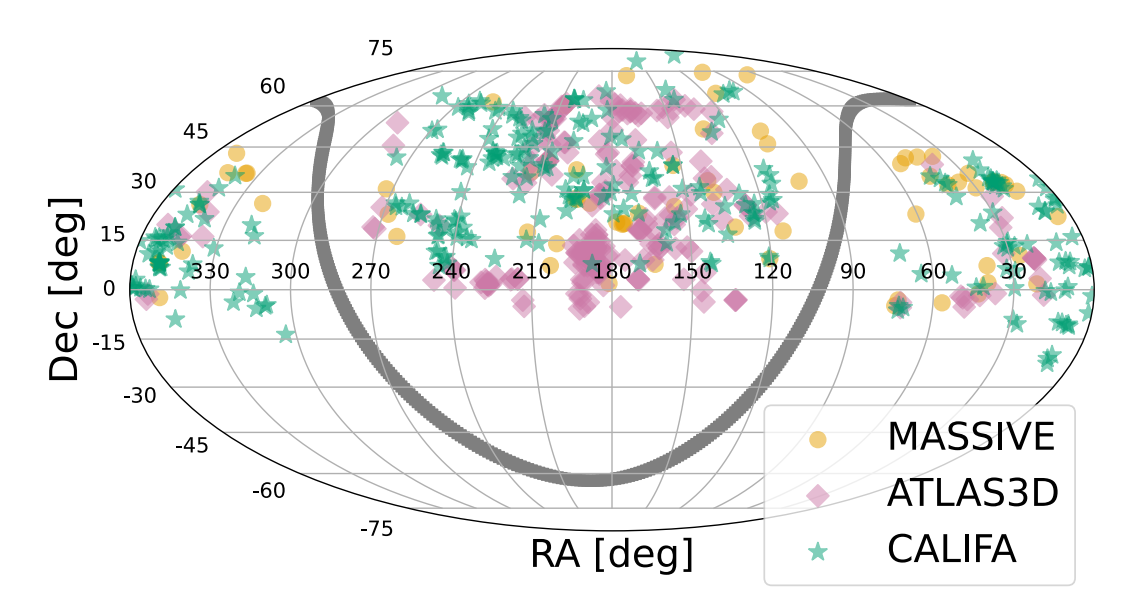


FIGURE 2.2: Sky map of the location of the galaxies we use for our search of the potential host galaxies of SMBHBs. The archival galaxy datasets we use (MASSIVE, ATLAS<sup>3D</sup> and CALIFA) cover most of the local massive galaxies in the northern sky. The gray line traces the Galactic plane.

SMBHBs detectable by PTAs requires a comparison to a mass-matched control sample of galaxies. Previous studies have asserted from cosmological simulations that PTA-detectable SMBHBs live in galaxies that are more massive, redder in color, more metal rich and less star-forming than the overall population of galaxies or the overall population of SMBHB host galaxies (Cella, Taylor, and Kelley, 2024; Saeedzadeh et al., 2024). However, because PTAs are more sensitive to the most massive SMBHBs, we expect their host galaxies to be more massive, which should naturally correlate with higher metallicity and lower star formation rate through galaxy scaling relations. In Figure 2.3, we show the  $M_* - Z$  and  $M_* - sSFR$  relations for MASSIVE (Davis et al., 2016; Greene et al., 2019), ATLAS<sup>3D</sup> (Davis et al., 2014; McDermid et al., 2015), and CALIFA galaxies (Sánchez et al., 2017; Catalán-Torrecilla et al., 2015) for which metallicity and star formation rates have been derived (for a total of 14, 88 and 291 galaxies from MASSIVE, ATLAS<sup>3D</sup> and CALIFA, respectively). We note that the wide range of star formation among the CALIFA galaxies is due to the CALIFA survey probing a different volume in mass and distance than MASSIVE and ATLAS<sup>3D</sup>, thus resulting in galaxies of different morphologies, while ATLAS<sup>3D</sup> and MASSIVE mostly contain E and S0 galaxies, which are usually less star-forming (González Delgado et al., 2015). As expected from global mass-scaling relations ( $M_* - Z$ ; Tremonti

et al. 2004; Ma et al. 2016, and  $M_*$ –sSFR; Brinchmann et al. 2004; Bauer et al. 2013), Figure 2.3 reveals a correlation between galaxy stellar mass and metallicity, and an anti-correlation between galaxy stellar mass and specific star formation rate. These correlations are consistent with the paradigm that more massive galaxies tend to have older stellar populations, which through time have enriched the interstellar medium with metals, resulting in higher stellar metallicity, and have exhausted the available gas required to form stars, resulting in lower specific star formation rate (e.g., Kennicutt, 1998; Madau and Dickinson, 2014). Since PTA-detectable SMBHBs are the most massive SMBHBs (with  $M_{\rm BH} \gtrsim 10^8 M_{\odot}$ ; Sesana, Vecchio, and Volonteri, 2009; Ellis et al., 2023), they reside in galaxies with high stellar mass. These galaxies are thus naturally more metal-rich and less star-forming compared to the overall population of SMBHB host galaxies or to the overall population of galaxies. These correlations reflect galaxy scaling relations, rather than truly distinctive properties of SMBHB host galaxies.

Using the ROMULUS25 simulations, we find that the stellar metallicity and sSFR are not reliable discriminants to identify SMBH merger and binary host galaxies from a mass- and redshift-matched control sample. To assess if Z and sSFR can be used as discriminants of SMBHB host galaxies, we train the LDA equation using Z and sSFR to distinguish the SMBH merger and binary host galaxy sample from the mass- and redshift-matched control galaxy sample in ROMULUS25. First, we extract the stellar metallicity and star-formation rate values for each galaxy in our samples from the ROMULUS25 simulation stellar particle data. We then train the LDA using the metallicity and sSFR parameters individually. We find that the resulting accuracy of the LDA classification is low ( $\lesssim$  65%), as shown in Figure 2.1. We also find that combining both Z and sSFR into the LDA equation does not increase its accuracy. This confirms that PTA-detectable SMBHB host galaxies do not have distinctivelyhigh metallicities and low star formation rates. Rather, they are simply more massive than the overall population of galaxies and SMBHB host galaxies. In contrast, our stellar kinematic LDA predictor in Equation 2.2 is not affected by galaxy scaling relations, and reflects truly distinctive properties of SMBHB host galaxies. Hence, we compute the LDA score using Equation 2.2 for galaxies in our archival IFU surveys to identify galaxies most likely to host a SMBHB.

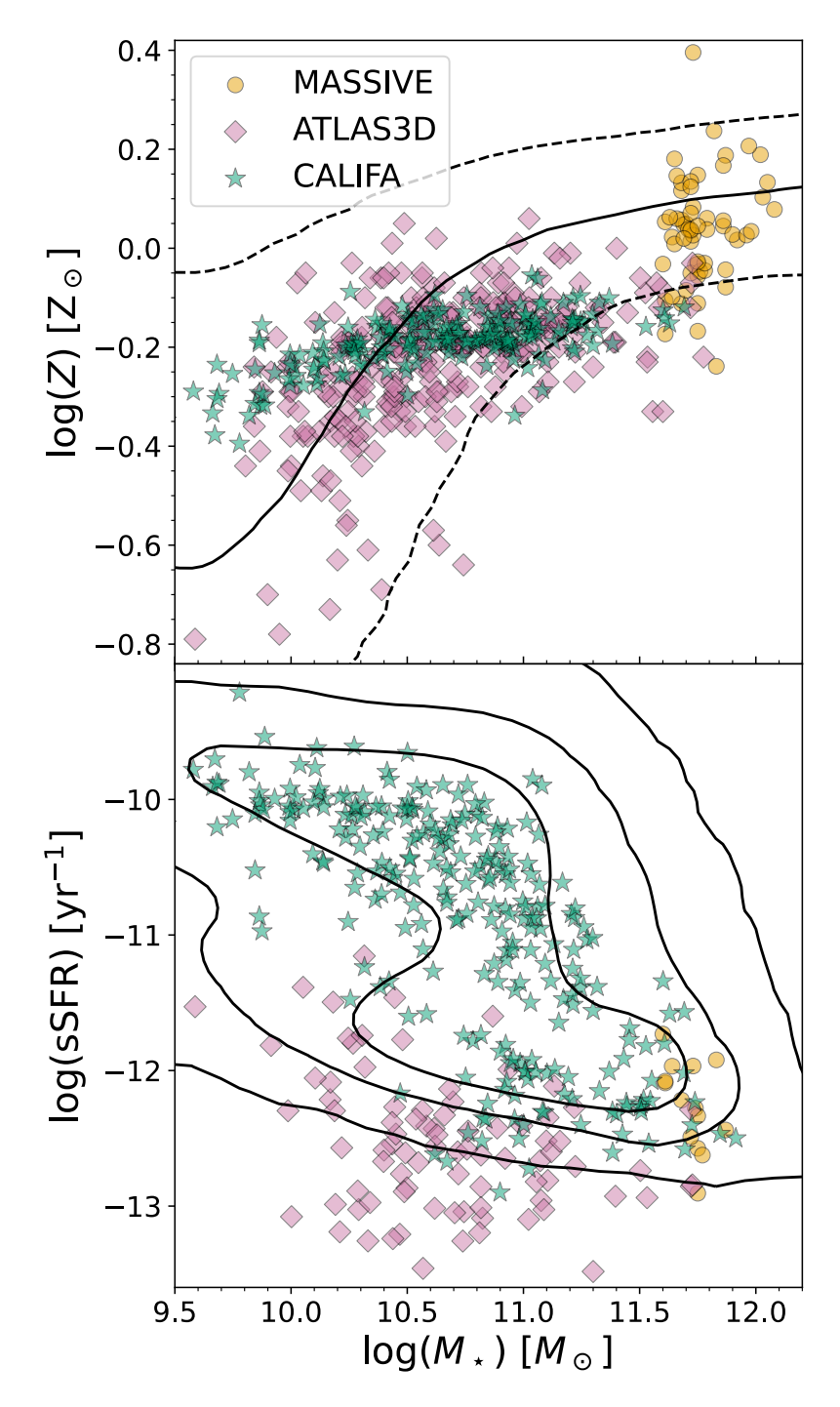


FIGURE 2.3: Galaxies within our sample obey well-known global scaling relations. Top panel: stellar mass-metallicity relation  $(M_*-Z)$  for the MASSIVE, ATLAS³D, and CALIFA galaxies for which  $\lambda_{R_e}$  and  $\Delta$ PA are available. The solid black line represents the empirical  $M_*-Z$  relation from SDSS galaxies from Gallazzi et al. (2005), with the dashed lines representing the  $\pm 1\sigma$  interval. Bottom panel: stellar mass-sSFR relation  $(M_*-sSFR)$  for all ATLAS³D, MASSIVE and CALIFA galaxies in the top panel for which SFR has also been derived. The contour lines enclose 68%, 95%, 99% of galaxies from the JHU-MPA SDSS galaxy catalog (Brinchmann et al., 2004).

# Chapter 3

# Characterizing SMBHB Host Galaxy Candidates with Stellar Kinematics and GWs

# 3.1 Identifying SMBHB Host Galaxy Candidates in Archival IFU Surveys

#### 3.1.1 Retrieval of Stellar Kinematic Parameters

To identify SMBHB host galaxy candidates from their distinct stellar kinematic properties using Equation 2.2, we first retrieve the stellar kinematic parameters of galaxies from archival datasets. Specifically, we retrieve the  $\lambda_{R_e}$  and  $\Delta$ PA parameters from ATLAS<sup>3D</sup> (Emsellem et al., 2011; Krajnović et al., 2011) and MASSIVE (Veale et al., 2017; Ene et al., 2018), and  $\lambda_{R_e}$  from CALIFA (Falcón-Barroso et al., 2019). A few MASSIVE galaxies have no reported value for  $\Delta$ PA due to not having identifiable kinematic axes (Ene et al., 2018). Furthermore, only a subset of the full CALIFA sample (galaxies with good quality data and non-disturbed morphologies) have reported values for  $\lambda_{R_e}$  (Falcón-Barroso et al., 2017). With these cuts, the stellar kinematic parameters are available for 71, 260 and 291 galaxies from MASSIVE, CALIFA and ATLAS<sup>3D</sup>, respectively.

Although the CALIFA survey does not provide the  $\Delta PA$  parameter for its galaxies, we measure  $\Delta PA$  by computing the morphological position angle  $PA_{morph}$  and

the kinematic position angle  $PA_{kin}$  from the flux and line-of-sight velocity dispersion (LOSVD) maps, respectively, as produced by the CALIFA collaboration (Falcón-Barroso et al., 2017). We retrieve the V1200 (medium resolution) stellar kinematic maps<sup>1</sup>, and run StatMorph (Rodriguez-Gomez et al., 2019) over the flux and noise maps to compute the morphological position angle  $PA_{morph}$ . We also compute the kinematic position angle  $PA_{kin}$  by following the technique by Nevin et al. (2019), and use the bounded Absolute Radon Transform by Stark et al. (2018) on the line-of-sight velocity dispersion (LOSVD) maps. This enables us to compute the  $\Delta PA$  parameter for all 291 CALIFA galaxies in our sample.

#### 3.1.2 Selection of Massive Galaxies

To identify the galaxies in our archival galaxy datasets that are the most likely to host a SMBHB detectable by PTAs, we first select the galaxies whose SMBH mass  $M_{\rm BH}$  are the highest. PTA experiments are only sensitive to the most massive SMBHB systems, so we select galaxies harboring the most massive SMBHs in the MASSIVE, ATLAS<sup>3D</sup> and CALIFA IFU surveys. We estimate the  $M_{\rm BH}$  of each galaxy using the empirical  $M_* - M_{\rm BH}$  relation for early-type galaxies from Sahu, Graham, and Davis (2019), and we justify this choice in Section 4.3.1. The resulting SMBH mass  $M_{\rm BH}$  distribution of our sample of galaxies is shown in Figure 3.1.

We use a fiducial minimum  $M_{\rm BH}=10^{8.4}M_{\odot}$  as the threshold to select the most massive galaxies in our sample. This threshold matches the sensitivity from PTA experiments, and corresponds to a chirp mass  $M_{chirp}\sim 10^8 M_{\odot}$  for a binary with a mass ratio q=1 (i.e., an equal-mass binary). Previously, B24B showed that the LDA predictor from Equation 2.2 has an accuracy of  $\gtrsim$ 85% in discriminating simulated SMBH merger and binary host galaxies from a mass- and redshift-matched control galaxy sample for SMBHs with a chirp mass  $M_{chirp}>10^{8.2}M_{\odot}$ . Notably, they found that this accuracy does not decrease significantly when the minimum chirp mass threshold is lowered from  $10^{8.2}M_{\odot}$  to  $10^8M_{\odot}$ . Thus, we still expect the LDA predictor to reach  $\sim$ 85% accuracy with our adopted minimum SMBH mass

<sup>1</sup>https://califa.caha.es/FTP-PUB/dataproducts/Stellar\_Kinematics\_V1200/

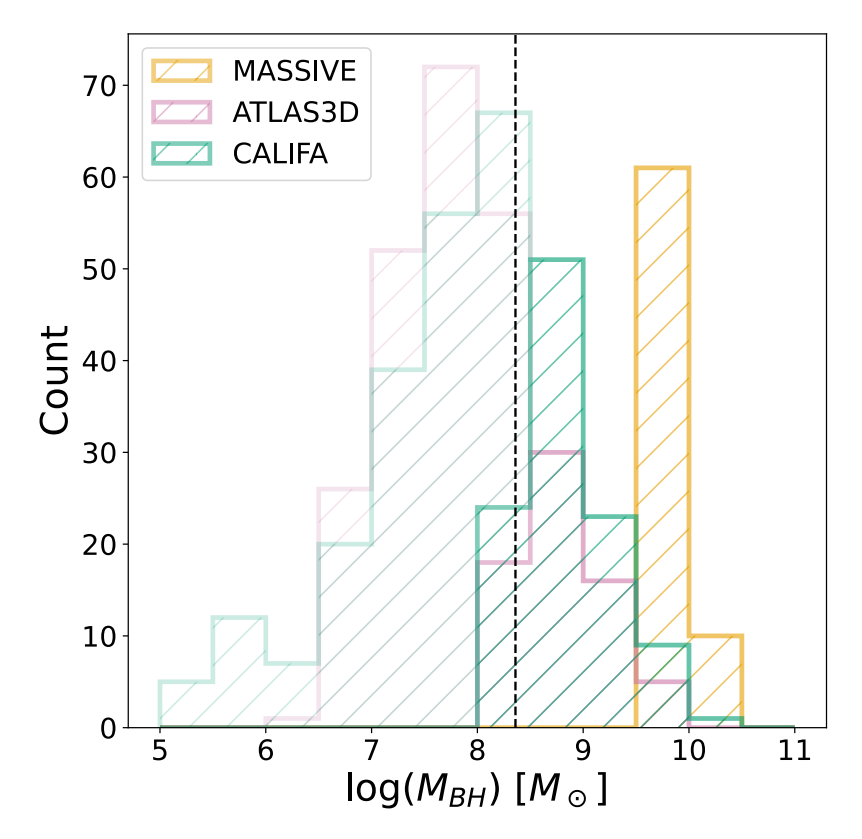


FIGURE 3.1: Distribution of the SMBH mass  $M_{\rm BH}$  of the galaxies in the archival IFU surveys. We search for PTA-detectable SMBHB host galaxies only among galaxies that host the most massive SMBHs ( $M_{\rm BH} \gtrsim 10^{8.4} M_{\odot}$ , corresponding to  $M_{chirp} \gtrsim 10^8 M_{\odot}$ ). This minimum SMBH mass threshold is indicated by a black dashed line. The bins with darker lines correspond to galaxies above this threshold.

Kinematics and GWs

threshold of  $M_{\rm BH}=10^{8.4}M_{\odot}$ , which corresponds to a minimum chirp mass threshold of  $M_{chirp}\sim10^8M_{\odot}$ . Our selection of the most massive galaxies yields 71, 69 and 106 galaxies in MASSIVE, ATLAS<sup>3D</sup> and CALIFA, respectively.

#### 3.1.3 LDA Score and Correlations

with  $\lambda_{R_e}$ ,  $\Delta PA$ ,  $M_*$ , Z, and sSFR

After retrieving the  $\lambda_{R_e}$  and  $\Delta PA$  parameters and selecting the most massive galaxies, we compute the LDA score for each galaxy. We normalize each parameter by subtracting the mean and dividing by the standard deviation of each parameter's distribution, following the method of B24A and B24B, to prevent any one particular parameter from dominating the LDA equation. We then input the normalized parameters in Equation 2.2 to determine the LDA score of each galaxy.

As expected, we find that the LDA score is strongly correlated with  $\lambda_{R_e}$ , and has a weaker correlation with  $\log \Delta PA$ . In the first and second panels from the top of Figure 3.2, we show the correlation between the LDA score and the  $\lambda_{R_e}$  and  $\Delta PA$  parameters for our sample of massive  $(M_{\rm BH} \gtrsim 10^{8.4} M_{\odot})$  galaxies. From the LDA predictor (Equation 2.2), the absolute values of the coefficients of each parameter are indicative of their relative importance. Thus, it makes sense that the strongest correlation occurs with the  $\lambda_{R_e}$  parameter in Figure 3.2, as its coefficient has an absolute value of 2.81, compared to 0.51 for  $\log \Delta PA$ . The sign of the coefficients indicates either an anti-correlation (coefficient < 0) or positive correlation (coefficient > 0). This is why  $\lambda_{R_e}$  (with a coefficient of -2.81) has a strong anti-correlation with the LDA score, while  $\log \Delta PA$  (with a coefficient of +0.51) has a weaker positive correlation with the LDA score. To verify this, we compute Pearson's r (see, e.g., Bravais, 1844; Stigler, 1989) for the LDA  $-\lambda_{R_e}$  and LDA  $-\log \Delta PA$  distributions, and find values of  $\sim -1$  and  $\sim 0.6$ , respectively, which is consistent with our expectations.

We also find that the LDA predictor does not simply select the most massive galaxies, further confirming that the LDA predictor is identifying the true distinctive stellar kinematic signatures of SMBH merger and binary host galaxies. In the third, fourth, and fifth panels from the top of Figure 3.2, we show the correlations between the LDA score from Equation 2.2 and galaxy stellar mass, metallicity, and sSFR, respectively. In contrast to  $\lambda_{R_e}$  and log  $\Delta$ PA, these parameters have little to no

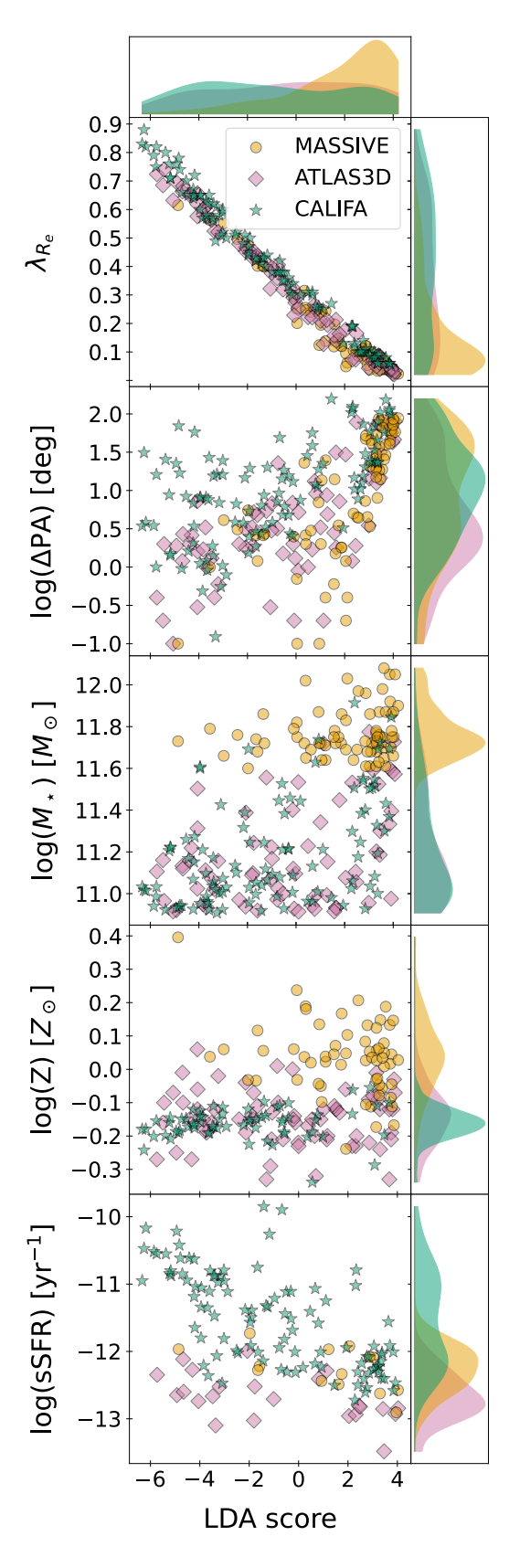


FIGURE 3.2: Correlations between various galaxy properties and the LDA score (from top to bottom:  $\lambda_{R_e}$ ,  $\log \Delta PA$ , stellar mass  $M_*$ , stellar metallicity Z, and specific star formation rate sSFR). Overall, the LDA score has a strong negative correlation with  $\lambda_{R_e}$ , and a weaker positive correlation with  $\log \Delta PA$ , but little to no correlation with stellar mass, Z, and sSFR.

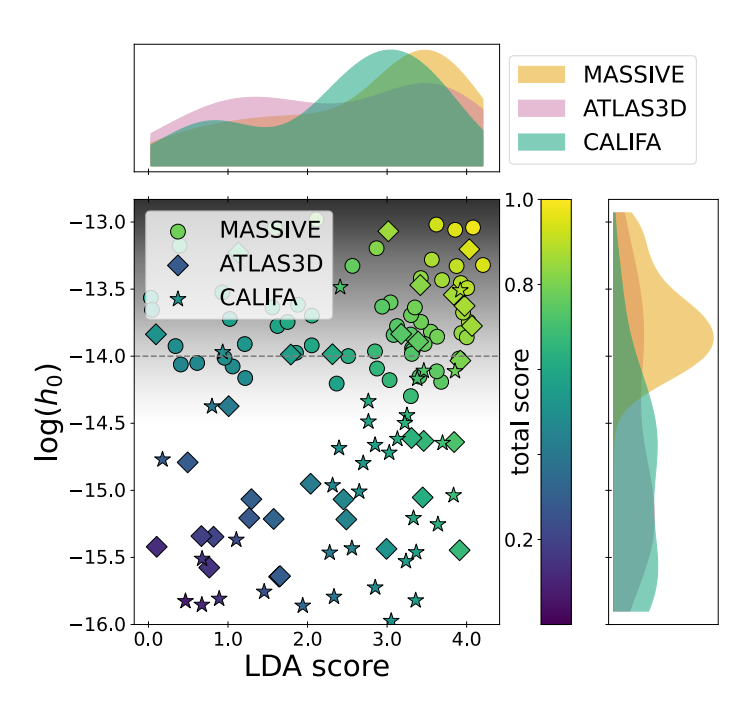


FIGURE 3.3: Distribution of LDA score and GW strain for our galaxies in our sample with an LDA score > 0. The color scale represents the total score of each galaxy (Equation 3.2). The gray dashed line represents the approximate  $h_0$  sensitivity limit from the 15-year NANOGrav dataset near f=10 nHz (Agazie, Antoniadis, and Anumarlapudi, 2024). Since we calculated the GW strain of the hypothetical SMBHBs within our galaxies using a black hole mass based on their stellar mass, an assumed emitted GW frequency of 10 nHz, and an assumed mass ratio of q=1, the dashed line is not a strict but rather an approximate limit, as represented by the gray shaded region around it.

correlation with the LDA score. We compute Pearson's r for each of their correlation with the LDA, and find values of  $\sim$ 0.5,  $\sim$ 0.3 and  $\sim$  -0.3 for log  $M_{\star}$ , log Z and log sSFR, respectively. As such, our results show that the LDA predictor is not simply selecting the most massive, metal-rich and least star-forming galaxies, and instead is likely identifying the true distinctive signature of SMBH merger and binary host galaxies.

## 3.2 Calculating the GW strain of Hypothetical SMBHBs

We calculate the GW strain of the hypothetical SMBHB systems in our galaxies. We use the GW strain equation for an equal-mass binary from Schutz and Ma, 2016:

$$h_0 = 6.9 \times 10^{-15} \left(\frac{M_{\rm BH}}{10^9 M_{\odot}}\right)^{5/3} \left(\frac{10 \text{ Mpc}}{d_L}\right) \left(\frac{f}{10^{-8} \text{Hz}}\right)^{2/3},$$
 (3.1)

where  $h_0$  is the GW strain of the hypothetical SMBHB,  $M_{\rm BH}$  is the total mass of the two black holes  $(M_1 + M_2)$ ,  $d_L$  is the luminosity distance to the host galaxy, and f is the frequency at which the GWs are assumed to be emitted. Since we have no information about the mass ratio of the potential binary systems, we assume equal-mass SMBHBs (i.e., fiducial mass ratio q = 1). Since we also do not know the separation between the two black holes, we further assume that the GWs are emitted at a frequency near the highest sensitivity of PTA experiments, around 10 nHz (Arzoumanian et al., 2020); this corresponds to a separation of  $\sim$ 5 milliparsecs between two black holes of mass  $M_{\rm BH} = 10^{10} M_{\odot}$  (Schutz and Ma, 2016). We discuss the caveats of this hypothetical  $h_0$  in Section 4.3.

We combine the GW strain and the LDA score into a total score for each galaxy, based on (1) how likely the galaxy is to host a hypothetical SMBHB, and (2) the amplitude of the GW strain  $h_0$  computed with Equation 3.1. We normalize both the LDA score and the GW strain  $h_0$  between 0 and 1, and add them in quadrature to compute a total score. We assign equal weights to each score to remain agnostic about the relative importance between these two metrics towards the likelihood of a PTA detection. We normalize the total score between 0 and 1, such that:

$$total\ score = \frac{1}{\sqrt{2}} \sqrt{\widehat{\text{LDA}}^2 + \widehat{\log h_0}^2}, \tag{3.2}$$

where LDA is the normalized LDA score and  $\log h_0$  is the normalized log GW strain score. We compute this total score for each of the massive galaxies in our sample with positive LDA scores. The resulting top ten ranked galaxies are listed in Table 3.1, while all ranked galaxies are listed in Table A.1 in the Appendix. In Figure 3.3, we present our sample of galaxies with a positive LDA score in the LDA  $-h_0$  plane, where the color of each galaxy reflects its total score from Equation 3.2. Galaxies with a high LDA score are predicted to be more likely to host a SMBHB, and galaxies whose SMBHBs have a high GW strain  $h_0$  are more likely to be detected by PTAs. We discuss some caveats on the interpretation of Figure 3.3 in Section 4.3.

TABLE 3.1: The top ten highest-ranking galaxies using the total score from Equation 3.2. Columns include: galaxy name, total score rank, luminosity distance D, IFU survey, log of the black hole mass  $M_{\rm BH}$ , log of the hypothetical GW strain  $h_0$ , LDA score (Equation 2.2), normalized log hypothetical strain  $\widehat{\log h_0}$ , normalized LDA score  $\widehat{\rm LDA}$ , total score (Equation 3.2), and the inner light profile classification from the literature, when available (where 'C'=core, 'P'=power-law, and 'I'=intermediate). The full list is provided in Table A.1 of the Appendix.

Name To	otal Score	e D	Survey log M <sub>BH</sub>	$\log h_0$	LDA	$\widehat{\log h_0}$	<u></u> <u> </u>	Total	Light
	Rank	[Mpc]	$[M_{\odot}]$		Score		Score	Score	Profile
NGC4073	1	91.50	MASSIVE 10.25	-13.04	4.08	0.98	0.99	0.99	С
NGC1016	2	95.20	MASSIVE 10.25	-13.06	3.86	0.98	0.97	0.97	С
NGC2832	3	105.20	MASSIVE 10.30	-13.02	3.62	0.99	0.94	0.97	С
NGC4486	4	17.20	ATLAS3D 9.72	-13.20	4.03	0.93	0.98	0.96	С
NGC1060	5	67.40	MASSIVE 10.00	-13.32	4.21	0.90	1.00	0.95	_
NGC0533	6	77.90	MASSIVE 10.03	-13.33	3.87	0.90	0.97	0.93	_
NGC4472	7	17.10	ATLAS3D 9.80	-13.07	3.02	0.97	0.89	0.93	C
NGC4874	8	102.00	MASSIVE 10.13	-13.28	3.56	0.91	0.94	0.92	C
NGC0410	9	71.30	MASSIVE 9.94	-13.45	3.93	0.86	0.97	0.92	_
NGC7265	10	82.80	MASSIVE 9.95	-13.49	4.01	0.85	0.98	0.92	

# Chapter 4

# Applications & Caveats of SMBHB Host Galaxy Identification

## 4.1 Interpretations of the Ranked List of Galaxies

In our ranked list of galaxies, high-LDA scoring galaxies are the most likely to host SMBHBs, although it is possible that the two SMBHs have either already merged or have yet to form a gravitationally-bound system. As discussed in Chapter 2, galaxies with a high LDA score possess the stellar kinematic signatures of SMBH merger and binary host galaxies, as informed from the ROMULUS25 cosmological simulations. However, the stellar kinematic signatures identified in ROMULUS25 (slow rotation and misaligned kinematic/photometric axes) are for SMBHB that have a broad range of separations, from ≤700 pc (i.e., SMBH pairs) to 0 pc (i.e., recently merged). For observed galaxies in the IFU surveys, the separation of their hypothetical two SMBHs is unknown. Thus, we caution that it is likely that the high-LDA scoring galaxies in our list are contaminated by galaxies harboring SMBHB that have merged in the past Gyr, or have current separations of ≤100 pc and thus have not yet hardened into a binary system. However, this issue of contamination should not hamper the use of our ranked list of galaxies for targeted continuous GW sources for PTA experiments. Furthermore, the presence of these contaminants in our ranked list enables other science goals, such as searches for close dual AGNs and recoiling AGNs. We discuss these different use cases for our ranked list in Section 4.2 below.

We suggest that the host galaxies of gravitationally-unbound SMBH pairs could

be distinguished from nHz GW-emitting SMBHB host galaxies based on their inner galaxy surface brightness profile. If the two SMBHs have hardened to a binary system by scouring the galaxy nucleus through three-body interactions with nearby stars, this would result in an observable surface brightness core in the inner light profile of the galaxy (e.g., Begelman, Blandford, and Rees, 1980; Hills, 1983; Quinlan, 1996). However, other mechanisms such as gravitational wave-induced recoil and tidal deposition have also been proposed to explain the origin of observed surface brightness cores (Nasim et al., 2021; Khonji et al., 2024; Rawlings et al., 2025), and so this interpretation warrants caution. Nevertheless, we provide the inner surface brightness profile classification of the massive galaxies in our search as found in the literature (Lauer et al., 1995; Faber et al., 1997; Ravindranath et al., 2001; Rest et al., 2001; Laine et al., 2003; Lauer et al., 2005; Lauer et al., 2007a; Krajnović et al., 2013) in Table 3.1 and Table A.1, if one desires to interpret it as a discriminant between potential SMBH pair and SMBHB host galaxies.

### 4.2 Use Cases of the Ranked List of Galaxies

The most basic use of our ranked list of galaxies in Tables 3.1 and A.1 is to identify the most likely host galaxy counterpart to an individual PTA source. Once PTA experiments identify an individual source of continuous GWs, nearby massive galaxies in its sky localization region that are also highest-ranked in our list are the most likely counterparts. However, even before such a PTA detection, our ranked list of galaxies can be used for several science cases, as discussed below.

#### 4.2.1 Targeted Searches for Individual Continuous GW Sources by PTAs

The highest-ranked galaxies in our ranked list can already be used in targeted searches for individual continuous GW sources in PTA data. PTA searches for continuous GWs from an individual SMBHB typically fit pulsar timing residual data to models with many parameters, such as the sky position, the GW frequency f, the orbital phase, the GW polarization angle, the orbital inclination, and others, depending on the chosen model (e.g., Arzoumanian et al., 2020; Liu and Vigeland, 2021). These searches are computationally expensive, but can be sped up by fixing one or more

of these parameters. For example, targeted searches fix the location in the sky of the GW source to observed galaxies, which improves the detection sensitivity (e.g., Liu et al., 2023; Charisi et al., 2024). Our high-ranking galaxies are among the best PTA-detectable SMBHB host galaxy candidates in the northern sky, and thus targeted PTA searches can focus on them for faster and more sensitive searches.

# 4.2.2 Independent Corroboration of Candidate SMBHBs Discovered Through Other Means

Our ranked list of galaxies can be used to independently corroborate candidate SMB-HBs discovered through other means (e.g., light curve periodicities), based on the host galaxy stellar kinematic properties. Our full galaxy list in Table A.1 provides the stellar kinematic properties of the overall population of massive nearby galaxies, spanning those likely to host SMBHBs (high LDA score) to those unlikely (low LDA score). For a candidate SMBHB discovered through other means, a comparison of its host galaxy stellar kinematics to our full galaxy list can provide independent evidence to either reinforce or weaken the hypothesis that its central SMBH is indeed a SMBHB. Specifically, the stellar kinematic parameters  $\lambda_{R_e}$  and  $\Delta PA$  of the candidate SMBHB's host galaxy can be measured from IFU spectroscopy, and used to compute a LDA score using Equation 2.2. The resultant LDA score can then be compared to our full galaxy list in Table A.1; if the SMBHB candidate has a high LDA score compared to the galaxies in our full list, this corroborates the hypothesis that the galaxy hosts a SMBHB, and conversely. We emphasize that since this comparison does not involve the GW strain  $h_0$ , it is the LDA score (Equation 2.2) in Table A.1 that should be considered, rather than the total score (Equation 3.2). We also note that the LDA score in Equation 2.2 requires normalized values of  $\lambda_{R_e}$  and  $\Delta PA$  for the candidate SMBHB's host galaxy. To perform this normalization, one should subtract the mean value of the parameter from our distribution and divide by its standard deviation (the mean and standard deviation of  $\lambda_{R_e}$  and log  $\Delta PA$  from our full list in Table A.1 are  $(\mu_{\lambda_{Re}}, \sigma_{\lambda_{Re}}) = (0.31, 0.24)$  and  $(\mu_{\log \Delta PA}, \sigma_{\log \Delta PA}) = (0.87, 0.73)$ , respectively). The resulting normalized values of  $\lambda_{R_e}$  and  $\Delta PA$  for the candidate SMBHB's host galaxy can then be directly inserted into Equation 2.2 to calculate its LDA score.

# 4.2.3 Identifying Candidate Dual AGNs and Recoiling AGNs for Follow-Up Observations

Our list of galaxies can also be used to select candidate closely separated ( $\lesssim$ 100 pc) dual AGN, which can be confirmed with follow-up observations. As discussed in Section 4.1, some of our top-ranked galaxies may instead host close ( $\lesssim 100 \text{ pc}$ ) SMBH pairs, since their host galaxy stellar kinematics are similar to SMBHBs and thus contaminate our ranked list. If both SMBHs in the pair are accreting, then they could be observable as a close dual AGN. Follow-up telescope imaging of these candidates with high spatial resolution in the infrared, X-ray, or radio could spatially resolve the two AGNs for confirmation. Furthermore, if the two SMBHs have not yet formed a bound ~parsec-scale binary (and are thus potentially resolvable in follow-up observations), the inner surface brightness profiles of the host galaxy would not have been modified by scouring yet. In this scenario, the host galaxies would thus display a power-law inner surface brightness profile (rather than a core), which can be used as an additional selection cut to maximize the efficiency of target selection for follow-up observations. Within our sample, six galaxies (NGC 6703, NGC 3414, NGC 474, NGC 4494, NGC 3226 and NGC 4596) have a positive LDA score and a power-law inner surface brightness profile.

In addition to dual AGN, we suggest that our ranked list of galaxies can be used to select candidate recoiling AGN that can be verified with follow-up observations. As discussed in Section 4.1, our top-ranked galaxies are also likely to host SMB-HBs that have merged in the past <Gyr. For a merging SMBHB, anisotropic emission of GWs produce a recoil kick on the merged SMBH (e.g., Campanelli et al., 2007; Schnittman and Buonanno, 2007; Blecha et al., 2011), with velocities ranging from  $\leq$ 500 km/s to 4000 km/s depending on the binary parameters (Bogdanović, Reynolds, and Miller, 2007; Campanelli et al., 2007). If the kicked SMBH is accreting, it could be observed as an AGN with spatial or kinematic offsets from the host galaxy. Such methods have already been employed towards detecting AGN recoil candidates, for example using HST images (e.g., Lena et al., 2014). In contrast with the dual AGN discussed above, the inner light profile of the host galaxy of a recently-merged SMBHB would be scoured and display a core. Follow-up observations of

our top-ranked galaxies, especially those with cores, could reveal these spatial or kinematic offsets (Blecha et al., 2011; Kim et al., 2016).

## 4.3 Uncertainties in Calculating the GW Strain $h_0$

#### 4.3.1 Black Hole Mass

Our calculation of the SMBH mass  $M_{\rm BH}$  carries a statistical error stemming from our use of an empirical scaling relation, which causes the GW strain  $h_0$  as shown in Figure 3.3 to be approximate. Specifically, the empirical  $M_* - M_{BH}$  relation we use from Sahu, Graham, and Davis, 2019 has a scatter of  $\sim$ 0.5 dex. Since  $h_0 \propto M_{chirv}^{5/3} \propto M_{BH}^{5/3}$ , this would lead to a scatter of a factor of  $\sim$ 7 in  $h_0$ , which corresponds to an uncertainty of  $\sim$ 0.8 dex on the y-axis of Figure 3.3. Among our top ranking galaxies in Table 3.1, two (NGC 4486 (M87) and NGC 4374 (M84)) have dynamically-or directlymeasured SMBH masses in the literature. The SMBH mass of M87 has been directly measured from the black hole's shadow by the Event Horizon Telescope Collaboration et al. (2019) to be  $M_{\rm BH}\sim 6.5\times 10^9 M_{\odot}$ , within  $1\sigma$  of our value found with stellar mass. The SMBH mass of M84 has been measured through gas kinematics by Bower et al. (1998) to be  $M_{\rm BH} \sim 1.5 \times 10^9 M_{\odot}$ , also within  $1\sigma$  of our stellar mass value. SMBH masses of other galaxies such as NGC 2832 and NGC 4874 have also been published, although they were found through the  $M_* - \sigma_e$  empirical relation (Schutz and Ma, 2016; Dullo, 2019). Their values are below our adopted estimates using a  $M_* - M_{\rm BH}$  relation (a difference of up to 1.5 dex), which is consistent with recent studies suggesting that the  $M_* - \sigma_e$  relation systematically underestimates  $M_{\rm BH}$  for the most massive galaxies, and is therefore a less robust method to determine  $M_{\rm BH}$  of local massive galaxies (e.g., Lauer et al., 2007b; Dullo, Gil de Paz, and Knapen, 2021; Liepold and Ma, 2024). This further justifies our choice of the  $M_* - M_{\rm BH}$  relation to compute  $M_{\rm BH}$ .

#### 4.3.2 Black Hole Mass Ratio

Our assumption of an equal mass ratio q = 1 in the calculation of the chirp mass  $M_{chirp}$  also leads to a systematic error in the gravitational wave strain  $h_0$ . Although the mass ratio of hypothetical SMBHBs in our galaxies is unknown, our choice of

q=1 may be justified because accretion onto the binary would drive it towards equal mass (Young and Clarke, 2015). However, hypothetical SMBHBs in our galaxy dataset might have a mass ratio  $0 < q \le 1$ . Since  $h_0 \propto M_{chirp}^{5/3} \propto \frac{q}{(1+q)^2}$ , if we assume a SMBHB to have a mass ratio of q=1 while its actual mass ratio is, e.g., q=0.1, we would overestimate its GW strain  $h_0$  by a factor of  $\sim$ 3, which corresponds to a  $\sim$ 0.5 dex difference on the y-axis of Figure 3.3 (but still smaller than the uncertainty caused by the black hole mass). Therefore, the GW strain  $h_0$  of galaxies shown in Figure 3.3 is an upper limit.

#### 4.3.3 Binary Separation

Ultimately, our lack of constraints on the hypothetical SMBHB orbital separation is our most significant obstacle towards identifying potential PTA-detectable SMBHB candidate host galaxies. In Figure 3.3, we assume a GW emission frequency of 10 nHz to compute the GW strain  $h_0$ , which corresponds to a binary separation of  $\sim$ 5 milliparsecs for a system of mass  $M_{\rm BH} \sim 10^{10} M_{\odot}$  (Schutz and Ma, 2016). As discussed in Section 4.1, the exact separations can be anywhere between  $\sim$ 100 pc to 0 pc (already merged). PTA-detectable SMBHBs need separations of  $\sim$ milliparsec to emit nHz GWs, which we cannot constrain (although they would rank highly in our list if there are any in our archival galaxy datasets). Thus, the galaxies shown in Figure 3.3 that are above the current NANOGrav  $h_0$  sensitivity limit are not necessarily predicted to host SMBHBs currently detectable by PTAs, but may instead host SMBHB systems that have either already merged in the past Gyr, or that are currently at larger separations and have not yet hardened into a bound nHz-emitting SMBHB.

# 4.4 Cross-Referencing with Multi-AGN Catalogs

Through cross-referencing with multi-AGN catalogs, we find five candidate recoiling AGN host galaxies in our galaxy dataset, all of which have a positive LDA score, which is consistent with our interpretation. We use the Pfeifle et al. (2024) Big Multi-AGN Catalog, which is a census of all known and candidate multiple-AGN systems

in the literature, and identify the galaxies in our sample that are present in that catalog. Notably, we find that five of our ATLAS<sup>3D</sup> galaxies host candidate recoiling AGN (NGC 4486 (M87), NGC 4168, NGC 4278, NGC 4636 and NGC 5846, as identified by Lena et al., 2014). These five galaxies all have  $\lesssim$ 10 pc spatial offsets between the AGN and the galaxy center, which suggests recent ( $\lesssim$ 0.1 Myr) SMBH mergers assuming typical recoil velocities of  $\sim$ 100–1000 km s<sup>-1</sup> (Campanelli et al., 2007). We also find one galaxy (NGC 6338) from the CALIFA sample in the Pfeifle et al. (2024) catalog as identified by Comerford and Greene (2014) that hosts a candidate dual AGN, with a projected separation of 1.6 kiloparsec. All six of these galaxies have positive LDA scores, which is consistent with our expectation that the LDA score not only identifies SMBHB host galaxies, but also the host galaxies of SMBH pairs and recent SMBHB mergers.

Other observational evidence also suggests that many of the highest-ranked galaxies in our sample either have undergone a recent galaxy merger, host a SMBHB, or host a recent SMBH merger. In particular, our #1 scoring galaxy, NGC 4073, has been observed by Lauer et al. (2005) to display a local minimum in its surface brightness profile near its center. Surface brightness central minima have been hypothesized to result from the hardening and recent merger of a SMBHB (Holley-Bockelmann and Richstone, 2000; Lauer et al., 2002), which is consistent with expectations from our LDA score. Our #6 scoring galaxy, NGC 533, lies in a galaxy group that is suspected to have recently undergone a merger based on X-ray observations of its intragroup medium gas (Finoguenov et al., 2007; Gu et al., 2012). We also note that the majority (6/10) of our highest-ranked galaxies reside in either galaxy groups or low-mass clusters rather than massive galaxy clusters, based on cross-referencing with galaxy catalogs (Mahtessian, 1998). This is consistent with the scenario in which galaxy groups are more conducive to major mergers of massive galaxies that lead to the formation of SMBHBs, due to the lower velocity dispersions of galaxies in the group (Binney and Tremaine, 2008).

# 4.5 Discrepancies Among Overlapping Galaxies Between Different Surveys

Among the 71, 69, and 106 galaxies from the MASSIVE, ATLAS<sup>3D</sup>, and CALIFA surveys that we use to search for PTA-detectable SMBHBs, there are 18 galaxies that overlap between two different galaxy surveys, and none that are in all three. In particular, NGC 5353, NGC 4472, NGC 5557, and NGC 5322 are present in both MASSIVE and ATLAS<sup>3D</sup>, NGC 2592, NGC 5631, NGC 2880, NGC 5485, and NGC 6278 are present in both ATLAS<sup>3D</sup> and CALIFA, while NGC 7619, NGC 4816, NGC 1167, NGC 3615, NGC 3158, NGC 2513, NGC 0499, NGC 1060, and NGC 4874 are present in both MASSIVE and CALIFA. As such, many of these galaxies have different reported distances and stellar kinematic parameters, depending on the survey.

For overlapping galaxies, we find that the stellar kinematic parameters are similar between the different surveys within the uncertainties, whereas some galaxy distances have been measured differently and disagree. For the galaxy distances, we use those that have been corrected with the surface brightness fluctuation method or corrected for local peculiar velocity, whenever available. For example, NGC 1060 as observed by MASSIVE is ranked #5 in our list, but #11 as observed by CALIFA. Upon closer inspection, this difference arises not from a different LDA score (both are similar), but rather from a difference in GW strain  $h_0$  due to MASSIVE reporting a distance of  $67.4 \times 10^6$  parsec (67.4 Mpc) and CALIFA reporting a distance of 73.9 Mpc. Since the MASSIVE galaxy distance is smaller, its  $h_0$  is higher and its rank is higher. In this case, the distance of NGC 1060 from MASSIVE has been corrected for its local peculiar velocity, and thus we rely on the distance reported in MASSIVE.

#### 4.6 Redshift Difference Between

#### the Simulated and Observational Galaxy Datasets

Although the redshift range of the IFU surveys we use is lower than the redshift range of the ROMULUS25 simulated galaxies, this does not significantly affect our results, because the distinct stellar kinematic signatures of simulated SMBH merger and binary host galaxies do not display redshift evolution. The simulated galaxies in

ROMULUS25 used by B24B to derive the LDA predictor have redshifts of  $0.5 \lesssim z \lesssim 2$  (mean of  $z \sim 1.5$ ). As such, it is possible that the stellar kinematic signatures of SMBH merger and binary host galaxies identified by B24B are different for lower redshift galaxies, such as those at  $z \lesssim 0.03$  in the IFU surveys we use. Although the ROMULUS25 simulation does not contain enough SMBH merger and binary host galaxies to directly assess if the LDA predictor in Equation 2.2 applies at  $z \sim 0$ , we test whether this LDA predictor evolves over redshift. Specifically, we retrain the LDA predictor only for a subset of simulated galaxies around redshift  $z \sim 0.5$ , and find that the resulting LDA equation is similar to Equation 2.2 in terms of parameters and parameter coefficients. This explicitly demonstrates that the distinct stellar kinematic properties of simulated SMBH merger and binary host galaxies do not evolve with redshift, and should apply even to galaxies at lower redshifts.

Despite the different redshift ranges of the simulated and observed galaxies, the synthetic IFU data used by B24B to compute the LDA predictor probe similar physical scales in the galaxies compared to the observational IFU datasets, which enables us to directly use the LDA predictor on our archival galaxy datasets. As a consequence of the difference in redshift range between the simulated and observed galaxies, if the physical scale probed by the synthetic IFU data for the simulated galaxies used to compute the LDA predictor is much smaller than the physical scale probed by the observational dataset, the LDA predictor may not be directly applicable to the observational IFU dataset. In particular, the pixel spatial resolution of the synthetic stellar kinematic maps produced by B24B probes physical scales of 400 to 900 pc in each galaxy, depending on the redshift of the simulated galaxy. On the other hand, the physical scales probed by the stellar kinematic maps from CALIFA, ATLAS $^{
m 3D}$ , and MASSIVE range from  $\sim$ 300–1200 parsec, depending on redshift and instrument resolution. Thus, despite the difference in redshift ranges, the physical scales probed are similar, enabling us to directly apply the LDA predictor in Equation 2.2 to the MASSIVE, ATLAS<sup>3D</sup> and CALIFA galaxy IFU datasets.

#### Chapter 5

## **Conclusions**

#### 5.1 Science Summary

We mined archival galaxy IFU surveys to search for potential candidate host galaxies of individual SMBHBs that could be detected in GWs by PTAs. To do this, we used results from the ROMULUS25 cosmological simulations to identify the optimal set of parameters that discriminate simulated SMBH merger and binary host galaxies from a mass- and redshift-matched control sample. This selection is embedded in a LDA predictor. We then compute the LDA score for galaxies from archival IFU surveys to identify nearby galaxies that display the distinct signatures of SMBH binary and merger host galaxies. Assuming that their hypothetical two SMBHs are equal mass and are at  $\sim$ milliparsec separations, we calculate their expected gravitational wave strain  $h_0$ . We combine the LDA score with  $h_0$  to calculate a total score for each galaxy that reflects both (1) how likely they are to host a SMBHB, and (2) the strength of their hypothetical gravitational wave strain. Our main findings are as follows:

- 1. Using the ROMULUS25 cosmological simulations, we determine that among the full set of morphological and stellar kinematic parameters, it is the set of stellar kinematic parameters that optimally discriminates SMBH merger and binary host galaxies from a mass- and redshift-matched control sample. By selecting simulated galaxies with chirp mass  $M_{\rm chirp} > 10^8 M_{\odot}$  and mass ratio q > 0.5, the accuracy of this classification reaches  $\gtrsim 85\%$ .
- 2. We derive the stellar kinematic signatures of simulated SMBH merger and binary host galaxies using a mass- and redshift-matched control sample, such

that our results are not affected by galaxy scaling relations. We apply these distinctive stellar kinematic signatures (slower rotation and stronger kinematic/photometric misalignments) to archival IFU observations of massive nearby galaxies, to predict which ones are the most likely to host a SMBH merger or binary.

3. We produce a ranked list of galaxies that correspond to the best candidates for the host galaxies of individual SMBHBs in the northern sky that will be detected in GWs by PTAs. Even before a PTA detection, this list can be used to (1) perform targeted searches for individual sources of continuous GW in PTA data, (2) to corroborate candidate SMBHBs discovered through other means, and (3) to select candidate closely-separated (≤100 pc) dual AGNs and recoiling AGN for follow-up observations.

The quest to detect continuous nHz GWs from an individual SMBHB is ongoing through multiple PTA experiments. While we focus here on identifying potential PTA GW sources among massive nearby galaxies using archival IFU surveys in the northern sky, ongoing galaxy IFU surveys in the south such as the Hector Galaxy Survey¹ can extend these efforts for full sky coverage of individual PTA sources. Such a search may become especially pressing given the recent tentative detection of a GW hotspot by the MeerKAT PTA collaboration at southern declinations not covered here (Grunthal et al., 2024). When the host galaxy of an individual SMBHB detected through GWs by PTAs is identified, telescope follow-up across the electromagnetic spectrum will provide insights on the formation and environments of SMBHBs that remain mysterious.

<sup>&</sup>lt;sup>1</sup>https://hector.survey.org.au/

#### 5.2 General Perspectives

The work presented in this thesis represents a step towards the discovery of the first SMBHB in GWs by PTA experiments in the future. In Chapter 1, we notably covered how current PTA data analysis predicts that the localization region of a nHz GW source cannot be constrained to a single host galaxy, and that there will be many candidates. In the pursuit of singling out the unique GW source host galaxy, searching for the host galaxy stellar kinematic signature is promising because it can be universally characterized and does not depend on, e.g., dust obscuration or projection alignment. The results shown here are additionally interesting because our analysis has enabled the exploration of complementary science goals, such as the search for closely separated dual AGNs and recoiling SMBHs, whose identification is traditionally challenging. As such, we hope that the results presented in this thesis will be conducive, in the future, to a better understanding of the evolution of SMBHs and their merging processes, from being gravitationally unbound to emitting GWs, and wandering galaxy nuclei upon merging.

### Appendix A

## **Ranked List of Galaxies**

TABLE A.1: Extended Table 3.1 for all the massive galaxies in our sample (with a SMBH mass  $M_{\rm BH} > 10^{8.4} M_{\odot}$ , or equivalently with a chirp mass  $M_{chirp} > 10^8 M_{\odot}$ ). Columns include: galaxy name, total score rank, luminosity distance D, IFU survey, log of the black hole mass  $M_{\rm BH}$ , log of the hypothetical strain  $h_0$ , LDA score (Equation 2.2), normalized log hypothetical GW strain  $\log h_0$ , normalized LDA score  $\widehat{\rm LDA}$ , total score (Equation 3.2), and the inner light profile classification from the literature, when available (where 'C'=core, 'P'=power-law, and 'I'=intermediate).

Name To	otal Score	e D	Survey log M	$I_{\rm BH} \log h_0$	LDA	$\widehat{\log h_0}$	ĹDA	Total	Light
	Rank	[Mpc]	$[M_{\odot}]$	]	Score		Score	Score	Profile
NGC4073	1	91.50	MASSIVE 10.2	5 -13.04	4.08	0.98	0.99	0.99	С
NGC1016	2	95.20	MASSIVE 10.2	5 -13.06	3.86	0.98	0.97	0.97	С
NGC2832	3	105.20	MASSIVE 10.3	0 -13.02	3.62	0.99	0.94	0.97	C
NGC4486	4	17.20	ATLAS3D 9.72	2 -13.20	4.03	0.93	0.98	0.96	C
NGC1060	5	67.40	MASSIVE 10.0	0 -13.32	4.21	0.90	1.00	0.95	-
NGC0533	6	77.90	MASSIVE 10.0	3 -13.33	3.87	0.90	0.97	0.93	_
NGC4472	7	17.10	ATLAS3D 9.80	-13.07	3.02	0.97	0.89	0.93	C
NGC4874	8	102.00	MASSIVE 10.1	3 -13.28	3.56	0.91	0.94	0.92	C
NGC0410	9	71.30	MASSIVE 9.94	4 -13.45	3.93	0.86	0.97	0.92	_
NGC7265	10	82.80	MASSIVE 9.9	5 -13.49	4.01	0.85	0.98	0.92	_
NGC1060	11	73.90	CALIFA 9.9	1 -13.51	3.92	0.84	0.97	0.91	_
NGC0777	12	72.20	MASSIVE 9.9	5 -13.43	3.69	0.86	0.95	0.91	_
NGC0315	13	70.30	MASSIVE 10.2	2 -12.98	2.11	1.00	0.80	0.91	_
NGC1129	14	73.90	MASSIVE 10.1	0 -13.20	2.87	0.94	0.87	0.90	-

Name	Rank	D	Survey lo	og M <sub>BH</sub>	$\log h_0$	LDA	$\widehat{\log h_0}$	$\widehat{LDA}$	Total	Light
		[Mpc]		$[M_{\odot}]$					Score	Profile
NGC4406	15	16.80	ATLAS3D	9.51	-13.54	3.84	0.83	0.97	0.90	С
NGC0507	16	69.80	MASSIVE	9.95	-13.42	3.42	0.87	0.93	0.90	С
NGC4374	17	18.50	ATLAS3D	9.48	-13.63	3.97	0.81	0.98	0.90	С
NGC4261	18	30.80	ATLAS3D	9.71	-13.47	3.42	0.85	0.93	0.89	С
NGC2258	19	59.00	MASSIVE	9.75	-13.68	3.96	0.79	0.98	0.89	_
NGC0708	20	69.00	MASSIVE	9.75	-13.74	4.03	0.77	0.98	0.88	_
NGC5846	21	24.20	ATLAS3D	9.46	-13.77	4.07	0.76	0.99	0.88	C
NGC4472	22	16.70	MASSIVE	9.80	-13.04	1.59	0.98	0.75	0.87	С
NGC7436	23	106.60	MASSIVE	10.12	-13.33	2.56	0.90	0.84	0.87	_
NGC2783	24	101.40	MASSIVE	9.80	-13.83	3.93	0.74	0.97	0.87	_
NGC5557	25	51.00	MASSIVE	9.61	-13.86	4.00	0.73	0.98	0.87	С
NGC7626	26	54.00	MASSIVE	9.75	-13.64	3.35	0.80	0.92	0.86	I
NGC3842	27	99.40	MASSIVE	9.94	-13.60	3.04	0.81	0.89	0.85	С
NGC4914	28	74.50	MASSIVE	9.80	-13.69	3.30	0.78	0.91	0.85	_
NGC2274	29	73.80	MASSIVE	9.77	-13.74	3.43	0.77	0.93	0.85	_
NGC0080	30	81.90	MASSIVE	9.75	-13.82	3.55	0.75	0.94	0.85	-
NGC1573	31	65.00	MASSIVE	9.67	-13.85	3.63	0.74	0.95	0.85	_
NGC5322	32	34.20	MASSIVE	9.64	-13.63	2.94	0.80	0.88	0.84	C
NGC3209	33	94.60	MASSIVE	9.67	-14.02	3.90	0.69	0.97	0.84	_
NGC4636	34	14.30	ATLAS3D	9.17	-14.03	3.92	0.68	0.97	0.84	C
NGC7436B	35	107.80	CALIFA	10.02	-13.49	2.41	0.85	0.83	0.84	_
NGC1132	36	97.60	MASSIVE	9.79	-13.84	3.30	0.74	0.91	0.83	_
NGC3562	37	101.00	MASSIVE	9.75	-13.91	3.47	0.72	0.93	0.83	_
NGC2672	38	61.50	MASSIVE	9.70	-13.78	3.13	0.76	0.90	0.83	_
NGC4365	39	23.30	ATLAS3D	9.38	-13.89	3.39	0.72	0.92	0.83	С
NGC4874	40	114.00	CALIFA	9.66	-14.11	3.85	0.66	0.97	0.83	С
NGC5813	41	31.30	ATLAS3D	9.49	-13.83	3.18	0.74	0.90	0.83	С
NGC4649	42	17.30	ATLAS3D	9.70	-13.23	1.13	0.93	0.71	0.82	C

Name	Rank	D	Survey lo	og M <sub>BH</sub>	$\log h_0$	LDA	$\widehat{\log h_0}$	$\widehat{LDA}$	Total	Light
		[Mpc]		$[M_{\odot}]$					Score	Profile
NGC0890	43	55.60	MASSIVE	9.64	-13.84	3.08	0.74	0.89	0.82	_
NGC0499	44	69.80	MASSIVE	9.64	-13.94	3.31	0.71	0.92	0.82	_
NGC3462	45	99.20	MASSIVE	9.72	-13.96	3.32	0.71	0.92	0.82	_
UGC02783	46	85.80	MASSIVE	9.59	-14.11	3.62	0.66	0.94	0.81	_
NGC7386	47	99.10	MASSIVE	9.70	-13.98	3.31	0.70	0.92	0.81	_
NGC0910	48	79.80	MASSIVE	9.52	-14.19	3.68	0.63	0.95	0.81	C
NGC6173	49	136.70	CALIFA	9.71	-14.11	3.46	0.66	0.93	0.81	_
NGC3158	50	103.40	MASSIVE	10.20	-13.18	0.39	0.94	0.64	0.80	_
NGC7274	51	82.80	MASSIVE	9.56	-14.15	3.41	0.65	0.92	0.80	_
NGC6338	52	126.40	CALIFA	9.66	-14.17	3.38	0.64	0.92	0.79	_
NGC4555	53	103.60	MASSIVE	9.94	-13.62	1.88	0.81	0.78	0.79	_
NGC3937	54	101.20	MASSIVE	9.72	-13.96	2.85	0.70	0.87	0.79	_
NGC7556	55	103.00	MASSIVE	9.89	-13.70	2.05	0.78	0.80	0.79	_
NGC1684	56	63.50	MASSIVE	9.52	-14.09	2.87	0.66	0.87	0.78	_
NGC7619	57	54.00	MASSIVE	9.75	-13.64	1.56	0.80	0.75	0.78	C
NGC4816	58	102.00	MASSIVE	9.52	-14.30	3.30	0.60	0.91	0.77	_
IC0310	59	77.50	MASSIVE	9.52	-14.18	3.03	0.64	0.89	0.77	_
UGC03683	60	85.10	MASSIVE	9.66	-14.00	2.51	0.69	0.84	0.77	_
NGC5557	61	38.80	ATLAS3D	9.07	-14.64	3.84	0.50	0.97	0.77	C
NGC7052	62	69.30	MASSIVE	9.75	-13.74	1.75	0.77	0.77	0.77	C
NGC2320	63	89.40	MASSIVE	9.95	-13.53	0.93	0.84	0.69	0.77	_
NGC5322	64	30.30	ATLAS3D	9.39	-13.99	2.31	0.70	0.82	0.76	C
NGC7550	65	73.80	CALIFA	9.23	-14.65	3.70	0.50	0.95	0.76	_
NGC6482	66	61.40	MASSIVE	9.70	-13.77	1.62	0.76	0.75	0.76	_
NGC2513	67	70.80	MASSIVE	9.66	-13.92	2.05	0.72	0.80	0.76	_
NGC0741	68	78.70	CALIFA	9.37	-14.44	3.25	0.56	0.91	0.75	_
NGC4841A	69	108.00	CALIFA	9.42	-14.50	3.22	0.54	0.91	0.75	_
NGC4168	70	30.90	ATLAS3D	9.01	-14.63	3.46	0.50	0.93	0.75	C

Name	Rank	D	Survey lo	og M <sub>BH</sub>	$\log h_0$	LDA	$\widehat{\log h_0}$	$\widehat{\text{LDA}}$	Total	Light
		[Mpc]		$[M_{\odot}]$					Score	Profile
NGC4552	71	15.80	ATLAS3D	8.85	-14.61	3.31	0.51	0.91	0.74	С
NGC2513	72	71.10	CALIFA	9.41	-14.34	2.76	0.59	0.86	0.74	_
UGC03894	73	97.20	MASSIVE	9.70	-13.97	1.86	0.70	0.78	0.74	_
NGC1700	74	54.40	MASSIVE	9.70	-13.72	1.02	0.78	0.70	0.74	C
NGC3816	75	99.40	MASSIVE	9.57	-14.20	2.37	0.63	0.83	0.73	_
NGC4382	76	17.90	ATLAS3D	9.26	-13.99	1.79	0.70	0.77	0.73	C
UGC12127	77	121.70	CALIFA	9.13	-15.04	3.84	0.38	0.96	0.73	_
NGC4816	78	110.10	CALIFA	9.35	-14.62	3.13	0.51	0.90	0.73	_
NGC0383	79	71.30	MASSIVE	9.87	-13.56	0.03	0.82	0.60	0.72	_
NGC0810	80	109.40	CALIFA	9.43	-14.49	2.77	0.54	0.86	0.72	_
NGC5490	81	78.60	MASSIVE	9.69	-13.91	1.21	0.72	0.72	0.72	_
NGC5029	82	136.00	CALIFA	9.35	-14.72	3.03	0.47	0.89	0.71	_
NGC6703	83	25.90	ATLAS3D	8.48	-15.45	3.91	0.25	0.97	0.71	P
NGC0499	84	62.90	CALIFA	9.18	-14.66	2.85	0.49	0.87	0.71	_
NGC5198	85	39.60	ATLAS3D	8.82	-15.05	3.45	0.37	0.93	0.71	C
NGC1453	86	56.40	MASSIVE	9.75	-13.66	0.04	0.80	0.61	0.71	_
UGC10695	87	129.30	CALIFA	9.01	-15.25	3.64	0.31	0.95	0.70	_
NGC2693	88	74.40	MASSIVE	9.82	-13.67	-0.09	0.79	0.59	0.70	_
NGC3158	89	107.90	CALIFA	9.73	-13.97	0.93	0.70	0.69	0.70	_
NGC6575	90	106.00	MASSIVE	9.70	-14.01	0.96	0.69	0.69	0.69	_
IC1079	91	137.90	CALIFA	9.06	-15.21	3.33	0.33	0.92	0.69	-
NGC2418	92	74.10	MASSIVE	9.57	-14.08	1.06	0.67	0.70	0.69	-
NGC6125	93	77.00	CALIFA	9.15	-14.80	2.70	0.45	0.86	0.68	_
NGC0997	94	90.40	MASSIVE	9.57	-14.16	1.22	0.64	0.72	0.68	_
NGC2768	95	21.80	ATLAS3D	9.40	-13.84	0.09	0.74	0.61	0.68	Ι
UGC10693	96	129.80	CALIFA	9.35	-14.69	2.40	0.48	0.83	0.68	_
NGC6223	97	86.70	MASSIVE	9.70	-13.92	0.34	0.71	0.63	0.68	_
NGC6515	98	106.20	CALIFA	8.84	-15.46	3.37	0.25	0.92	0.67	_

Name	Rank	D	Survey lo	og M <sub>BH</sub>	$\log h_0$	LDA	$\widehat{\log h_0}$	<b>LDA</b>	Total	Light
		[Mpc]		$[M_{\odot}]$					Score	Profile
NGC6375	99	95.80	MASSIVE	9.66	-14.05	0.61	0.68	0.66	0.67	
NGC6411	100	61.30	CALIFA	8.65	-15.53	3.24	0.23	0.91	0.66	_
NGC7562	101	52.70	CALIFA	8.92	-15.01	2.65	0.39	0.85	0.66	_
NGC5129	102	107.50	MASSIVE	9.94	-13.63	-1.35	0.80	0.47	0.66	_
NGC6020	103	71.80	CALIFA	8.52	-15.82	3.36	0.14	0.92	0.66	_
NGC7618	104	76.30	MASSIVE	9.59	-14.06	0.41	0.67	0.64	0.66	_
NGC3608	105	22.30	ATLAS3D	8.44	-15.44	2.99	0.26	0.88	0.65	C
NGC5614	106	65.40	CALIFA	9.01	-14.96	2.31	0.40	0.82	0.65	_
NGC3414	107	24.50	ATLAS3D	8.69	-15.07	2.45	0.37	0.83	0.64	P
NGC3607	108	22.20	ATLAS3D	9.08	-14.37	1.01	0.58	0.70	0.64	C
NGC5485	109	25.20	ATLAS3D	8.61	-15.22	2.49	0.32	0.84	0.63	C
UGC00029	110	127.50	CALIFA	8.58	-15.97	3.05	0.09	0.89	0.63	_
NGC4278	111	15.60	ATLAS3D	8.64	-14.95	2.04	0.40	0.79	0.63	C
NGC6146	112	137.30	CALIFA	9.55	-14.37	0.80	0.58	0.68	0.63	_
NGC5631	113	36.30	CALIFA	8.40	-15.72	2.85	0.17	0.87	0.63	_
NGC0155	114	89.20	CALIFA	8.81	-15.43	2.56	0.26	0.84	0.62	-
NGC1167	115	70.20	MASSIVE	9.74	-13.78	-1.65	0.76	0.44	0.62	_
NGC0524	116	23.30	ATLAS3D	9.18	-14.23	-0.14	0.62	0.59	0.60	C
NGC3665	117	33.10	ATLAS3D	9.43	-13.96	-1.22	0.70	0.48	0.60	_
NGC5485	118	36.70	CALIFA	8.56	-15.46	2.28	0.25	0.82	0.60	C
NGC3615	119	101.20	MASSIVE	9.70	-13.99	-1.30	0.69	0.48	0.60	_
NGC3303	120	98.80	CALIFA	8.62	-15.79	2.33	0.15	0.82	0.59	_
NGC0665	121	74.60	MASSIVE	9.64	-13.97	-1.58	0.70	0.45	0.59	_
NGC1167	122	70.60	CALIFA	9.66	-13.91	-1.96	0.72	0.41	0.59	_
NGC7426	123	80.00	MASSIVE	9.82	-13.70	-3.55	0.78	0.26	0.58	_
NGC5353	124	41.10	MASSIVE	9.61	-13.77	-2.98	0.76	0.32	0.58	_
NGC3805	125	99.40	MASSIVE	9.77	-13.87	-2.41	0.73	0.37	0.58	_
NGC3379	126	10.30	ATLAS3D	8.38	-15.21	1.57	0.32	0.75	0.58	С

Name	Rank	D	Survey lo	og M <sub>BH</sub>	$\log h_0$	LDA	$\widehat{\log h_0}$	<u>LDA</u>	Total	Light
		[Mpc]		$[M_{\odot}]$					Score	Profile
NGC3193	127	33.10	ATLAS3D	8.77	-15.07	1.29	0.37	0.72	0.57	С
NGC7619	128	54.90	CALIFA	8.42	-15.86	1.94	0.13	0.78	0.56	C
NGC4494	129	16.60	ATLAS3D	8.51	-15.21	1.27	0.33	0.72	0.56	P
NGC7025	130	75.40	CALIFA	9.39	-14.39	-0.58	0.57	0.55	0.56	_
NGC3613	131	28.30	ATLAS3D	8.89	-14.79	0.49	0.45	0.65	0.56	C
NGC0661	132	30.60	ATLAS3D	8.40	-15.64	1.65	0.20	0.76	0.55	_
NGC0474	133	30.90	ATLAS3D	8.40	-15.64	1.64	0.19	0.76	0.55	P
NGC2918	134	105.10	CALIFA	9.25	-14.77	0.18	0.46	0.62	0.54	_
NGC3106	135	96.40	CALIFA	8.87	-15.37	1.10	0.28	0.71	0.54	_
NGC7623	136	54.50	CALIFA	8.49	-15.76	1.45	0.16	0.74	0.53	_
UGC10097	137	94.60	CALIFA	9.27	-14.68	-0.25	0.49	0.58	0.53	_
NGC4621	138	14.90	ATLAS3D	8.71	-14.81	-0.11	0.45	0.59	0.52	P
NGC1497	139	87.80	MASSIVE	9.51	-14.26	-1.98	0.61	0.41	0.52	_
NGC3226	140	22.90	ATLAS3D	8.51	-15.35	0.82	0.28	0.68	0.52	P
NGC4753	141	22.90	ATLAS3D	9.16	-14.26	-2.07	0.61	0.40	0.52	_
NGC4477	142	16.50	ATLAS3D	8.42	-15.34	0.67	0.29	0.66	0.51	I
NGC5208	143	105.00	MASSIVE	9.72	-13.98	-4.86	0.70	0.14	0.50	_
NGC5638	144	25.60	ATLAS3D	8.40	-15.58	0.76	0.22	0.67	0.50	_
NGC0447	145	80.10	CALIFA	8.73	-15.51	0.67	0.23	0.66	0.50	_
NGC0821	146	23.40	ATLAS3D	8.67	-15.07	-0.03	0.37	0.60	0.50	I
NGC5966	147	73.50	CALIFA	8.53	-15.81	0.89	0.14	0.69	0.50	_
NGC7194	148	118.90	CALIFA	9.25	-14.82	-0.71	0.44	0.53	0.49	_
NGC4429	149	16.50	ATLAS3D	8.79	-14.72	-0.99	0.47	0.51	0.49	P
NGC4526	150	16.40	ATLAS3D	8.92	-14.51	-1.74	0.54	0.44	0.49	_
NGC3615	151	105.40	CALIFA	9.15	-14.94	-0.47	0.41	0.56	0.49	_
NGC0169	152	66.20	CALIFA	9.51	-14.13	-3.95	0.65	0.23	0.49	_
NGC5353	153	35.20	ATLAS3D	9.35	-14.13	-4.06	0.65	0.22	0.49	_
NGC3640	154	26.30	ATLAS3D	8.88	-14.77	-1.01	0.46	0.51	0.48	С

Name	Rank	D	Survey lo	$\log M_{ m BH}$	$\log h_0$	LDA	$\widehat{\log h_0}$	<u>LDA</u>	Total	Light
		[Mpc]		$[M_{\odot}]$					Score	Profile
NGC7563	155	60.80	CALIFA	8.46	-15.85	0.67	0.13	0.66	0.48	_
NGC4697	156	11.40	ATLAS3D	8.63	-14.84	-1.06	0.44	0.50	0.47	P
NGC4596	157	16.50	ATLAS3D	8.37	-15.42	0.10	0.26	0.61	0.47	P
NGC2554	158	64.00	CALIFA	8.87	-15.19	-0.31	0.33	0.57	0.47	_
NGC0932	159	57.50	CALIFA	8.46	-15.83	0.47	0.14	0.65	0.47	_
NGC4473	160	15.30	ATLAS3D	8.40	-15.35	-0.08	0.28	0.59	0.47	С
NGC5866	161	14.90	ATLAS3D	8.52	-15.14	-0.53	0.35	0.55	0.46	_
NGC5784	162	86.60	CALIFA	8.87	-15.31	-0.31	0.30	0.57	0.45	_
NGC6945	163	59.30	CALIFA	9.16	-14.67	-2.11	0.49	0.40	0.45	_
NGC0529	164	69.00	CALIFA	8.66	-15.56	-0.13	0.22	0.59	0.44	_
UGC10905	165	122.70	CALIFA	9.52	-14.39	-3.95	0.57	0.23	0.44	_
NGC6314	166	105.30	CALIFA	8.87	-15.41	-0.55	0.27	0.55	0.43	_
NGC7722	167	58.30	CALIFA	8.92	-15.06	-1.32	0.37	0.48	0.43	-
NGC6021	168	78.50	CALIFA	8.53	-15.84	-0.15	0.13	0.59	0.43	_
NGC0936	169	22.40	ATLAS3D	9.03	-14.46	-4.06	0.55	0.22	0.42	P
NGC0680	170	37.50	ATLAS3D	8.56	-15.47	-0.74	0.25	0.53	0.41	_
NGC2859	171	27.00	ATLAS3D	8.47	-15.48	-0.78	0.25	0.53	0.41	P
NGC7738	172	97.80	CALIFA	8.65	-15.74	-0.67	0.17	0.54	0.40	_
NGC1349	173	93.90	CALIFA	8.40	-16.14	-0.50	0.05	0.55	0.39	_
UGC11228	174	90.30	CALIFA	8.67	-15.67	-0.97	0.19	0.51	0.38	_
NGC4956	175	77.70	CALIFA	8.49	-15.90	-0.78	0.12	0.53	0.38	_
NGC2962	176	34.00	ATLAS3D	8.68	-15.23	-1.78	0.32	0.43	0.38	P
NGC5473	177	33.20	ATLAS3D	8.66	-15.25	-1.81	0.31	0.43	0.38	_
NGC6081	178	85.00	CALIFA	8.71	-15.57	-1.25	0.22	0.48	0.37	_
NGC7824	179	88.10	CALIFA	8.92	-15.24	-1.90	0.32	0.42	0.37	_
NGC4459	180	16.10	ATLAS3D	8.38	-15.40	-1.59	0.27	0.45	0.37	P
UGC05771	181	114.30	CALIFA	9.04	-15.15	-2.16	0.34	0.40	0.37	_
NGC5838	182	21.80	ATLAS3D	8.78	-14.87	-3.20	0.43	0.30	0.37	P

Name	Rank	D	Survey lo	$\log M_{ m BH}$	$\log h_0$	LDA	$\widehat{\log h_0}$	<u>LDA</u>	Total	Light
		[Mpc]		$[M_{\odot}]$					Score	Profile
NGC6150	183	135.80	CALIFA	9.22	-14.93	-3.10	0.41	0.31	0.36	_
NGC3998	184	13.70	ATLAS3D	8.41	-15.27	-2.08	0.31	0.40	0.36	I
UGC08107	185	128.60	CALIFA	8.63	-15.89	-1.18	0.12	0.49	0.36	_
NGC4281	186	24.40	ATLAS3D	8.88	-14.75	-4.30	0.46	0.19	0.36	P
NGC0023	187	65.70	CALIFA	8.58	-15.67	-1.41	0.19	0.47	0.36	_
NGC7711	188	58.80	CALIFA	8.60	-15.59	-1.65	0.21	0.44	0.35	_
NGC6278	189	48.60	CALIFA	8.38	-15.88	-1.43	0.12	0.46	0.34	P
UGC10205	190	104.60	CALIFA	8.51	-15.99	-1.66	0.09	0.44	0.32	_
NGC5687	191	27.20	ATLAS3D	8.47	-15.48	-2.34	0.24	0.38	0.32	_
NGC0160	192	75.20	CALIFA	8.57	-15.76	-1.93	0.16	0.42	0.32	_
NGC2974	193	20.90	ATLAS3D	8.74	-14.92	-4.68	0.41	0.16	0.31	P
NGC7671	194	60.00	CALIFA	8.44	-15.87	-1.93	0.13	0.42	0.31	_
NGC5987	195	50.80	CALIFA	8.86	-15.10	-3.85	0.36	0.24	0.30	_
NGC4036	196	24.60	ATLAS3D	8.78	-14.91	-5.48	0.42	0.08	0.30	_
NGC5308	197	31.50	ATLAS3D	8.78	-15.03	-4.38	0.38	0.19	0.30	P
NGC3945	198	23.20	ATLAS3D	8.55	-15.27	-3.36	0.31	0.28	0.29	P
UGC05113	199	103.60	CALIFA	8.68	-15.70	-2.46	0.18	0.37	0.29	_
UGC08234	200	124.80	CALIFA	8.74	-15.69	-2.51	0.18	0.36	0.29	_
NGC4233	201	33.90	ATLAS3D	8.64	-15.30	-3.48	0.30	0.27	0.29	_
NGC5406	202	84.40	CALIFA	8.97	-15.14	-4.18	0.35	0.20	0.28	_
NGC3230	203	40.80	ATLAS3D	8.70	-15.27	-3.73	0.31	0.25	0.28	_
NGC4762	204	22.60	ATLAS3D	8.69	-15.03	-5.73	0.38	0.06	0.27	P
NGC5908	205	55.40	CALIFA	8.88	-15.10	-5.18	0.36	0.11	0.27	_
NGC2639	206	52.70	CALIFA	8.79	-15.23	-4.43	0.32	0.18	0.26	_
UGC06036	207	101.60	CALIFA	8.80	-15.50	-3.41	0.24	0.28	0.26	_
NGC4521	208	39.70	ATLAS3D	8.71	-15.24	-4.65	0.32	0.16	0.25	_
NGC0217	209	56.70	CALIFA	8.68	-15.45	-3.71	0.25	0.25	0.25	_
UGC06312	210	100.70	CALIFA	8.57	-15.88	-2.87	0.12	0.33	0.25	_

Name	Rank	D	Survey 1	og M <sub>BH</sub>	$\log h_0$	LDA	$\widehat{\log h_0}$	<u>LDA</u>	Total	Light
		[Mpc]		$[M_{\odot}]$					Score	Profile
NGC4003	211	103.60	CALIFA	8.64	-15.78	-3.02	0.15	0.31	0.25	_
NGC7683	212	54.20	CALIFA	8.55	-15.65	-3.32	0.19	0.29	0.24	_
IC0944	213	112.40	CALIFA	8.95	-15.30	-4.52	0.30	0.17	0.24	-
NGC0774	214	65.20	CALIFA	8.39	-15.99	-3.02	0.09	0.31	0.23	_
UGC00036	215	90.50	CALIFA	8.52	-15.92	-3.16	0.11	0.30	0.23	_
UGC10380	216	137.90	CALIFA	8.53	-16.08	-3.02	0.06	0.31	0.23	_
NGC2695	217	31.50	ATLAS3D	8.41	-15.64	-3.69	0.19	0.25	0.22	_
NGC5422	218	30.80	ATLAS3D	8.43	-15.60	-3.82	0.21	0.24	0.22	I
NGC6278	219	42.90	ATLAS3D	8.56	-15.53	-4.06	0.23	0.22	0.22	P
NGC6497	220	95.50	CALIFA	8.58	-15.84	-3.44	0.13	0.27	0.22	_
UGC08781	221	120.90	CALIFA	8.61	-15.89	-3.39	0.12	0.28	0.21	-
IC0674	222	116.70	CALIFA	8.36	-16.29	-3.26	0.00	0.29	0.21	_
UGC12274	223	112.10	CALIFA	8.77	-15.60	-4.20	0.21	0.20	0.21	-
NGC7311	224	66.90	CALIFA	8.63	-15.60	-4.24	0.21	0.20	0.20	_
NGC7684	225	74.30	CALIFA	8.49	-15.88	-3.69	0.12	0.25	0.20	_
NGC0364	226	72.80	CALIFA	8.45	-15.93	-3.66	0.11	0.25	0.19	_
UGC03995	227	71.80	CALIFA	8.39	-16.04	-3.58	0.08	0.26	0.19	_
IC4566	228	92.30	CALIFA	8.44	-16.06	-3.61	0.07	0.26	0.19	_
UGC09537	229	138.50	CALIFA	8.88	-15.50	-5.17	0.24	0.11	0.19	-
NGC5888	230	136.50	CALIFA	8.86	-15.54	-5.22	0.23	0.11	0.18	_
NGC3160	231	106.90	CALIFA	8.44	-16.12	-3.94	0.05	0.23	0.16	_
NGC2577	232	30.80	ATLAS3D	8.39	-15.67	-4.93	0.19	0.13	0.16	_
NGC5493	233	38.80	ATLAS3D	8.46	-15.65	-5.43	0.19	0.09	0.15	_
IC1755	234	113.50	CALIFA	8.39	-16.23	-4.23	0.02	0.20	0.14	_
NGC6547	235	40.80	ATLAS3D	8.38	-15.81	-5.06	0.14	0.12	0.13	_
NGC5934	236	91.30	CALIFA	8.42	-16.09	-4.71	0.06	0.15	0.12	_
NGC6060	237	73.70	CALIFA	8.41	-16.02	-4.83	0.08	0.14	0.12	_
NGC6941	238	94.80	CALIFA	8.42	-16.10	-4.79	0.06	0.15	0.11	_

Name	Rank	D	Survey	$\log M_{ m BH}$	$\log h_0$	LDA	$\widehat{\log h_0}$	<u>LDA</u>	Total	Light
		[Mpc]		$[M_{\odot}]$					Score	Profile
NGC7321	239	104.90	CALIFA	8.40	-16.18	-4.94	0.03	0.13	0.10	_
NGC6978	240	91.60	CALIFA	8.57	-15.84	-6.33	0.14	0.00	0.10	_
NGC0180	241	75.30	CALIFA	8.39	-16.06	-5.37	0.07	0.09	0.08	_
NGC2347	242	67.10	CALIFA	8.42	-15.96	-5.86	0.10	0.05	0.08	_
NGC6478	243	105.10	CALIFA	8.54	-15.95	-6.18	0.10	0.01	0.07	_
UGC10337	244	138.60	CALIFA	8.57	-16.02	-5.75	0.08	0.06	0.07	_
NGC6301	245	129.50	CALIFA	8.55	-16.03	-6.26	0.08	0.01	0.06	-
UGC10710	246	130.10	CALIFA	8.49	-16.12	-5.76	0.05	0.05	0.05	-

- Abbott, B. P. et al. (Feb. 2016). "Observation of Gravitational Waves from a Binary Black Hole Merger". In: 116.6, 061102, p. 061102. DOI: 10.1103/PhysRevLett. 116.061102. arXiv: 1602.03837 [gr-qc].
- Abbott, B. P. et al. (Jan. 2017). "The basic physics of the binary black hole merger GW150914". In: *Annalen der Physik* 529.1-2, 1600209, p. 1600209. DOI: 10.1002/andp.201600209. arXiv: 1608.01940 [gr-qc].
- Agazie, G., J. Antoniadis, and A. Anumarlapudi (May 2024). "Comparing Recent Pulsar Timing Array Results on the Nanohertz Stochastic Gravitational-wave Background". In: 966.1, 105, p. 105. DOI: 10.3847/1538-4357/ad36be. arXiv: 2309.00693 [astro-ph.HE].
- Agazie, Gabriella et al. (July 2023a). "The NANOGrav 15 yr Data Set: Evidence for a Gravitational-wave Background". In: 951.1, L8, p. L8. DOI: 10.3847/2041-8213/acdac6. arXiv: 2306.16213 [astro-ph.HE].
- Agazie, Gabriella et al. (July 2023b). "The NANOGrav 15 yr Data Set: Observations and Timing of 68 Millisecond Pulsars". In: 951.1, L9, p. L9. DOI: 10.3847/2041-8213/acda9a. arXiv: 2306.16217 [astro-ph.HE].
- Alcock, C. et al. (Oct. 2000). "The MACHO Project: Microlensing Results from 5.7 Years of LargeMagellanic Cloud Observations". en. In: *The Astrophysical Journal* 542.1. Publisher: IOP Publishing, p. 281. ISSN: 0004-637X. DOI: 10.1086/309512. URL: https://iopscience.iop.org/article/10.1086/309512/meta (visited on 07/18/2025).
- Alexander, D. M. and R. C. Hickox (June 2012). "What drives the growth of black holes?" In: 56.4, pp. 93–121. DOI: 10.1016/j.newar.2011.11.003. arXiv: 1112. 1949 [astro-ph.GA].

An, T., P. Mohan, and S. Frey (Oct. 2018). "VLBI Studies of DAGN and SMBHB Hosting Galaxies". In: *Radio Science* 53.10, pp. 1211–1217. DOI: 10.1029/2018RS006647. arXiv: 1808.07651 [astro-ph.GA].

- Antonini, Fabio and David Merritt (Jan. 2012). "Dynamical Friction around Supermassive Black Holes". In: 745.1, 83, p. 83. DOI: 10.1088/0004-637X/745/1/83. arXiv: 1108.1163 [astro-ph.GA].
- Armitage, Philip J. and Priyamvada Natarajan (Mar. 2002). "Accretion during the Merger of Supermassive Black Holes". In: 567.1, pp. L9–L12. DOI: 10.1086/339770. arXiv: astro-ph/0201318 [astro-ph].
- Arzoumanian, Z. et al. (Oct. 2014). "Gravitational Waves from Individual Supermassive Black Hole Binaries in Circular Orbits: Limits from the North American Nanohertz Observatory for Gravitational Waves". In: 794.2, 141, p. 141. DOI: 10.1088/0004-637X/794/2/141. arXiv: 1404.1267 [astro-ph.GA].
- Arzoumanian, Zaven et al. (Sept. 2020). "Multimessenger Gravitational-wave Searches with Pulsar Timing Arrays: Application to 3C 66B Using the NANOGrav 11-year Data Set". In: 900.2, 102, p. 102. DOI: 10.3847/1538-4357/ababa1. arXiv: 2005.07123 [astro-ph.GA].
- Baldwin, J. A., M. M. Phillips, and R. Terlevich (Feb. 1981). "Classification parameters for the emission-line spectra of extragalactic objects." In: 93, pp. 5–19. DOI: 10.1086/130766.
- Bardati, Jaeden et al. (2024a). "Signatures of Massive Black Hole Merger Host Galaxies from Cosmological Simulations. I. Unique Galaxy Morphologies in Imaging". In: *The Astrophysical Journal* 961.1, p. 34. DOI: 10.3847/1538-4357/ad055a. URL: https://dx.doi.org/10.3847/1538-4357/ad055a.
- Bardati, Jaeden et al. (2024b). Signatures of Massive Black Hole Merger Host Galaxies from Cosmological Simulations II: Unique Stellar Kinematics in Integral Field Unit Spectroscopy. arXiv: 2407.14061 [astro-ph.GA]. URL: https://arxiv.org/abs/2407.14061.
- Barth, Aaron J. et al. (Sept. 2003). "Iron Emission in the z = 6.4 Quasar SDSS J114816.64+525150.3". In: 594.2, pp. L95–L98. DOI: 10.1086/378735. arXiv: astro-ph/0308005 [astro-ph].

Bauer, Amanda E. et al. (Sept. 2013). "Galaxy And Mass Assembly (GAMA): linking star formation histories and stellar mass growth". In: 434.1, pp. 209–221. DOI: 10.1093/mnras/stt1011. arXiv: 1306.2424 [astro-ph.CO].

- Begelman, Mitchell C, Roger D Blandford, and Martin J Rees (1980). "Massive black hole binaries in active galactic nuclei". In: *Nature* 287.5780, pp. 307–309.
- Begelman, Mitchell C., Marta Volonteri, and Martin J. Rees (July 2006). "Formation of supermassive black holes by direct collapse in pre-galactic haloes". In: 370.1, pp. 289–298. DOI: 10.1111/j.1365-2966.2006.10467.x. arXiv: astro-ph/0602363 [astro-ph].
- Benítez, Erika et al. (Jan. 2013). "Characterization of a Sample of Intermediate-type AGNs. I. Spectroscopic Properties and Serendipitous Discovery of New Dual AGNs". In: 763.1, 36, p. 36. DOI: 10.1088/0004-637X/763/1/36. arXiv: 1212.1189 [astro-ph.CO].
- Binney, James and Scott Tremaine (2008). Galactic Dynamics: Second Edition.
- Blecha, Laura et al. (Apr. 2011). "Recoiling black holes in merging galaxies: relationship to active galactic nucleus lifetimes, starbursts and the MBH-\* relation". In: Monthly Notices of the Royal Astronomical Society 412.4, pp. 2154–2182. ISSN: 0035-8711. DOI: 10.1111/j.1365-2966.2010.18042.x. eprint: https://academic.oup.com/mnras/article-pdf/412/4/2154/3325987/mnras0412-2154.pdf. URL: https://doi.org/10.1111/j.1365-2966.2010.18042.x.
- Bogdanović, Tamara, M. Coleman Miller, and Laura Blecha (Dec. 2022). "Electromagnetic counterparts to massive black-hole mergers". In: *Living Reviews in Relativity* 25.1, 3, p. 3. DOI: 10.1007/s41114-022-00037-8. arXiv: 2109.03262 [astro-ph.HE].
- Bogdanović, Tamara, Christopher S. Reynolds, and M. Coleman Miller (June 2007).

  "Alignment of the Spins of Supermassive Black Holes Prior to Coalescence". In:

  661.2, pp. L147–L150. DOI: 10.1086/518769. arXiv: astro-ph/0703054 [astro-ph].
- Bois, Maxime et al. (Sept. 2011). "The ATLAS<sup>3D</sup> project VI. Simulations of binary galaxy mergers and the link with fast rotators, slow rotators and kinematically distinct cores". In: 416.3, pp. 1654–1679. DOI: 10.1111/j.1365-2966.2011. 19113.x. arXiv: 1105.4076 [astro-ph.CO].

Bolton, C. T. (Feb. 1972). "Identification of Cygnus X-1 with HDE 226868". In: 235.5336, pp. 271–273. DOI: 10.1038/235271b0.

- Bower, G. A. et al. (Jan. 1998). "Kinematics of the Nuclear Ionized Gas in the Radio Galaxy M84 (NGC 4374)". In: 492.2, pp. L111–L114. DOI: 10.1086/311109. arXiv: astro-ph/9710264 [astro-ph].
- Bravais, A. (1844). Analyse mathématique sur les probabilités des erreurs de situation d'un point. fr. Google-Books-ID: 7g\_hAQAACAAJ. Impr. Royale.
- Brinchmann, J. et al. (July 2004). "The physical properties of star-forming galaxies in the low-redshift Universe". In: 351.4, pp. 1151–1179. DOI: 10.1111/j.1365-2966.2004.07881.x. arXiv: astro-ph/0311060 [astro-ph].
- Bundy, Kevin et al. (2014). "OVERVIEW OF THE SDSS-IV MaNGA SURVEY: MAPPING NEARBY GALAXIES AT APACHE POINT OBSERVATORY". In: *The Astrophysical Journal* 798.1, p. 7. DOI: 10.1088/0004-637X/798/1/7. URL: https://dx.doi.org/10.1088/0004-637X/798/1/7.
- Burke-Spolaor, Sarah et al. (June 2019). "The astrophysics of nanohertz gravitational waves". In: 27.1, 5, p. 5. DOI: 10.1007/s00159-019-0115-7. arXiv: 1811.08826 [astro-ph.HE].
- Campanelli, Manuela et al. (June 2007). "Maximum Gravitational Recoil". In: *Physical Review Letters* 98.23. ISSN: 1079-7114. DOI: 10.1103/physrevlett.98.231102. URL: http://dx.doi.org/10.1103/PhysRevLett.98.231102.
- Cappellari, Michele et al. (May 2011). "The ATLAS<sup>3D</sup> project I. A volume-limited sample of 260 nearby early-type galaxies: science goals and selection criteria". In: 413.2, pp. 813–836. DOI: 10.1111/j.1365-2966.2010.18174.x. arXiv: 1012.1551 [astro-ph.CO].
- Carr, B. J., J. R. Bond, and W. D. Arnett (Feb. 1984). "Cosmological consequences of Population III stars". In: 277, pp. 445–469. DOI: 10.1086/161713.
- Carr, Bernard J. (2003). "Primordial Black Holes as a Probe of Cosmology and High Energy Physics". In: *Quantum Gravity: From Theory to Experimental Search*. Ed. by Domenico Giulini, Claus Kiefer, and Claus Laemmerzahl. Vol. 631, pp. 301–321. DOI: 10.1007/978-3-540-45230-0\_7.
- Casares, Jorge (Apr. 2007). "Observational evidence for stellar-mass black holes". In: Black Holes from Stars to Galaxies – Across the Range of Masses. Ed. by Vladimír

Karas and Giorgio Matt. Vol. 238. IAU Symposium, pp. 3–12. DOI: 10.1017/S1743921307004590. arXiv: astro-ph/0612312 [astro-ph].

- Catalán-Torrecilla, C. et al. (Dec. 2015). "Star formation in the local Universe from the CALIFA sample. I. Calibrating the SFR using integral field spectroscopy data". In: 584, A87, A87. DOI: 10.1051/0004-6361/201526023. arXiv: 1507.03801 [astro-ph.GA].
- Cella, Katharine, Stephen R. Taylor, and Luke Zoltan Kelley (July 2024). "Host Galaxy Demographics Of Individually Detectable Supermassive Black-hole Binaries with Pulsar Timing Arrays". In: *arXiv e-prints*, arXiv:2407.01659, arXiv:2407.01659. DOI: 10.48550/arXiv.2407.01659. arXiv: 2407.01659 [astro-ph.GA].
- Chandrasekhar, S. (July 1931). "The Maximum Mass of Ideal White Dwarfs". In: 74, p. 81. DOI: 10.1086/143324.
- (Mar. 1943). "Dynamical Friction. I. General Considerations: the Coefficient of Dynamical Friction." In: 97, p. 255. DOI: 10.1086/144517.
- Charisi, Maria et al. (Feb. 2024). "Efficient Large-Scale, Targeted Gravitational-Wave Probes of Supermassive Black-Hole Binaries". In: 132.6, 061401, p. 061401. DOI: 10.1103/PhysRevLett.132.061401. arXiv: 2304.03786 [gr-qc].
- Chiara Guzzetti, Maria et al. (May 2016). "Gravitational waves from inflation". In: arXiv e-prints, arXiv:1605.01615, arXiv:1605.01615. DOI: 10.48550/arXiv.1605.01615. arXiv: 1605.01615 [astro-ph.CO].
- Clark, Paul C., Simon C. O. Glover, and Ralf S. Klessen (Jan. 2008). "The First Stellar Cluster". In: 672.2, pp. 757–764. DOI: 10.1086/524187.
- Comerford, Julia M. and Jenny E. Greene (July 2014). "Offset Active Galactic Nuclei as Tracers of Galaxy Mergers and Supermassive Black Hole Growth". In: 789.2, 112, p. 112. DOI: 10.1088/0004-637X/789/2/112. arXiv: 1405.6711 [astro-ph.GA].
- Condon, J. J. (Jan. 1992). "Radio emission from normal galaxies." In: 30, pp. 575–611.

  DOI: 10.1146/annurev.aa.30.090192.003043.
- Davis, Timothy A. et al. (Nov. 2014). "The ATLAS<sup>3D</sup> Project XXVIII. Dynamically driven star formation suppression in early-type galaxies". In: 444.4, pp. 3427–3445. DOI: 10.1093/mnras/stu570. arXiv: 1403.4850 [astro-ph.GA].

Davis, Timothy A. et al. (Jan. 2016). "The MASSIVE survey - III. Molecular gas and a broken Tully-Fisher relation in the most massive early-type galaxies". In: 455.1, pp. 214–226. DOI: 10.1093/mnras/stv2313. arXiv: 1510.00729 [astro-ph.GA].

- De Rosa, Alessandra et al. (Dec. 2019). "The quest for dual and binary supermassive black holes: A multi-messenger view". In: *New Astronomy Reviews* 86, p. 101525. ISSN: 1387-6473. DOI: 10.1016/j.newar.2020.101525. URL: http://dx.doi.org/10.1016/j.newar.2020.101525.
- Deane, R. P. et al. (July 2014). "A close-pair binary in a distant triple supermassive black hole system". In: 511.7507, pp. 57–60. DOI: 10.1038/nature13454. arXiv: 1406.6365 [astro-ph.GA].
- Devecchi, B. and M. Volonteri (Mar. 2009). "Formation of the First Nuclear Clusters and Massive Black Holes at High Redshift". In: 694.1, pp. 302–313. DOI: 10.1088/0004-637X/694/1/302. arXiv: 0810.1057 [astro-ph].
- Di Matteo, Tiziana, Volker Springel, and Lars Hernquist (Feb. 2005). "Energy input from quasars regulates the growth and activity of black holes and their host galaxies". In: *Nature* 433. ADS Bibcode: 2005Natur.433..604D, pp. 604–607. ISSN: 0028-0836. DOI: 10.1038/nature03335. URL: https://ui.adsabs.harvard.edu/abs/2005Natur.433..604D (visited on 05/30/2025).
- Dong-Páez, Chi An et al. (Aug. 2023). "Multi-messenger study of merging massive black holes in the OBELISK simulation: Gravitational waves, electromagnetic counterparts, and their link to galaxy and black-hole populations". In: 676, A2, A2. DOI: 10.1051/0004-6361/202346435. arXiv: 2303.09569 [astro-ph.HE].
- D'Orazio, Daniel J., Zoltán Haiman, and Andrew MacFadyen (Dec. 2013). "Accretion into the central cavity of a circumbinary disc". In: 436.4, pp. 2997–3020. DOI: 10. 1093/mnras/stt1787. arXiv: 1210.0536 [astro-ph.GA].
- Dullo, Bililign T. (Dec. 2019). "The Most Massive Galaxies with Large Depleted Cores: Structural Parameter Relations and Black Hole Masses". In: 886.2, 80, p. 80. DOI: 10.3847/1538-4357/ab4d4f. arXiv: 1910.10240 [astro-ph.GA].
- Dullo, Bililign T., Armando Gil de Paz, and Johan H. Knapen (Feb. 2021). "Ultramassive Black Holes in the Most Massive Galaxies:  $M_{BH}$ - $\sigma$  versus  $M_{BH}$ - $R_b$ ". In: 908.2, 134, p. 134. DOI: 10.3847/1538-4357/abceae. arXiv: 2012.04471 [astro-ph.GA].

Einstein, Albert (Jan. 1915). "Die Feldgleichungen der Gravitation". In: Sitzungsberichte der Königlich Preussischen Akademie der Wissenschaften, pp. 844–847. URL: https://ui.adsabs.harvard.edu/abs/1915SPAW.....844E (visited on 05/05/2025).

- Ellis, John et al. (Aug. 2023). "Prospects for future binary black hole gravitational wave studies in light of PTA measurements". In: 676, A38, A38. DOI: 10.1051/0004-6361/202346268. arXiv: 2301.13854 [astro-ph.C0].
- Emsellem, Eric et al. (Aug. 2007). "The SAURON project IX. A kinematic classification for early-type galaxies". In: 379.2, pp. 401–417. DOI: 10.1111/j.1365-2966.2007.11752.x. arXiv: astro-ph/0703531 [astro-ph].
- Emsellem, Eric et al. (June 2011). "The ATLAS<sup>3D</sup> project III. A census of the stellar angular momentum within the effective radius of early-type galaxies: unveiling the distribution of fast and slow rotators". In: 414.2, pp. 888–912. DOI: 10.1111/j.1365-2966.2011.18496.x. arXiv: 1102.4444 [astro-ph.CO].
- Ene, Irina et al. (Sept. 2018). "The MASSIVE Survey X. Misalignment between kinematic and photometric axes and intrinsic shapes of massive early-type galaxies". In: 479.2, pp. 2810–2826. DOI: 10.1093/mnras/sty1649. arXiv: 1802.00014 [astro-ph.GA].
- Enoki, Motohiro et al. (Nov. 2004). "Gravitational Waves from Supermassive Black Hole Coalescence in a Hierarchical Galaxy Formation Model". In: 615.1, pp. 19–28. DOI: 10.1086/424475. arXiv: astro-ph/0404389 [astro-ph].
- EPTA Collaboration et al. (Oct. 2023). "The second data release from the European Pulsar Timing Array. III. Search for gravitational wave signals". In: 678, A50, A50. DOI: 10.1051/0004-6361/202346844. arXiv: 2306.16214 [astro-ph.HE].
- Eracleous, Michael and Jules P. Halpern (Jan. 1994). "Double-peaked Emission Lines in Active Galactic Nuclei". In: 90, p. 1. DOI: 10.1086/191856.
- Eracleous, Michael et al. (Nov. 1997). "Rejection of the Binary Broad-Line Region Interpretation of Double-peaked Emission Lines in Three Active Galactic Nuclei". In: 490.1, pp. 216–226. DOI: 10.1086/304859. arXiv: astro-ph/9706222 [astro-ph].

Eracleous, Michael et al. (Aug. 2012). "A Large Systematic Search for Close Supermassive Binary and Rapidly Recoiling Black Holes". In: 201.2, 23, p. 23. DOI: 10.1088/0067-0049/201/2/23. arXiv: 1106.2952 [astro-ph.CO].

- Event Horizon Telescope Collaboration et al. (Apr. 2019). "First M87 Event Horizon Telescope Results. VI. The Shadow and Mass of the Central Black Hole". In: 875.1, L6, p. L6. DOI: 10.3847/2041-8213/ab1141. arXiv: 1906.11243 [astro-ph.GA].
- Event Horizon Telescope Collaboration et al. (May 2022). "First Sagittarius A\* Event Horizon Telescope Results. I. The Shadow of the Supermassive Black Hole in the Center of the Milky Way". In: 930.2, L12, p. L12. DOI: 10.3847/2041-8213/ac6674.
- Faber, S. M. et al. (Nov. 1997). "The Centers of Early-Type Galaxies with HST. IV. Central Parameter Relations." In: 114, p. 1771. DOI: 10.1086/118606. arXiv: astro-ph/9610055 [astro-ph].
- Falcón-Barroso, J. et al. (Jan. 2017). "Stellar kinematics across the Hubble sequence in the CALIFA survey: general properties and aperture corrections". In: 597, A48, A48. DOI: 10.1051/0004-6361/201628625. arXiv: 1609.06446 [astro-ph.GA].
- Falcón-Barroso, J. et al. (Dec. 2019). "The CALIFA view on stellar angular momentum across the Hubble sequence". In: 632, A59, A59. DOI: 10.1051/0004-6361/201936413. arXiv: 1910.06236 [astro-ph.GA].
- Ferrarese, Laura and Holland Ford (Feb. 2005). "Supermassive Black Holes in Galactic Nuclei: Past, Present and Future Research". en. In: *Space Science Reviews* 116.3, pp. 523–624. ISSN: 1572-9672. DOI: 10.1007/s11214-005-3947-6. URL: https://doi.org/10.1007/s11214-005-3947-6 (visited on 05/30/2025).
- Ferrarese, Laura and David Merritt (Aug. 2000). "A Fundamental Relation between Supermassive Black Holes and Their Host Galaxies". In: *The Astrophysical Journal* 539. Publisher: IOP ADS Bibcode: 2000ApJ...539L...9F, pp. L9–L12. ISSN: 0004-637X. DOI: 10.1086/312838. URL: https://ui.adsabs.harvard.edu/abs/2000ApJ...539L...9F (visited on 05/30/2025).
- Finoguenov, A. et al. (Jan. 2007). "XMM-Newton study of 0.012 < z < 0.024 groups I. Overview of the IGM thermodynamics". In: 374.2, pp. 737–760. DOI: 10.1111/j.1365-2966.2006.11194.x. arXiv: astro-ph/0611846 [astro-ph].

Fu, Hai et al. (Jan. 2012). "The Nature of Double-peaked [O III] Active Galactic Nuclei". In: 745.1, 67, p. 67. DOI: 10.1088/0004-637X/745/1/67. arXiv: 1107.3564 [astro-ph.CO].

- Gallazzi, Anna et al. (Sept. 2005). "The ages and metallicities of galaxies in the local universe". In: 362.1, pp. 41–58. DOI: 10.1111/j.1365-2966.2005.09321.x. arXiv: astro-ph/0506539 [astro-ph].
- Gebhardt, Karl et al. (Aug. 2000). "A Relationship between Nuclear Black Hole Mass and Galaxy Velocity Dispersion". In: *The Astrophysical Journal* 539. Publisher: IOP ADS Bibcode: 2000ApJ...539L..13G, pp. L13–L16. ISSN: 0004-637X. DOI: 10.1086/312840. URL: https://ui.adsabs.harvard.edu/abs/2000ApJ...539L..13G (visited on 05/30/2025).
- Gerke, Brian F. et al. (May 2007). "The DEEP2 Galaxy Redshift Survey: AEGIS Observations of a Dual AGN at z=0.7". In: 660.1, pp. L23–L26. DOI: 10.1086/517968. arXiv: astro-ph/0608380 [astro-ph].
- Ghez, A. M. et al. (Dec. 1998). "High Proper-Motion Stars in the Vicinity of Sagittarius A\*: Evidence for a Supermassive Black Hole at the Center of Our Galaxy". In: 509.2, pp. 678–686. DOI: 10.1086/306528. arXiv: astro-ph/9807210 [astro-ph].
- Ghez, A. M. et al. (Sept. 2000). "The accelerations of stars orbiting the Milky Way's central black hole". In: 407.6802, pp. 349–351. DOI: 10.1038/35030032. arXiv: astro-ph/0009339 [astro-ph].
- Goldstein, Janna M. et al. (July 2018). "Null-stream analysis of Pulsar Timing Array data: localization of resolvable gravitational wave sources". In: 477.4, pp. 5447–5459. DOI: 10.1093/mnras/sty892. arXiv: 1712.03975 [astro-ph.IM].
- Goldstein, Janna M. et al. (May 2019). "Associating host galaxy candidates to massive black hole binaries resolved by pulsar timing arrays". In: 485.1, pp. 248–259.

  DOI: 10.1093/mnras/stz420. arXiv: 1812.02670 [astro-ph.IM].
- González Delgado, R. M. et al. (Sept. 2015). "The CALIFA survey across the Hubble sequence. Spatially resolved stellar population properties in galaxies". In: 581, A103, A103. DOI: 10.1051/0004-6361/201525938. arXiv: 1506.04157 [astro-ph.GA].

Graham, Matthew J. et al. (Feb. 2015). "A possible close supermassive black-hole binary in a quasar with optical periodicity". In: 518.7537, pp. 74–76. DOI: 10. 1038/nature14143. arXiv: 1501.01375 [astro-ph.GA].

- Greene, Jenny E. et al. (Mar. 2019). "The MASSIVE Survey. XII. Connecting Stellar Populations of Early-type Galaxies to Kinematics and Environment". In: 874.1, 66, p. 66. DOI: 10.3847/1538-4357/ab01e3. arXiv: 1901.01271 [astro-ph.GA].
- Grunthal, Kathrin et al. (Dec. 2024). "The MeerKAT Pulsar Timing Array: Maps of the gravitational-wave sky with the 4.5 year data release". In: *arXiv e-prints*, arXiv:2412.01214, arXiv:2412.01214. DOI: 10.48550/arXiv.2412.01214. arXiv: 2412.01214 [astro-ph.HE].
- Gu, Jun-Hua et al. (Jan. 2012). "Group-scale asymmetric abundance structures in the NGC 533 group". In: *Research in Astronomy and Astrophysics* 12.1, pp. 63–74. DOI: 10.1088/1674-4527/12/1/005.
- Haehnelt, Martin G. and Martin J. Rees (July 1993). "The formation of nuclei in newly formed galaxies and the evolution of the quasar population". In: 263.1, pp. 168–178. DOI: 10.1093/mras/263.1.168.
- Häring, Nadine and Hans-Walter Rix (Apr. 2004). "On the Black Hole Mass-Bulge Mass Relation". In: 604.2, pp. L89–L92. DOI: 10.1086/383567. arXiv: astro-ph/0402376 [astro-ph].
- Harms, Richard J. et al. (Nov. 1994). "HST FOS Spectroscopy of M87: Evidence for a Disk of Ionized Gas around a Massive Black Hole". In: 435, p. L35. DOI: 10.1086/187588.
- Herrera Ruiz, N. et al. (May 2016). "Unveiling the origin of the radio emission in radio-quiet quasars". In: 589, L2, p. L2. DOI: 10.1051/0004-6361/201628302. arXiv: 1603.07136 [astro-ph.GA].
- Hills, J. G. (Aug. 1983). "The effect of low-velocity, low-mass intruders (collisionless gas) on the dynamical evolution of a binary system". In: 88, pp. 1269–1283. DOI: 10.1086/113418.
- Hobbs, G. (Nov. 2013). "The Parkes Pulsar Timing Array". In: *Classical and Quantum Gravity* 30.22, 224007, p. 224007. DOI: 10.1088/0264-9381/30/22/224007. arXiv: 1307.2629 [astro-ph.IM].

Holley-Bockelmann, Kelly and Douglas O. Richstone (Mar. 2000). "The Role of a Massive Central Singularity in Galactic Mergers on the Survival of the Core Fundamental Plane". In: 531.1, pp. 232–244. DOI: 10.1086/308447. arXiv: astro-ph/9908258 [astro-ph].

- Holz, Daniel E. and Scott A. Hughes (Aug. 2005). "Using Gravitational-Wave Standard Sirens". In: 629.1, pp. 15–22. DOI: 10.1086/431341. arXiv: astro-ph/0504616 [astro-ph].
- Hopkins, Philip F. et al. (May 2010). "Mergers and Bulge Formation in ΛCDM: Which Mergers Matter?" In: 715.1, pp. 202–229. DOI: 10.1088/0004-637X/715/1/202. arXiv: 0906.5357 [astro-ph.CO].
- Hopkins, Philip F. et al. (Nov. 2014). "Galaxies on FIRE (Feedback In Realistic Environments): stellar feedback explains cosmologically inefficient star formation".

  In: 445.1, pp. 581–603. DOI: 10.1093/mnras/stu1738. arXiv: 1311.2073 [astro-ph.CO].
- Horlaville, Patrick et al. (Apr. 2025). "Predicting Potential Host Galaxies of Supermassive Black Hole Binaries Based on Stellar Kinematics in Archival IFU Surveys". In: *arXiv e-prints*, arXiv:2504.21145, arXiv:2504.21145. DOI: 10.48550/arXiv. 2504.21145. arXiv: 2504.21145 [astro-ph.GA].
- Hu, Betty X. et al. (July 2020). "Spikey: self-lensing flares from eccentric SMBH binaries". In: 495.4, pp. 4061–4070. DOI: 10.1093/mnras/staa1312. arXiv: 1910.05348 [astro-ph.HE].
- Ivezić, Željko et al. (Nov. 2002). "Optical and Radio Properties of Extragalactic Sources Observed by the FIRST Survey and the Sloan Digital Sky Survey". en. In: *The Astronomical Journal* 124.5. Publisher: IOP Publishing, p. 2364. ISSN: 1538-3881. DOI: 10.1086/344069. URL: https://iopscience.iop.org/article/10.1086/344069/meta (visited on 07/19/2025).
- Izquierdo-Villalba, David, Alberto Sesana, and Monica Colpi (Feb. 2023). "Unveiling the hosts of parsec-scale massive black hole binaries: morphology and electromagnetic signatures". In: 519.2, pp. 2083–2100. DOI: 10.1093/mnras/stac3677. arXiv: 2207.04064 [astro-ph.GA].
- Jaffe, A. H. and D. C. Backer (Feb. 2003). "Gravitational Waves Probe the Coalescence Rate of Massive Black Hole Binaries". In: 583.2, pp. 616–631. DOI: 10.1086/345443. arXiv: astro-ph/0210148 [astro-ph].

Jahnke, Knud and Andrea V. Macciò (June 2011). "The Non-causal Origin of the Black-hole-galaxy Scaling Relations". In: 734.2, 92, p. 92. DOI: 10.1088/0004-637X/734/2/92. arXiv: 1006.0482 [astro-ph.CO].

- Johnson, Jarrett L. and Volker Bromm (Feb. 2007). "The aftermath of the first stars: massive black holes". In: 374.4, pp. 1557–1568. DOI: 10.1111/j.1365-2966.2006. 11275.x. arXiv: astro-ph/0605691 [astro-ph].
- Kelley, Luke Zoltan, Laura Blecha, and Lars Hernquist (Jan. 2017). "Massive black hole binary mergers in dynamical galactic environments". In: 464.3, pp. 3131–3157. DOI: 10.1093/mnras/stw2452. arXiv: 1606.01900 [astro-ph.HE].
- Kennicutt Jr., Robert C. (Jan. 1998). "Star Formation in Galaxies Along the Hubble Sequence". In: 36, pp. 189–232. DOI: 10.1146/annurev.astro.36.1.189. arXiv: astro-ph/9807187 [astro-ph].
- Khlopov, M. Yu., S. G. Rubin, and A. S. Sakharov (Mar. 2005). "Primordial structure of massive black hole clusters". In: *Astroparticle Physics* 23.2, pp. 265–277. DOI: 10.1016/j.astropartphys.2004.12.002. arXiv: astro-ph/0401532 [astro-ph].
- Khonji, Nader et al. (Oct. 2024). "Core Formation by Binary Scouring and Gravitational Wave Recoil in Massive Elliptical Galaxies". In: 974.2, 204, p. 204. DOI: 10.3847/1538-4357/ad7390. arXiv: 2408.12537 [astro-ph.GA].
- Kim, D. C. et al. (June 2016). "Kinematically Identified Recoiling Supermassive Black Hole Candidates in SDSS QSOs with z>0.25". In: 824.2, 122, p. 122. DOI: 10. 3847/0004-637X/824/2/122. arXiv: 1604.05604 [astro-ph.GA].
- King, Andrew (Oct. 2003). "Black Holes, Galaxy Formation, and the  $M_{BH}$ - $\sigma$  Relation". In: 596.1, pp. L27–L29. DOI: 10.1086/379143. arXiv: astro-ph/0308342 [astro-ph].
- Klessen, Ralf S. and Simon C. O. Glover (Aug. 2023). "The First Stars: Formation, Properties, and Impact". In: 61, pp. 65–130. DOI: 10.1146/annurev-astro-071221-053453. arXiv: 2303.12500 [astro-ph.CO].
- Komossa, S. et al. (Jan. 2003). "Discovery of a Binary Active Galactic Nucleus in the Ultraluminous Infrared Galaxy NGC 6240 Using Chandra". In: 582.1, pp. L15–L19. DOI: 10.1086/346145. arXiv: astro-ph/0212099 [astro-ph].
- Kormendy, John and Luis C. Ho (Aug. 2013). "Coevolution (Or Not) of Supermassive Black Holes and Host Galaxies". In: *Annual Review of Astronomy and Astrophysics*

51. ADS Bibcode: 2013ARA&A..51..511K, pp. 511-653. ISSN: 0066-4146. DOI: 10. 1146/annurev-astro-082708-101811. URL: https://ui.adsabs.harvard.edu/abs/2013ARA&A..51..511K (visited on 05/30/2025).

- Kormendy, John and Douglas Richstone (Jan. 1995). "Inward Bound—The Search For Supermassive Black Holes In Galactic Nuclei". In: *Annual Review of Astronomy and Astrophysics* 33. ADS Bibcode: 1995ARA&A..33..581K, p. 581. ISSN: 0066-4146. DOI: 10.1146/annurev.aa.33.090195.003053. URL: https://ui.adsabs.harvard.edu/abs/1995ARA&A..33..581K (visited on 05/30/2025).
- Koss, Michael J. et al. (Nov. 2018). "A population of luminous accreting black holes with hidden mergers". In: 563.7730, pp. 214–216. DOI: 10.1038/s41586-018-0652-7. arXiv: 1811.03641 [astro-ph.GA].
- Koushiappas, Savvas M., James S. Bullock, and Avishai Dekel (Oct. 2004). "Massive black hole seeds from low angular momentum material". In: 354.1, pp. 292–304. DOI: 10.1111/j.1365-2966.2004.08190.x. arXiv: astro-ph/0311487 [astro-ph].
- Krajnović, Davor et al. (July 2011). "The ATLAS<sup>3D</sup> project II. Morphologies, kinemetric features and alignment between photometric and kinematic axes of early-type galaxies". In: 414.4, pp. 2923–2949. DOI: 10.1111/j.1365-2966.2011. 18560.x. arXiv: 1102.3801 [astro-ph.C0].
- Krajnović, Davor et al. (Aug. 2013). "The ATLAS<sup>3D</sup> Project XXIII. Angular momentum and nuclear surface brightness profiles". In: 433.4, pp. 2812–2839. DOI: 10.1093/mnras/stt905. arXiv: 1305.4973 [astro-ph.CO].
- Kramer, Michael and David J. Champion (Nov. 2013). "The European Pulsar Timing Array and the Large European Array for Pulsars". In: *Classical and Quantum Gravity* 30.22, 224009, p. 224009. DOI: 10.1088/0264-9381/30/22/224009.
- Krolik, Julian H. et al. (July 2019). "Population Estimates for Electromagnetically Distinguishable Supermassive Binary Black Holes". In: 879.2, 110, p. 110. DOI: 10.3847/1538-4357/ab24c9. arXiv: 1905.10450 [astro-ph.GA].
- Laine, Seppo et al. (Feb. 2003). "Hubble Space Telescope Imaging of Brightest Cluster Galaxies". In: 125.2, pp. 478–505. DOI: 10.1086/345823. arXiv: astro-ph/0211074 [astro-ph].

Laplace, Pierre Simon (1796). Exposition du système du monde. DOI: 10.3931/e-rara-497.

- Lauer, T. R. et al. (Dec. 1995). "The Centers of Early-Type Galaxies with HST.I.An Observational Survey". In: 110, p. 2622. DOI: 10.1086/117719.
- Lauer, Tod R. et al. (Oct. 2002). "Galaxies with a Central Minimum in Stellar Luminosity Density". In: 124.4, pp. 1975–1987. DOI: 10.1086/342932. arXiv: astro-ph/0206122 [astro-ph].
- Lauer, Tod R. et al. (May 2005). "The Centers of Early-Type Galaxies with Hubble Space Telescope. V. New WFPC2 Photometry". In: 129.5, pp. 2138–2185. DOI: 10. 1086/429565. arXiv: astro-ph/0412040 [astro-ph].
- Lauer, Tod R. et al. (July 2007a). "The Centers of Early-Type Galaxies with Hubble Space Telescope. VI. Bimodal Central Surface Brightness Profiles". In: 664.1, pp. 226–256. DOI: 10.1086/519229. arXiv: astro-ph/0609762 [astro-ph].
- Lauer, Tod R. et al. (June 2007b). "The Masses of Nuclear Black Holes in Luminous Elliptical Galaxies and Implications for the Space Density of the Most Massive Black Holes". In: 662.2, pp. 808–834. DOI: 10.1086/518223. arXiv: astro-ph/0606739 [astro-ph].
- Law-Smith, Jamie and Daniel J. Eisenstein (Feb. 2017). "The Color and Stellar Mass Dependence of Small-scale Galaxy Clustering in SDSS-III BOSS". In: 836.1, 87, p. 87. DOI: 10.3847/1538-4357/836/1/87. arXiv: 1702.03933 [astro-ph.GA].
- Lena, D. et al. (Nov. 2014). "Recoiling Supermassive Black Holes: A Search in the Nearby Universe". In: 795.2, 146, p. 146. DOI: 10.1088/0004-637X/795/2/146. arXiv: 1409.3976 [astro-ph.GA].
- Lentati, L. et al. (Nov. 2015). "European Pulsar Timing Array limits on an isotropic stochastic gravitational-wave background". In: 453.3, pp. 2576–2598. DOI: 10.1093/mnras/stv1538. arXiv: 1504.03692 [astro-ph.CO].
- Li, Kunyang et al. (July 2022). "Massive Black Hole Binaries from the TNG50-3 Simulation. I. Coalescence and LISA Detection Rates". In: 933.1, 104, p. 104. DOI: 10.3847/1538-4357/ac74b5. arXiv: 2201.11088 [astro-ph.GA].
- Liepold, Emily R. and Chung-Pei Ma (Aug. 2024). "Big Galaxies and Big Black Holes: The Massive Ends of the Local Stellar and Black Hole Mass Functions and the

Implications for Nanohertz Gravitational Waves". In: 971.2, L29, p. L29. DOI: 10. 3847/2041-8213/ad66b8. arXiv: 2407.14595 [astro-ph.GA].

- LIGO Virgo, KAGRA (2025). LIGO-Virgo-KAGRA Announce the 200th Gravitational Wave Detection of O4! URL: https://www.ligo.caltech.edu/news/ligo20250320 (visited on 07/19/2025).
- Liu, Tingting and Sarah J. Vigeland (Nov. 2021). "Multi-messenger Approaches to Supermassive Black Hole Binary Detection and Parameter Estimation: Implications for Nanohertz Gravitational Wave Searches with Pulsar Timing Arrays". In: 921.2, 178, p. 178. DOI: 10.3847/1538-4357/ac1da9. arXiv: 2105.08087 [astro-ph.HE].
- Liu, Tingting et al. (Mar. 2023). "Multi-messenger Approaches to Supermassive Black Hole Binary Detection and Parameter Estimation. II. Optimal Strategies for a Pulsar Timing Array". In: 945.1, 78, p. 78. DOI: 10.3847/1538-4357/acb492. arXiv: 2301.07135 [astro-ph.HE].
- Lobanov, A. P. and J. Roland (Mar. 2005). "A supermassive binary black hole in the quasar 3C 345". In: 431.3, pp. 831–846. DOI: 10.1051/0004-6361: 20041831. arXiv: astro-ph/0411417 [astro-ph].
- Loeb, Abraham and Frederic A. Rasio (Sept. 1994). "Collapse of Primordial Gas Clouds and the Formation of Quasar Black Holes". In: 432, p. 52. DOI: 10.1086/174548. arXiv: astro-ph/9401026 [astro-ph].
- Lotz, Jennifer M., Joel Primack, and Piero Madau (July 2004). "A New Nonparametric Approach to Galaxy Morphological Classification". In: 128.1, pp. 163–182.

  DOI: 10.1086/421849. arXiv: astro-ph/0311352 [astro-ph].
- Lynden-Bell, D. (Mar. 1978). "Gravity power." In: 17, pp. 185–191. DOI: 10.1088/0031-8949/17/3/009.
- Ma, Chung-Pei et al. (2014). "THE MASSIVE SURVEY. I. A VOLUME-LIMITED INTEGRAL-FIELD SPECTROSCOPIC STUDY OF THE MOST MASSIVE EARLY-TYPE GALAXIES WITHIN 108 Mpc". In: *The Astrophysical Journal* 795.2, p. 158. DOI: 10.1088/0004-637X/795/2/158. URL: https://dx.doi.org/10.1088/0004-637X/795/2/158.

Ma, Xiangcheng et al. (Feb. 2016). "The origin and evolution of the galaxy mass-metallicity relation". In: 456.2, pp. 2140–2156. DOI: 10.1093/mnras/stv2659. arXiv: 1504.02097 [astro-ph.GA].

- Madau, Piero and Mark Dickinson (Aug. 2014). "Cosmic Star-Formation History". In: 52, pp. 415–486. DOI: 10.1146/annurev-astro-081811-125615. arXiv: 1403. 0007 [astro-ph.CO].
- Mahtessian, A. P. (July 1998). "Groups of galaxies. III. Some empirical characteristics." In: *Astrophysics* 41.3, pp. 308–321. DOI: 10.1007/BF03036100.
- Malmquist, K. G. (Mar. 1922). "On some relations in stellar statistics". In: *Meddelanden fran Lunds Astronomiska Observatorium Serie I* 100, pp. 1–52.
- Mandel, Ilya (n.d.). Eddington luminosity or Eddington limit. URL: https://ilyamandel.github.io/BackOfTheEnvelopeNotes/Eddington.pdf.
- Massonneau, Warren et al. (Feb. 2023). "How the super-Eddington regime regulates black hole growth in high-redshift galaxies". In: 670, A180, A180. DOI: 10.1051/0004-6361/202243170. arXiv: 2201.08766 [astro-ph.GA].
- Mateos, S. et al. (June 2017). "Survival of the Obscuring Torus in the Most Powerful Active Galactic Nuclei". In: 841.2, L18, p. L18. DOI: 10.3847/2041-8213/aa7268. arXiv: 1705.04323 [astro-ph.HE].
- Matthews, Thomas A. and Allan R. Sandage (July 1963). "Optical Identification of 3C 48, 3C 196, and 3C 286 with Stellar Objects." In: 138, p. 30. DOI: 10.1086/147615.
- McDermid, Richard M. et al. (Apr. 2015). "The ATLAS<sup>3D</sup> Project XXX. Star formation histories and stellar population scaling relations of early-type galaxies". In: 448.4, pp. 3484–3513. DOI: 10.1093/mnras/stv105. arXiv: 1501.03723 [astro-ph.GA].
- Michell, John (Jan. 1784). "VII. On the means of discovering the distance, magnitude, &c. of the fixed stars, in consequence of the diminution of the velocity of their light, in case such a diminution should be found to take place in any of them, and such other data should be procured from observations, as would be farther necessary for that purpose. By the Rev. John Michell, B.D. F.R.S. In a letter to Henry Cavendish, Esq. F.R.S. and A.S". In: *Philosophical Transactions of the Royal Society of London* 74. Publisher: Royal Society, pp. 35–57. DOI: 10.1098/rstl. 1784.0008. URL: https://royalsocietypublishing.org/doi/10.1098/rstl. 1784.0008 (visited on 04/07/2025).

Miller-Jones, James C. A. et al. (Mar. 2021). "Cygnus X-1 contains a 21-solar mass black hole—Implications for massive star winds". In: *Science* 371.6533, pp. 1046–1049. DOI: 10.1126/science.abb3363. arXiv: 2102.09091 [astro-ph.HE].

- Milosavljević, Miloš, Sean M. Couch, and Volker Bromm (May 2009). "Accretion Onto Intermediate-Mass Black Holes in Dense Protogalactic Clouds". In: 696.2, pp. L146–L149. DOI: 10.1088/0004-637X/696/2/L146. arXiv: 0812.2516 [astro-ph].
- Miyoshi, Makoto et al. (Jan. 1995). "Evidence for a black hole from high rotation velocities in a sub-parsec region of NGC4258". In: 373.6510, pp. 127–129. DOI: 10.1038/373127a0.
- Naab, Thorsten et al. (Nov. 2014). "The ATLAS<sup>3D</sup> project XXV. Two-dimensional kinematic analysis of simulated galaxies and the cosmological origin of fast and slow rotators". In: 444.4, pp. 3357–3387. DOI: 10.1093/mnras/stt1919. arXiv: 1311.0284 [astro-ph.CO].
- Nasim, Imran Tariq et al. (Apr. 2021). "Formation of the largest galactic cores through binary scouring and gravitational wave recoil". In: 502.4, pp. 4794–4814. DOI: 10.1093/mnras/stab435. arXiv: 2011.04663 [astro-ph.GA].
- Netzer, Hagai (Aug. 2015). "Revisiting the Unified Model of Active Galactic Nuclei". In: 53, pp. 365–408. DOI: 10.1146/annurev-astro-082214-122302. arXiv: 1505.00811 [astro-ph.GA].
- Nevin, R. et al. (Feb. 2019). "Accurate Identification of Galaxy Mergers with Imaging". In: 872.1, 76, p. 76. DOI: 10.3847/1538-4357/aafd34. arXiv: 1901.01975 [astro-ph.GA].
- Oda, M. et al. (May 1971). "X-Ray Pulsations from Cygnus X-1 Observed from UHURU". In: 166, p. L1. DOI: 10.1086/180726.
- Omukai, K., R. Schneider, and Z. Haiman (Oct. 2008). "Can Supermassive Black Holes Form in Metal-enriched High-Redshift Protogalaxies?" In: 686.2, pp. 801–814. DOI: 10.1086/591636. arXiv: 0804.3141 [astro-ph].
- Oppenheimer, J. R. and G. M. Volkoff (Feb. 1939). "On Massive Neutron Cores". In: *Physical Review* 55.4. Publisher: American Physical Society, pp. 374–381. DOI: 10.1103/PhysRev.55.374. URL: https://link.aps.org/doi/10.1103/PhysRev.55.374 (visited on 07/12/2025).

Padovani, P. et al. (Aug. 2017). "Active galactic nuclei: what's in a name?" In: 25.1, 2, p. 2. DOI: 10.1007/s00159-017-0102-9. arXiv: 1707.07134 [astro-ph.GA].

- Page, D. N. and S. W. Hawking (May 1976). "Gamma rays from primordial black holes." In: 206, pp. 1–7. DOI: 10.1086/154350.
- Pawlik, M. M. et al. (Mar. 2016). "Shape asymmetry: a morphological indicator for automatic detection of galaxies in the post-coalescence merger stages". In: 456.3, pp. 3032–3052. DOI: 10.1093/mnras/stv2878. arXiv: 1512.02000 [astro-ph.GA].
- Pelupessy, Federico I., Tiziana Di Matteo, and Benedetta Ciardi (Aug. 2007). "How Rapidly Do Supermassive Black Hole "Seeds" Grow at Early Times?" In: 665.1, pp. 107–119. DOI: 10.1086/519235. arXiv: astro-ph/0703773 [astro-ph].
- Petrov, Polina et al. (June 2024). "Identifying Host Galaxies of Supermassive Black Hole Binaries Found by PTAs". In: *arXiv e-prints*, arXiv:2406.04409, arXiv:2406.04409.

  DOI: 10.48550/arXiv.2406.04409. arXiv: 2406.04409 [astro-ph.GA].
- Pfeifle, Ryan W. et al. (Apr. 2019). "Buried Black Hole Growth in IR-selected Mergers: New Results from Chandra". In: 875.2, 117, p. 117. DOI: 10.3847/1538-4357/ab07bc. arXiv: 1904.10955 [astro-ph.GA].
- Pfeifle, Ryan W. et al. (Nov. 2024). "Super-Size Me: The Big Multi-AGN Catalog (The Big MAC), Data Release 1: The Source Catalog". In: arXiv e-prints, arXiv:2411.12799, arXiv:2411.12799. DOI: 10.48550/arXiv.2411.12799. arXiv: 2411.12799 [astro-ph.GA].
- Popović, Luka Č. (Feb. 2012). "Super-massive binary black holes and emission lines in active galactic nuclei". In: 56.2-3, pp. 74–91. DOI: 10.1016/j.newar.2011.11. 001. arXiv: 1109.0710 [astro-ph.CO].
- Quinlan, Gerald D. (July 1996). "The dynamical evolution of massive black hole binaries I. Hardening in a fixed stellar background". In: 1.1, pp. 35–56. DOI: 10. 1016/S1384-1076(96)00003-6. arXiv: astro-ph/9601092 [astro-ph].
- Ragusa, Enrico, Giuseppe Lodato, and Daniel J. Price (Aug. 2016). "Suppression of the accretion rate in thin discs around binary black holes". In: 460.2, pp. 1243–1253. DOI: 10.1093/mnras/stw1081. arXiv: 1605.01730 [astro-ph.HE].
- Rajagopal, Mohan and Roger W. Romani (June 1995). "Ultra–Low-Frequency Gravitational Radiation from Massive Black Hole Binaries". In: 446, p. 543. DOI: 10. 1086/175813. arXiv: astro-ph/9412038 [astro-ph].

Ravindranath, Swara et al. (Aug. 2001). "Central Structural Parameters of Early-Type Galaxies as Viewed with Nicmos on the Hubble Space Telescope". In: 122.2, pp. 653–678. DOI: 10.1086/321175. arXiv: astro-ph/0105390 [astro-ph].

- Rawlings, Alexander et al. (Mar. 2025). "Identifying supermassive black hole recoil in elliptical galaxies". In: 537.4, pp. 3421–3447. DOI: 10.1093/mnras/staf238. arXiv: 2410.13942 [astro-ph.GA].
- Reardon, Daniel J. et al. (July 2023). "Search for an Isotropic Gravitational-wave Background with the Parkes Pulsar Timing Array". In: 951.1, L6, p. L6. DOI: 10.3847/2041-8213/acdd02. arXiv: 2306.16215 [astro-ph.HE].
- Regan, John A. and Martin G. Haehnelt (June 2009). "Pathways to massive black holes and compact star clusters in pre-galactic dark matter haloes with virial temperatures >~10000K". In: 396.1, pp. 343–353. DOI: 10.1111/j.1365-2966. 2009.14579.x. arXiv: 0810.2802 [astro-ph].
- Rest, Armin et al. (May 2001). "WFPC2 Images of the Central Regions of Early-Type Galaxies. I. The Data". In: 121.5, pp. 2431–2482. DOI: 10.1086/320370. arXiv: astro-ph/0102286 [astro-ph].
- Ricci, C. et al. (July 2014). "Iron Kα emission in type-I and type-II active galactic nuclei". In: 441.4, pp. 3622–3633. DOI: 10.1093/mnras/stu735. arXiv: 1405.7575 [astro-ph.GA].
- Richards, Gordon T. et al. (June 2006). "The Sloan Digital Sky Survey Quasar Survey: Quasar Luminosity Function from Data Release 3". In: 131.6, pp. 2766–2787. DOI: 10.1086/503559. arXiv: astro-ph/0601434 [astro-ph].
- Richstone, D. et al. (Oct. 1998). Supermassive black holes and the evolution of galaxies. ISSN: 0028-0836 Volume: 385 ADS Bibcode: 1998Natur.395A..14R. DOI: 10.48550/arXiv.astro-ph/9810378. URL: https://ui.adsabs.harvard.edu/abs/1998Natur.395A..14R (visited on 05/30/2025).
- Rodriguez, C. et al. (July 2006). "A Compact Supermassive Binary Black Hole System". In: *The Astrophysical Journal* 646. Publisher: IOP ADS Bibcode: 2006ApJ...646...49R, pp. 49–60. ISSN: 0004-637X. DOI: 10.1086/504825. URL: https://ui.adsabs.harvard.edu/abs/2006ApJ...646...49R (visited on 06/04/2025).
- Rodriguez-Gomez, Vicente et al. (Mar. 2019). "The optical morphologies of galaxies in the IllustrisTNG simulation: a comparison to Pan-STARRS observations".

In: 483.3, pp. 4140-4159. DOI: 10.1093/mnras/sty3345. arXiv: 1809.08239 [astro-ph.GA].

- Roedig, Constanze, Julian H. Krolik, and M. Coleman Miller (Apr. 2014). "Observational Signatures of Binary Supermassive Black Holes". In: 785.2, 115, p. 115. DOI: 10.1088/0004-637X/785/2/115. arXiv: 1402.7098 [astro-ph.HE].
- Romano, M. et al. (Sept. 2021). "The ALPINE-ALMA [CII] survey. The contribution of major mergers to the galaxy mass assembly at z  $\sim$  5". In: 653, A111, A111. DOI: 10.1051/0004-6361/202141306. arXiv: 2107.10856 [astro-ph.GA].
- Rosas-Guevara, Yetli M. et al. (Feb. 2019). "The abundances and properties of Dual AGN and their host galaxies in the EAGLE simulations". In: 483.2, pp. 2712–2720. DOI: 10.1093/mnras/sty3251. arXiv: 1805.01479 [astro-ph.GA].
- Saeedzadeh, Vida et al. (Feb. 2024). "Shining light on the hosts of the nano-Hertz gravitational wave sources: a theoretical perspective". In: *Monthly Notices of the Royal Astronomical Society* 529.4, pp. 4295–4310. ISSN: 0035-8711. DOI: 10.1093/mnras/stae513. eprint: https://academic.oup.com/mnras/article-pdf/529/4/4295/57143101/stae513.pdf. URL: https://doi.org/10.1093/mnras/stae513.
- Sahu, Nandini, Alister W. Graham, and Benjamin L. Davis (May 2019). "Black Hole Mass Scaling Relations for Early-type Galaxies. I. M <sub>BH</sub>-M <sub>\*, sph</sub> and M <sub>BH</sub>-M <sub>\*,gal</sub>". In: 876.2, 155, p. 155. DOI: 10.3847/1538-4357/ab0f32. arXiv: 1903.04738 [astro-ph.GA].
- Salpeter, E. E. (Aug. 1964). "Accretion of Interstellar Matter by Massive Objects." In: 140, pp. 796–800. DOI: 10.1086/147973.
- Sánchez, S. F. et al. (Feb. 2012). "CALIFA, the Calar Alto Legacy Integral Field Area survey. I. Survey presentation". In: 538, A8, A8. DOI: 10.1051/0004-6361/201117353. arXiv: 1111.0962 [astro-ph.CO].
- Sánchez, S. F. et al. (Aug. 2017). "The mass-metallicity relation revisited with CAL-IFA". In: 469.2, pp. 2121–2140. DOI: 10.1093/mnras/stx808. arXiv: 1703.09769 [astro-ph.GA].
- Sandage, A. (2000). "Malmquist Bias and Completeness Limits". In: *Encyclopedia of Astronomy and Astrophysics*. Ed. by P. Murdin, 1940, p. 1940. DOI: 10.1888/0333750888/1940.

Schneider, Raffaella et al. (July 2006). "Fragmentation of star-forming clouds enriched with the first dust". In: 369.3, pp. 1437–1444. DOI: 10.1111/j.1365-2966.2006.10391.x. arXiv: astro-ph/0603766 [astro-ph].

- Schnittman, Jeremy D. and Alessandra Buonanno (June 2007). "The Distribution of Recoil Velocities from Merging Black Holes". In: 662.2, pp. L63–L66. DOI: 10. 1086/519309. arXiv: astro-ph/0702641 [astro-ph].
- Schutz, B. F. (Sept. 1986). "Determining the Hubble constant from gravitational wave observations". In: 323.6086, pp. 310–311. DOI: 10.1038/323310a0.
- Schutz, Katelin and Chung-Pei Ma (June 2016). "Constraints on individual supermassive black hole binaries from pulsar timing array limits on continuous gravitational waves". In: 459.2, pp. 1737–1744. DOI: 10.1093/mnras/stw768. arXiv: 1510.08472 [astro-ph.GA].
- Schwarzschild, Karl (Jan. 1916). "Über das Gravitationsfeld eines Massenpunktes nach der Einsteinschen Theorie". In: Sitzungsberichte der Königlich Preussischen Akademie der Wissenschaften. ADS Bibcode: 1916SPAW......189S, pp. 189–196. URL: https://ui.adsabs.harvard.edu/abs/1916SPAW.....189S (visited on 04/22/2025).
- Sesana, A., A. Vecchio, and M. Volonteri (Apr. 2009). "Gravitational waves from resolvable massive black hole binary systems and observations with Pulsar Timing Arrays". In: 394.4, pp. 2255–2265. DOI: 10.1111/j.1365-2966.2009.14499.x. arXiv: 0809.3412 [astro-ph].
- Sesana, Alberto, Francesco Haardt, and Piero Madau (Oct. 2008). "Interaction of Massive Black Hole Binaries with Their Stellar Environment. III. Scattering of Bound Stars". In: 686.1, pp. 432–447. DOI: 10.1086/590651. arXiv: 0710.4301 [astro-ph].
- Sesana, Alberto and Alberto Vecchio (May 2010). "Measuring the parameters of massive black hole binary systems with pulsar timing array observations of gravitational waves". In: 81.10, 104008, p. 104008. DOI: 10.1103/PhysRevD.81.104008. arXiv: 1003.0677 [astro-ph.CO].
- Sesana, Alberto et al. (Aug. 2004). "Low-Frequency Gravitational Radiation from Coalescing Massive Black Hole Binaries in Hierarchical Cosmologies". In: 611.2, pp. 623–632. DOI: 10.1086/422185. arXiv: astro-ph/0401543 [astro-ph].

Shannon, R. M. et al. (Sept. 2015). "Gravitational waves from binary supermassive black holes missing in pulsar observations". In: *Science* 349.6255, pp. 1522–1525. DOI: 10.1126/science.aab1910. arXiv: 1509.07320 [astro-ph.CO].

- Shen, Yue and Abraham Loeb (Dec. 2010). "Identifying Supermassive Black Hole Binaries with Broad Emission Line Diagnosis". In: 725.1, pp. 249–260. DOI: 10. 1088/0004-637X/725/1/249. arXiv: 0912.0541 [astro-ph.C0].
- Silk, Joseph and Martin J. Rees (Mar. 1998). Quasars and galaxy formation. ISSN: 0004-6361 Volume: 331 ADS Bibcode: 1998A&A...331L...1S. DOI: 10.48550/arXiv.astro-ph/9801013. URL: https://ui.adsabs.harvard.edu/abs/1998A&A...331L...1S (visited on 05/30/2025).
- Simon, Joseph et al. (Mar. 2014). "Gravitational Wave Hotspots: Ranking Potential Locations of Single-source Gravitational Wave Emission". In: 784.1, 60, p. 60. DOI: 10.1088/0004-637X/784/1/60. arXiv: 1402.1140 [astro-ph.C0].
- Soltan, A. (July 1982). "Masses of quasars." In: 200, pp. 115–122. DOI: 10.1093/mnras/200.1.115.
- Stark, David V. et al. (Oct. 2018). "SDSS-IV MaNGA: characterizing non-axisymmetric motions in galaxy velocity fields using the Radon transform". In: 480.2, pp. 2217–2235. DOI: 10.1093/mnras/sty1991. arXiv: 1807.11503 [astro-ph.GA].
- Stigler, Stephen M. (May 1989). "Francis Galton's Account of the Invention of Correlation". In: *Statistical Science* 4.2. Publisher: Institute of Mathematical Statistics, pp. 73–79. ISSN: 0883-4237, 2168-8745. DOI: 10.1214/ss/1177012580. URL: https://projecteuclid.org/journals/statistical-science/volume-4/issue-2/Francis-Galtons-Account-of-the-Invention-of-Correlation/10.1214/ss/1177012580.full (visited on 04/25/2025).
- Sun, Luming et al. (Feb. 2016). "Keck/ESI Long-slit Spectroscopy of SBS 1421+511:

  A Recoiling Quasar Nucleus in an Active Galaxy Pair?" In: 818.1, 64, p. 64. DOI: 10.3847/0004-637X/818/1/64. arXiv: 1512.05877 [astro-ph.GA].
- Tisserand, P. et al. (July 2007). "Limits on the Macho content of the Galactic Halo from the EROS-2 Survey of the Magellanic Clouds". en. In: *Astronomy & Astrophysics* 469.2. Number: 2 Publisher: EDP Sciences, pp. 387–404. ISSN: 0004-6361, 1432-0746. DOI: 10.1051/0004-6361: 20066017. URL: https://www.aanda.

org/articles/aa/abs/2007/26/aa6017-06/aa6017-06.html (visited on 07/18/2025).

- Torbaniuk, O. et al. (Feb. 2024). "Probing supermassive black hole growth and its dependence on stellar mass and star formation rate in low-redshift galaxies". In: 527.4, pp. 12091–12108. DOI: 10.1093/mnras/stad3965. arXiv: 2312.13869 [astro-ph.GA].
- Tremmel, M. et al. (Sept. 2017). "The Romulus cosmological simulations: a physical approach to the formation, dynamics and accretion models of SMBHs". In: 470.1, pp. 1121–1139. DOI: 10.1093/mnras/stx1160. arXiv: 1607.02151 [astro-ph.GA].
- Tremonti, Christy A. et al. (Oct. 2004). "The Origin of the Mass-Metallicity Relation: Insights from 53,000 Star-forming Galaxies in the Sloan Digital Sky Survey". In: 613.2, pp. 898–913. DOI: 10.1086/423264. arXiv: astro-ph/0405537 [astro-ph].
- Truant, Riccardo J. et al. (Apr. 2025). "Lighting up the nano-hertz gravitational wave sky: opportunities and challenges of multimessenger astronomy with PTA experiments". In: *arXiv e-prints*, arXiv:2504.01074, arXiv:2504.01074. DOI: 10.48550/arXiv.2504.01074. arXiv: 2504.01074 [astro-ph.GA].
- Valtaoja, L., M. J. Valtonen, and G. G. Byrd (Aug. 1989). "Binary Pairs of Supermassive Black Holes: Formation in Merging Galaxies". In: 343, p. 47. DOI: 10.1086/167683.
- Veale, Melanie et al. (Oct. 2017). "The MASSIVE Survey VII. The relationship of angular momentum, stellar mass and environment of early-type galaxies". In: 471.2, pp. 1428–1445. DOI: 10.1093/mnras/stx1639. arXiv: 1703.08573 [astro-ph.GA].
- Vilenkin, Alexander (1985). "Cosmic Strings and Domain Walls". In: *Phys. Rept.* 121, pp. 263–315. DOI: 10.1016/0370-1573(85)90033-X.
- Villforth, Carolin and Fred Hamann (Mar. 2015). "The Host Galaxies and Narrow-Line Regions of Four Double-Peaked [OIII] AGNs". In: 149.3, 92, p. 92. DOI: 10. 1088/0004-6256/149/3/92. arXiv: 1501.00325 [astro-ph.GA].
- Vogelsberger, Mark et al. (Oct. 2014). "Introducing the Illustris Project: simulating the coevolution of dark and visible matter in the Universe". In: 444.2, pp. 1518–1547. DOI: 10.1093/mnras/stu1536. arXiv: 1405.2921 [astro-ph.CO].
- Volonteri, Marta (July 2010). "Formation of supermassive black holes". en. In: *The Astronomy and Astrophysics Review* 18.3, pp. 279–315. ISSN: 1432-0754. DOI: 10.

```
1007/s00159-010-0029-x. URL: https://doi.org/10.1007/s00159-010-0029-x (visited on 05/15/2025).
```

- Volonteri, Marta, Francesco Haardt, and Piero Madau (2003). "The Assembly and Merging History of Supermassive Black Holes in Hierarchical Models of Galaxy Formation". In: *The Astrophysical Journal* 582.2, p. 559. DOI: 10.1086/344675. URL: https://dx.doi.org/10.1086/344675.
- Volonteri, Marta, Giuseppe Lodato, and Priyamvada Natarajan (Jan. 2008). "The evolution of massive black hole seeds". In: 383.3, pp. 1079–1088. DOI: 10.1111/j.1365-2966.2007.12589.x. arXiv: 0709.0529 [astro-ph].
- Volonteri, Marta et al. (Oct. 2020). "Black hole mergers from dwarf to massive galaxies with the NewHorizon and Horizon-AGN simulations". In: 498.2, pp. 2219–2238. DOI: 10.1093/mnras/staa2384. arXiv: 2005.04902 [astro-ph.GA].
- Walcher, C. J. et al. (Sept. 2014). "CALIFA: a diameter-selected sample for an integral field spectroscopy galaxy survey". In: 569, A1, A1. DOI: 10.1051/0004-6361/201424198. arXiv: 1407.2939 [astro-ph.GA].
- Webster, B. Louise and Paul Murdin (Jan. 1972). "Cygnus X-1-a Spectroscopic Binary with a Heavy Companion?" In: 235.5332, pp. 37–38. DOI: 10.1038/235037a0.
- Willott, Chris J. et al. (June 2005). "Imaging of SDSS z > 6 Quasar Fields: Gravitational Lensing, Companion Galaxies, and the Host Dark Matter Halos". In: 626.2, pp. 657–665. DOI: 10.1086/430168. arXiv: astro-ph/0503202 [astro-ph].
- Wise, John H., Matthew J. Turk, and Tom Abel (Aug. 2008). "Resolving the Formation of Protogalaxies. II. Central Gravitational Collapse". In: 682.2, pp. 745–757.

  DOI: 10.1086/588209. arXiv: 0710.1678 [astro-ph].
- Wyithe, J. Stuart B. and Abraham Loeb (June 2003). "Low-Frequency Gravitational Waves from Massive Black Hole Binaries: Predictions for LISA and Pulsar Timing Arrays". In: 590.2, pp. 691–706. DOI: 10.1086/375187. arXiv: astro-ph/0211556 [astro-ph].
- Xu, Dawei and S. Komossa (Nov. 2009). "Narrow Double-Peaked Emission Lines of SDSS J131642.90+175332.5: Signature of a Single or a Binary AGN in a Merger, Jet-Cloud Interaction, or Unusual Narrow-Line Region Geometry". In: 705.1, pp. L20–L24. DOI: 10.1088/0004-637X/705/1/L20. arXiv: 0908.3140 [astro-ph.GA].

Xu, Heng et al. (July 2023). "Searching for the Nano-Hertz Stochastic Gravitational Wave Background with the Chinese Pulsar Timing Array Data Release I". In: Research in Astronomy and Astrophysics 23.7, 075024, p. 075024. DOI: 10.1088/1674-4527/acdfa5. arXiv: 2306.16216 [astro-ph.HE].

- York, Donald G. et al. (Sept. 2000). "The Sloan Digital Sky Survey: Technical Summary". In: 120.3, pp. 1579–1587. DOI: 10.1086/301513. arXiv: astro-ph/0006396 [astro-ph].
- Young, M. D. and C. J. Clarke (Sept. 2015). "Binary accretion rates: dependence on temperature and mass ratio". In: 452.3, pp. 3085–3091. DOI: 10.1093/mnras/stv1512. arXiv: 1507.01850 [astro-ph.SR].
- Yu, Qingjuan et al. (Sept. 2011). "The Low Frequency of Dual Active Galactic Nuclei versus the High Merger Rate of Galaxies: A Phenomenological Model". In: *The Astrophysical Journal* 738. Publisher: IOP ADS Bibcode: 2011ApJ...738...92Y, p. 92. ISSN: 0004-637X. DOI: 10.1088/0004-637X/738/1/92. URL: https://ui.adsabs.harvard.edu/abs/2011ApJ...738...92Y (visited on 06/04/2025).
- Zel'dovich, Ya. B. (Sept. 1964). "The Fate of a Star and the Evolution of Gravitational Energy Upon Accretion". In: *Soviet Physics Doklady* 9, p. 195.